

Journal Pre-proof

Design, synthesis and biological evaluation of novel naturally-inspired multifunctional molecules for the management of Alzheimer's disease

Yash Pal Singh, Gullanki Naga Venkata Charan Tej, Amruta Pandey, Khushbu Priya, Pankaj Pandey, Gauri Shankar, Prasanta Kumar Nayak, Geeta Rai, Amar G. Chittiboyina, Robert J. Doerksen, Swati Vishwakarma, Gyan Modi

PII: S0223-5234(20)30224-5

DOI: <https://doi.org/10.1016/j.ejmech.2020.112257>

Reference: EJMECH 112257

To appear in: *European Journal of Medicinal Chemistry*

Received Date: 15 February 2020

Revised Date: 17 March 2020

Accepted Date: 18 March 2020



Please cite this article as: Y.P. Singh, G.N.V.C. Tej, A. Pandey, K. Priya, P. Pandey, G. Shankar, P.K. Nayak, G. Rai, A.G. Chittiboyina, R.J. Doerksen, S. Vishwakarma, G. Modi, Design, synthesis and biological evaluation of novel naturally-inspired multifunctional molecules for the management of Alzheimer's disease, *European Journal of Medicinal Chemistry* (2020), doi: <https://doi.org/10.1016/j.ejmech.2020.112257>.

This is a PDF file of an article that has undergone enhancements after acceptance, such as the addition of a cover page and metadata, and formatting for readability, but it is not yet the definitive version of record. This version will undergo additional copyediting, typesetting and review before it is published in its final form, but we are providing this version to give early visibility of the article. Please note that, during the production process, errors may be discovered which could affect the content, and all legal disclaimers that apply to the journal pertain.

© 2020 Published by Elsevier Masson SAS.

Design, Synthesis and Biological Evaluation of Novel Naturally-Inspired Multifunctional Molecules for the Management of Alzheimer's Disease

Yash Pal Singh,[#] Gullanki Naga Venkata Charan Tej,[#] Amruta Pandey,^{#¶} Khushbu Priya,^{||} Pankaj Pandey,[§] Gauri Shankar,[#] Prasanta Kumar Nayak,[#] Geeta Rai,^{||} Amar G. Chittiboyina,[§] Robert J Doerksen,^Δ Swati Vishwakarma,^{#*} Gyan Modi^{#*}

[#]Department of Pharmaceutical Engineering & Technology, Indian Institute of Technology (Banaras Hindu University), Varanasi, 221005, India

^{||}Department of Molecular and Human Genetics, Institute of Science, Banaras Hindu University, Varanasi, 221005, India

[§]National Center for Natural Products Research, and ^ΔDepartment of BioMolecular Sciences, School of Pharmacy, University of Mississippi, University, MS 38677, United States

[¶]Current address: Zydus Research Center, Zydus Cadila, Moraiya, Ahmadabad, 382213, India

^{*}Current address: Biological R & D Center (A division of Aurobindo Pharma Limited), Survey No. 77 & 78, Indrakaran (V), Kandi (M), Sangareddy, Telangana, 502329, India

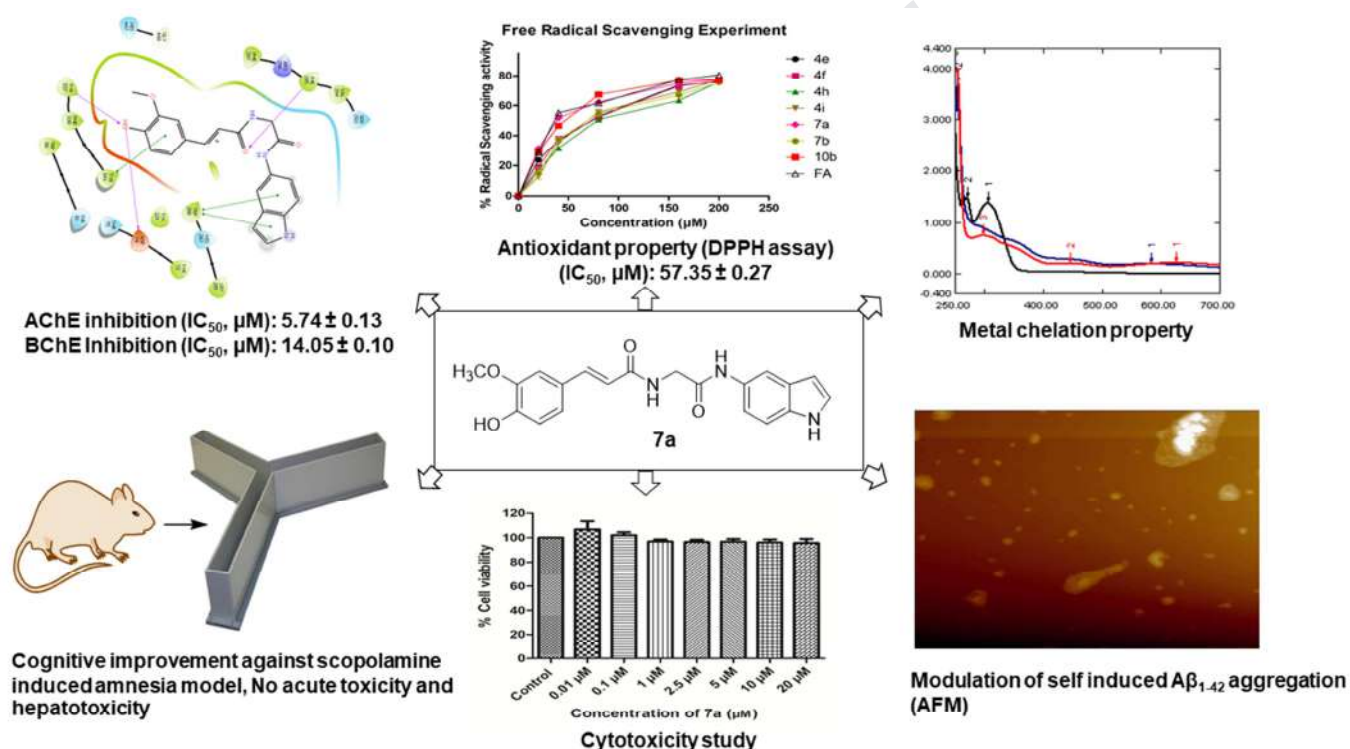
Abstract

In our overall goal to overcome the limitations associated with natural products for the management of Alzheimer's disease and to develop *in-vivo* active multifunctional cholinergic inhibitors, we embarked on the development of ferulic acid analogs. A systematic SAR study to improve upon the cholinesterase inhibition of ferulic acid with analogs that also had lower logP was carried out. Enzyme inhibition and kinetic studies identified compound **7a** as a lead molecule with preferential acetylcholinesterase inhibition (AChE IC₅₀ = 5.74 ± 0.13 μM; BChE IC₅₀ = 14.05 ± 0.10 μM) compared to the parent molecule ferulic acid (% inhibition of AChE and BChE at 20 μM, 15.19 ± 0.59 and 19.73 ± 0.91, respectively). Molecular docking and dynamics studies revealed that **7a** fits well into the active sites of AChE and BChE, forming stable and strong interactions with key residues Asp74, Trp286, and Tyr337 in AChE and with Tyr128, Trp231, Leu286, Ala328, Phe329, and Tyr341 in BChE. Compound **7a** was found to be an efficacious antioxidant in a DPPH assay (IC₅₀ = 57.35 ± 0.27 μM), and it also was able to chelate iron. Data from atomic force microscopy images demonstrated that **7a** was able to modulate aggregation of amyloid β₁₋₄₂. Upon oral administration, **7a** exhibited promising *in-vivo* activity in the scopolamine-induced AD animal model and was able to improve spatial memory in cognitive deficit mice in the Y-maze model. Analog **7a** could

effectively reverse the increased levels of AChE and BChE in scopolamine-treated animals and exhibited potent *ex-vivo* antioxidant properties. These findings suggest that **7a** can act as a lead molecule for the development of naturally-inspired multifunctional molecules for the management of Alzheimer's and other neurodegenerative disorders.

Keywords: Alzheimer's disease, ferulic acid, acetylcholinesterase, amyloid-beta, antioxidant, docking, multifunctional targeted ligands

Graphical abstract



1. Introduction

Alzheimer's disease (AD) is a multifactorial progressive neurodegenerative disorder characterized by gradual loss of neurons and synapses, particularly within the brain's cholinergic system, resulting in loss of memory and of other cognitive functions[1]. It is the sixth-leading cause of death in the United States [2]. One in nine people older than 65 in USA has AD. The total cost for all individuals with AD and other dementias is expected to rise to approximately \$1.1 trillion by 2050. Cholinesterases (ChEs) are responsible for the hydrolysis of acetylcholine, a major neurotransmitter that plays an important role in learning and

memory. Human ChEs can be divided into acetylcholine and butyrylcholinesterase (AChE and BChE), which share 65% structural homology in their amino acid sequences[3, 4]. AChE is classified as a serine protease and it is responsible for the degradation of acetylcholine into choline and acetic acid. Therefore, it plays a very critical role in cholinergic neurotransmission. Its active site can be divided into the anionic site, catalytic triad or esteratic site (ES), oxyanion hole, selectivity determinant acyl pocket and peripheral anionic site (PAS) [5]. BChE is a second human cholinesterase that is also present in the brain and that cleaves acetylcholine. Recent studies suggest that brain-targeted BChE not only lowers A β levels in transgenic mice but also improves cognitive performance in animals [6, 7]. The levels of both AChE and BChE change dramatically as AD progresses. Therefore, both enzymes have been widely explored as targets for a neuroprotective and disease-modifying therapy for AD [8].

The etiology of AD is not yet completely known but it is evident from the literature, including publications from our group, that low levels of neurotransmitters, especially acetylcholine; amyloid-beta (A β) aggregates; oxidative stress; and the concentrations of metals interdependently play key roles in the neurodegeneration process [9-17]. A pathological hallmark of AD is the presence of A β aggregates, including the accumulation of A β into insoluble plaques and soluble oligomers [18]. The presence of hydrophobic amino acid residues in the central region of the A β structure is mainly responsible for its aggregation potential [19-21]. The accumulation of A β aggregates stimulates a string of neurotoxic pathways such as apoptosis, inflammation and calcium dysregulation, which are hypothesized to cause the impairment of synapses and neurons [22, 23]. Further, excess production of A β aggregates can also damage various cellular organelles. Altered brain metal homeostasis is responsible for the pathogenesis of AD [24]. Although iron has paramount importance in several cellular functions including in the synthesis and metabolism of neurotransmitters, excess amounts of free iron are the leading cause for the generation of reactive oxygen species (ROS) via the Fenton reaction, the formation of toxic A β_{1-42} aggregates, and mitochondrial oxidation. The levels of iron increase with age due to multiple factors including but not limited to the leaky blood-brain barrier (BBB), inefficient chelating of iron in the brain and compromise in iron homeostasis. Excess iron can cause neuronal death due to an increase in oxidative stress, misfolding of A β_{1-42} , and tau hyperphosphorylation in AD [25-27].

Among various factors responsible for neurodegeneration in AD, an increased level of ROS is one of the major culprits which is thought to play a key role in the onset and progression of neurodegeneration. Apart from the presence of aggregated forms of A β ₁₋₄₂, AD brains have constantly shown the signature of ROS- and RNS-mediated injury. The brain is highly prone to oxidative imbalance due to the presence of highly metabolic oxidative polyunsaturated fatty acids (PUFAs) and metal ions especially iron [28]. The altered mitochondrial function, presence of A β , and high concentrations of metals can interdependently increase the level of ROS, thereby disrupting the electron transport chain and eventually leading to oxidative stress-induced neurodegeneration in AD. The close relationship of oxidative stress to other pathophysiological factors can cause overproduction of ROS which can alter the clearance of oxidative species, and thereby enhance the oxidative environment in the neurons. This imbalance between ROS production and antioxidant defense leads to an increase in the level of oxidative stress, resulting in accumulation of free radicals which eventually causes mitochondrial dysfunction [29].

Among the currently available AD drugs on the market, including donepezil (1), rivastigmine (2), galantamine (3) and memantine (4) (**Figure 1A**), AChE is an important target for 1-2. The best the existing drugs can provide is only symptomatic relief for the initial 1-2 years of the disease without addressing the aforesaid critical basic factors responsible for the neurodegeneration. Consequently, the progression of the disease continues despite the availability of the current drugs for AD. There is an urgent need for novel therapies that should not only alleviate the symptoms of the disease but also be able to provide neuroprotection via modification of the pathological factors such as A β ₁₋₄₂ aggregates, oxidative stress, and metal accumulation, to slow or stop the progression of neurodegeneration in AD. Our laboratory has been developing novel multifunctional neuroprotective molecules of varying selectivity towards the cholinergic system [5].

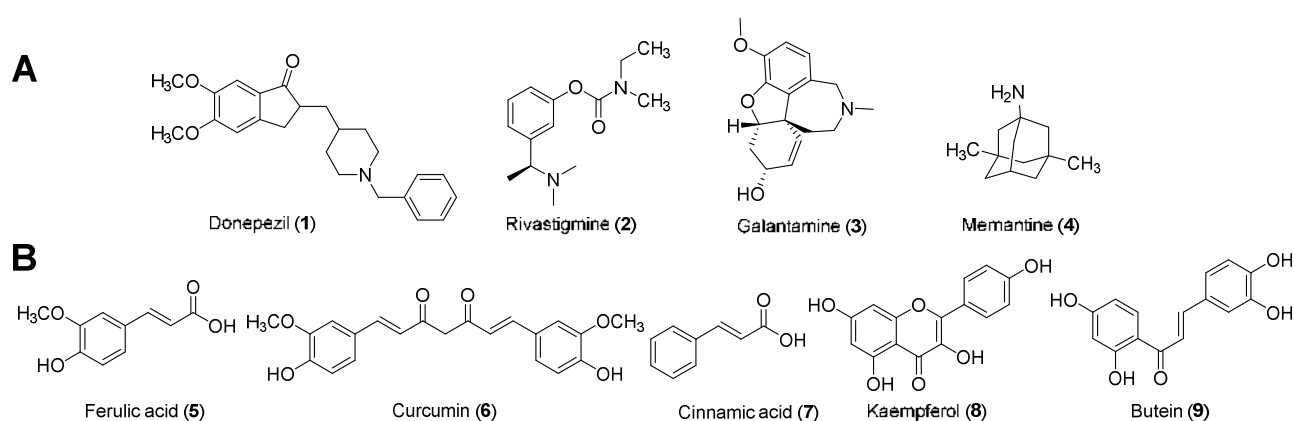


Fig. 1. Chemical structures of (A) Drug candidates available in the market for the treatment of AD; (B) Natural products that are known to modulate neurodegenerative disorders.

Plant-derived compounds represent one of the major sources of therapeutic tools for a variety of diseases including neurodegenerative disorders [30]. The presence of a trans-alkene attached to a phenyl ring bearing a hydroxyl group is the key structural feature in the majority of known anti-AD natural products such as ferulic acid (**FA**) (5), curcumin (6), cinnamic acid (7), kaempferol (8), butein (9), and others (Figure 1B). Several natural products including trans-4-hydroxy-3-methoxy cinnamic acid (**FA**) and their hybrid analogs are under investigation as neuroprotective agents for AD [31]. In *in-vitro* experiments, **FA** has shown promising neuroprotection. However, **FA** does not effectively interact with AChE and BChE (<20% inhibition of AChE and BChE at 20 μ M), which is evident from the literature and our experiments [32]. Further, its ability to cross the blood-brain barrier is limited due to its relatively low lipophilicity (cLog P \sim 1.5). The low logP value of **FA** is also responsible for its poor aqueous solubility. To develop naturally inspired *in-vivo* active neuroprotective molecules and to overcome the limitations associated with the natural compounds, we embarked on the development of novel **FA** analogs. In order to address the aforesaid limitations associated with **FA**, we systematically designed and developed novel diamide compounds in which **FA** is connected to various aromatic/substituted, aromatic/heterocyclic moieties to impart the cholinergic inhibition property, and to increase the logP of the designed molecules (Figure 2). The selection of linker and various hydrophobic or heterocyclic moieties are based on binding mode analysis of **FA** to the enzymes. The increase in logP of the designed molecules via the introduction of hydrophobic features should provide optimal logP values in the range of 2-4 and enable them to cross barriers to reach and interact with

the enzymes effectively. We are also taking into account the structure of the enzymes and our publication/patents contributions in this area for the improved design of the compounds [5].

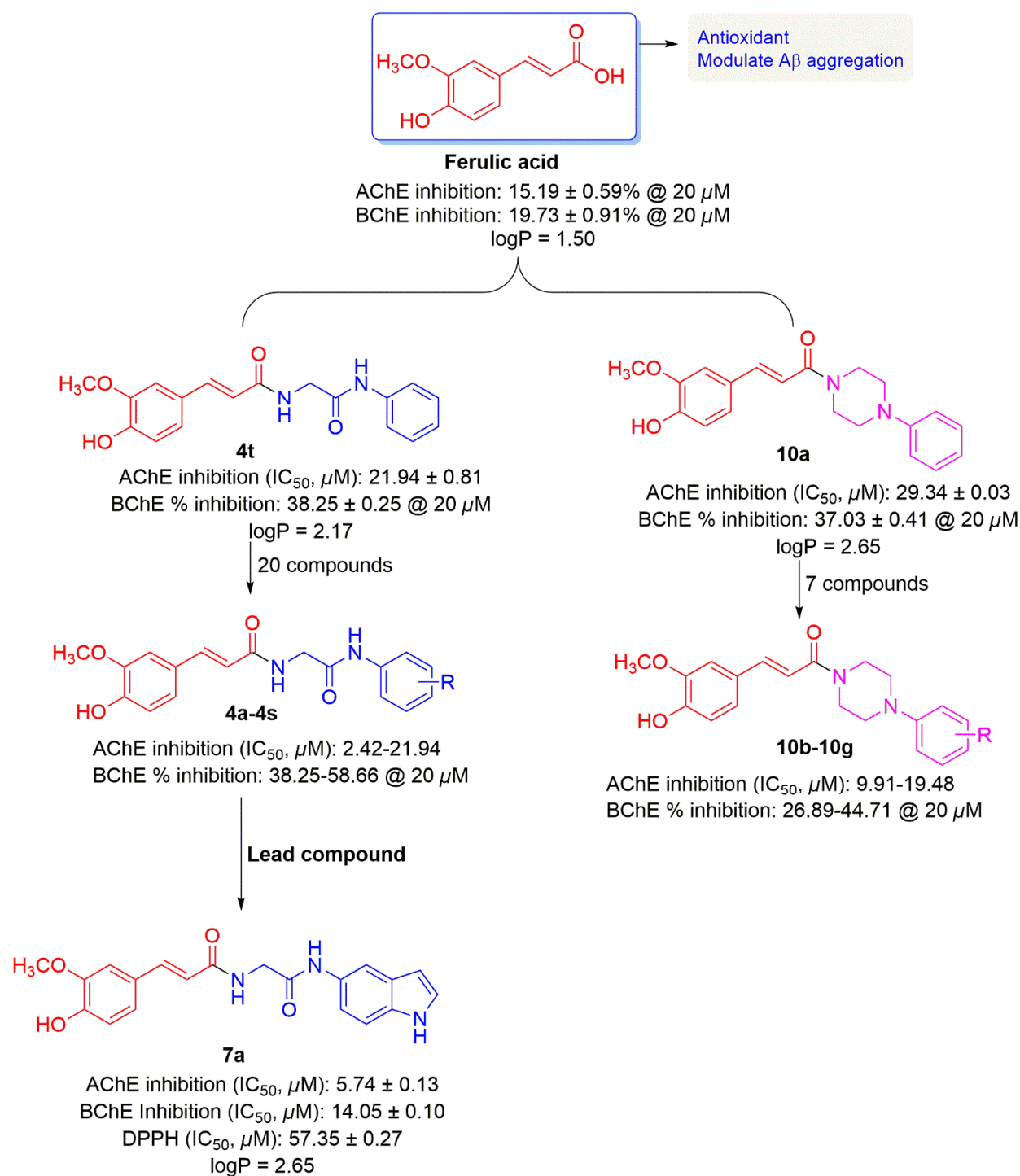


Fig. 2. Schematic pipeline toward the development of novel ferulic acid derivatives with favorable properties.

2. Results and discussion

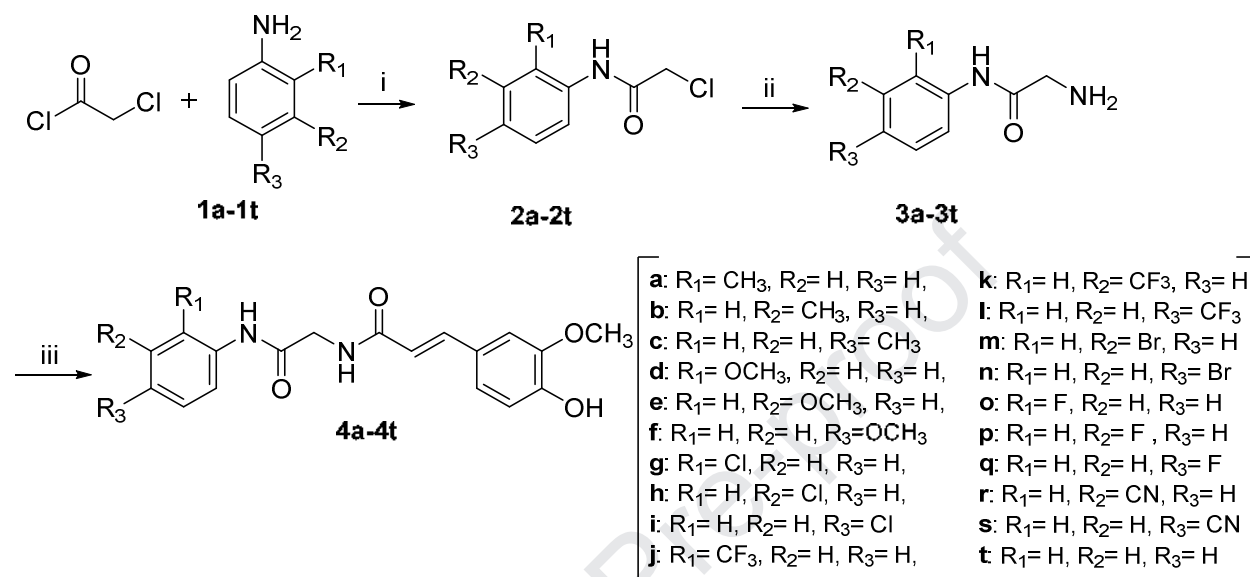
2.1. Chemistry

A novel synthetic route towards the development of ferulic acid derivatives has been optimized as shown in **Schemes 1** and **2**. In **Scheme 1**, we developed a novel method for the synthesis of 2-amino-N-phenyl substituted acetamides (**3a-3t** and **6a-6b**), from 2-chloro-N-phenyl substituted acetamides (**2a-2t**) which are the key intermediates for the target compounds (**4a-4t** and **7a-7b**). In our initial attempts, the reaction between glycine and substituted aniline in organic solvents did not work well due to the poor solubility of glycine. So, we switched to the conversion of substituted amines into the corresponding 2-chloro-N-phenyl substituted acetamides followed by reflux with aqueous ammonia. Commercially available substituted anilines **1a-1t**, **5-aminoindole**, and **6-aminoquinoline** underwent a nucleophilic acyl substitution reaction with chloroacetyl chloride in dichloromethane and K_2CO_3 as a base to give 2-chloro-N-phenyl substituted acetamides **2a-2t** and **5a-5b**. The synthesis of 2-amino-N-phenyl substituted acetamides **3a-3t** and **6a-6b** using *tert*-butoxycarbonyl (BOC)-protected glycine has been reported in the literature [33-36]. However, these methods are not viable due to limited commercial availability of the BOC-protected substrates, the requirement of functional group transformations with several reagents and solvents. Therefore, we developed direct and efficient routes towards the synthesis of 2-amino-N-phenyl substituted acetamide derivatives **3a-3t** and **6a-6b** under mild conditions in environmentally friendly aqueous media in a single step with good-to-high yields. 2-chloro-N-phenyl substituted acetamides **2a-2n** and **5a-5b** were refluxed at 60 °C in aqueous ammonia (NH_3) to afford precursor 2-amino-N-phenyl substituted acetamides **3a-3n** and **6a-6b** in good-to-excellent yields without purification. Finally, the target compounds **4a-4n** and **7a-7b** were generated using a standard amide coupling reaction of the 2-amino-N-phenyl substituted acetamide with ferulic acid in high yield.

Next, cf. **Scheme 3**, we introduced a piperazine moiety in order to impart rigidity and provide a site for protonation to help improve the solubility and ability to cross the BBB. The aryl amines, **8a-8g**, underwent a nucleophilic substitution reaction (S_N2) with bis(2-chloroethyl) amine hydrochloride to give the substituted phenyl piperazines **9a-9g**, following the literature method,[37] which were further reacted with ferulic acid to afford the target

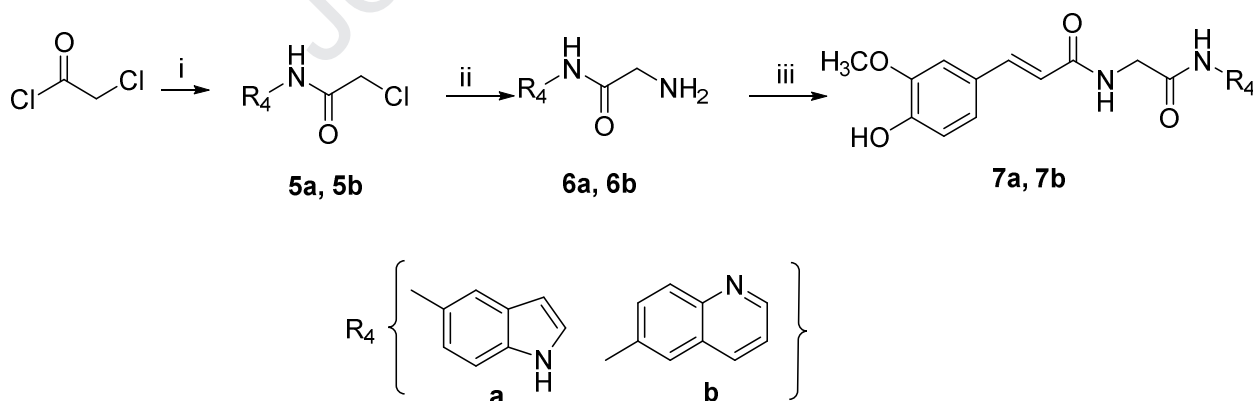
compounds **10a-10g**. The structures of the synthesized molecules were confirmed with the help of ^1H and ^{13}C NMR, and high-resolution mass spectrometry (Supporting Information).

Scheme 1. Synthesis of ferulic acid-acetamide derivatives **4a-4t**^a

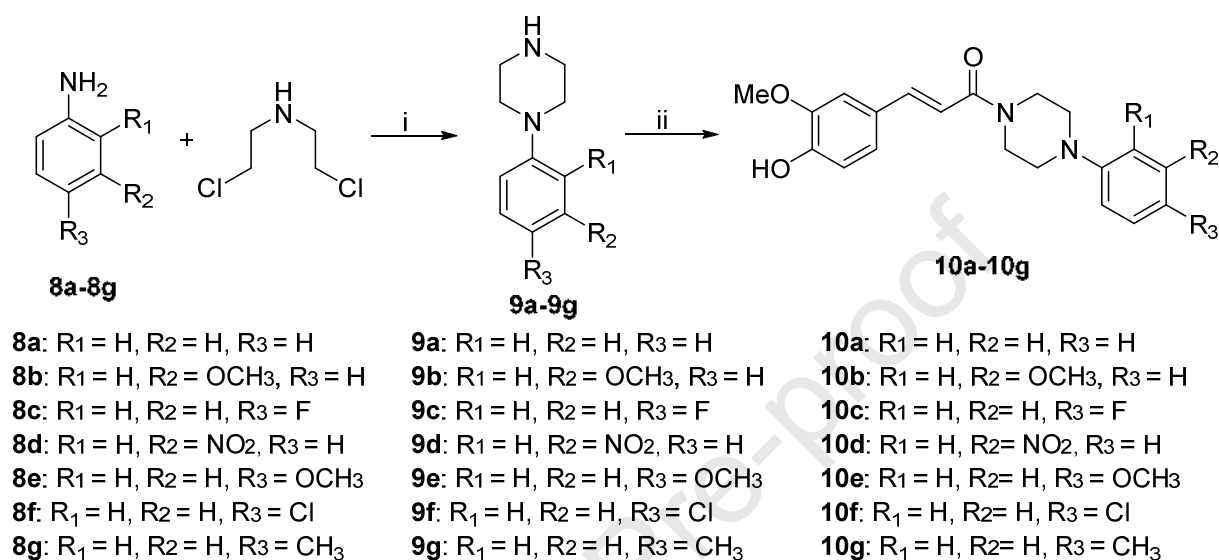


^aReagents and conditions: (i) K_2CO_3 , DCM, 0°C , 2h, 60-70%; (ii) Excess NH_3 solution, 60°C , 6h, 50-60%; (iii) Ferulic acid, EDCI, HOBT, DIPEA, DCM, rt, overnight, 65-75%

Scheme 2. Synthetic route of compounds **7a-7b**^a



^aReagents and conditions: (i) 5-aminoindole/6-aminoquinoline, K_2CO_3 , DCM, 0°C , 2h, 75-80%; (ii) Excess NH_3 solution, 60°C , 6h, 60-70%; (iii) Ferulic acid, EDCI, HOBT, DIPEA, DCM, rt, overnight, 65-70%.

Scheme 3. Synthesis of ferulic acid tethered to N-phenyl-piperazine scaffold **10a-10g**^a

^aReagents and conditions: (i) Diglyme, 150°C, 8-10 h, 65-70%; (ii) Ferulic acid, EDCI, HOBt, DIPEA, THF, rt, overnight, 80-85%.

2.2. Design of novel ferulic acid analogs and cholinesterases inhibition studies

The deficiency of brain acetylcholine (ACh) and other related neurotransmitters is one of the major factors in the progression of AD. Clinically, it is well explored that cholinesterase inhibitors are effective in improving the behavior and slowing down cognitive decline in patients with AD. Thus, the inhibitory activity of the newly synthesized compounds against human AChE and *equine* BChE was measured by using the spectroscopic method of Ellman *et al.* and expressed as IC₅₀, i.e., the inhibitor concentration that reduces the cholinesterase activity by 50 [38]. In this study, **DPZ** served as the reference drug and ferulic acid was used as the negative control.

The crystal structure analysis of AChE revealed the location of the active site at the bottom of a deep and 20 Å long narrow gorge. The choline part of the substrate, ACh, binds into the anionic subsite of the active site surrounded by Trp86, Tyr337, and Phe338 while the esteric moiety interacts with the catalytic triad composed of Ser203, Glu334, and His447 of the

esteratic site. A docking study with the R enantiomer of **DPZ** on AChE (PDB ID:4EY7) was carried out as shown in **Figure 3A**. The binding mode analysis of **DPZ** involves residues that span the length of the active site gorge and multiple key interactions with critical residues thought to be important in the enzyme mechanism. The benzyl ring stacks against Trp86 in the active site while the indanone ring forms π - π interactions with Trp286 in the peripheral anionic site. The carbonyl group of **DPZ** binds with Phe295 while the piperidine nitrogen makes hydrogen bonding to Trp86, Tyr337, and Phe338.

It is evident from the literature that **FA** is a poor inhibitor of AChE. We carried out docking studies for **FA** followed by AChE inhibition studies and compared the results with those for the reference drug **DPZ**. As expected, in both the studies **FA** exhibited significantly poorer interactions compared to **DPZ** (IC_{50} , $\mu M = 0.03 \pm 0.07$ for **DPZ**, and $15.19 \pm 0.59\%$ inhibition of AChE at $20 \mu M$ for **FA**). Given the nature of the long active site of AChE and the relatively short structure of **FA**, it was expected that docking studies would be helpful for predicting which structural modifications should be carried out to improve the binding of **FA** to AChE. The overlay of docked **DPZ** and co-crystallized **DPZ** is included in the supporting information (**Figure S1**). It demonstrates that the docking method works well, because of the close agreement between the two poses of **DPZ**. Interestingly, the docking studies of **FA** (**Figure 3B**) with AChE revealed that the majority of the interactions with the critical amino acids are missing as compared to **DPZ** (**Figure 3A**). It is noteworthy that the presence of acid and phenol functional groups in **FA** provides a lot of scope for possible structural modifications to develop novel analogs. Two of the major goals behind our design of the novel **FA** analogs were to improve the AChE inhibition and to modify the logP values in this first generation of **FA** derived compounds. The structural modifications are centered on the acid functional group of **FA**.

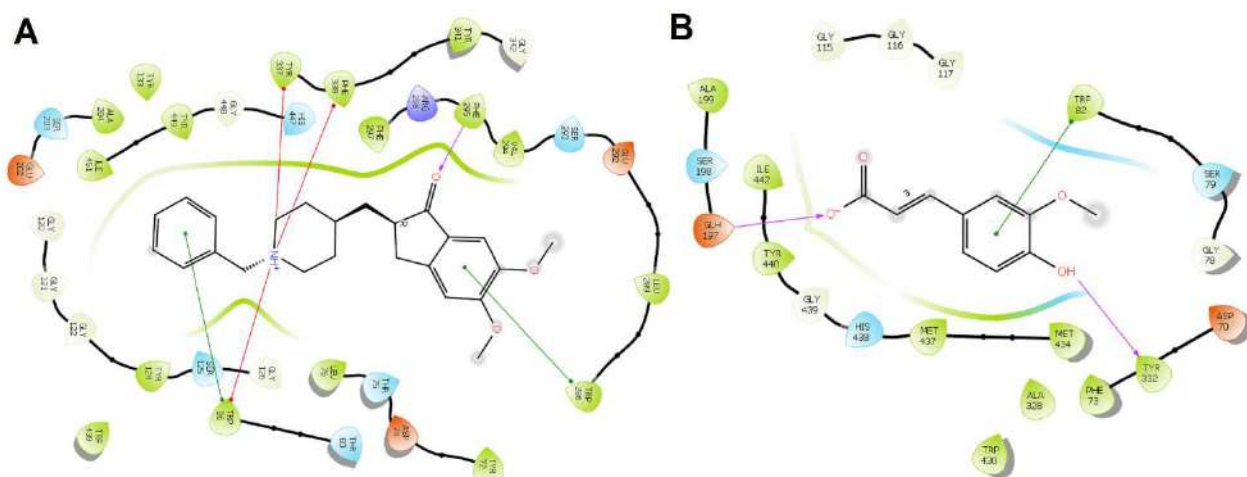


Fig. 3. 2D interaction diagram of (A) **DPZ** and (B) **FA** with various amino acids of the AChE cavity.

We started with the introduction of an amide linker followed by aromatic features into the designed molecules to reach the active site of the enzymes. The aromatic features also improved the lipophilicity and helped the analogs to be able to interact with the essential hydrophobic residues. The presence of an amide bond near the aromatic substitutions on the right-hand side of the molecule could allow H-bonding with Phe295. Our first goal was to find out if the peripheral phenyl ring could be tolerated at the enzyme sites. Therefore, compound **4t** was designed, synthesized and evaluated for enzyme inhibition. To our interest, in the enzyme inhibition studies, **4t** was found to be a potent inhibitor of AChE. The significant improvement in AChE inhibition as compared to **FA** was observed (**4t** $IC_{50} = 21.94 \pm 0.81 \mu M$ for AChE, while **FA** exhibited only $19.73 \pm 0.91\%$ inhibition of AChE at $20 \mu M$). This result indicated that novel amide compounds with aromatic features are well tolerated on the enzyme sites. Further, the methyl group was introduced on various positions of the phenyl ring located on the right-hand side of the molecule. Compounds **4a-4c** were designed, synthesized and evaluated for enzyme inhibition. In the AChE inhibition assay, **4c**, bearing a methyl group in the *p*-position of the phenyl ring, turned out to be the most potent in comparison to the *ortho*-or *meta*-substituted compounds **4a** and **4b** (IC_{50} , AChE, 16.27 ± 0.62 , 18.9 ± 0.17 , and $12.62 \pm 0.05 \mu M$ for **4a**, **4b**, and **4c**, respectively) (Table 1). Interestingly, **4c** was found to be approximately 1.5 times more potent compared to unsubstituted **4t** (IC_{50} , AChE (μM) 21.94 ± 0.81 vs. 12.62 ± 0.05 for **4t** and **4c**, respectively). However, in the BChE inhibition assay no such significant difference in the enzyme inhibition

was observed among the compounds developed so far (% inhibition at 20 μ M 36.82 ± 1.10 , 36.12 ± 0.22 , 35.60 ± 0.84 and 38.25 ± 0.25 for **4a**, **4b**, **4c**, and **4t**, respectively). It is noteworthy that **4a** and **4t** are twice as potent in BChE inhibition compared to **FA** (BChE inhibition at 20 μ M 19.73 ± 0.91 for **FA**).

For the next set of compounds, monomethoxy or monochloro functional groups were introduced at various positions of the distal phenyl ring of the earlier developed **4t**, which led to the generation of **4d-4f**, and **4g-4i**, respectively. Interestingly, compounds **4e** and **4i** showed the maximum inhibition for AChE among all the synthesized derivatives of this class (IC_{50} , AChE (μ M), **4e** = 2.42 ± 0.32 , **4i** = 3.43 ± 0.03 , BChE (μ M), **4e** = 15.29 ± 0.14 , **4f** = 19.54 ± 0.01 , respectively) (**Table 1**). This result indicated that the introduction of electron-withdrawing groups on the phenyl ring at the *para*-position or electron-donating groups at the *meta*-position drastically improved AChE and BChE inhibition. This may be due to strong hydrogen bonding with Tyr124 and Arg296, and aromatic- π interaction with Tyr337 and Phe338 of **4e** (**Figure 4A & 4B**).

We further introduced electron-withdrawing groups in various positions of the terminal phenyl ring to find out the role played by electronic features on the inhibition of the enzymes. The introduction of *o*-CF₃, *m*-CF₃, *p*-CF₃, *m*-Br and *p*-Br led to development of compounds **4j-4n** with IC_{50} , AChE (μ M), **4j** = 15.15 ± 0.31 , **4k** = 9.31 ± 0.03 , **4l** = 8.23 ± 0.12 , **4m** = 13.07 ± 0.05 , and **4n** = 10.24 ± 0.14 (**Table 1**). These results suggested that the introduction of electron-withdrawing groups on the phenyl ring could significantly improve the AChE inhibitory activity compared to **FA**. However, in the BChE inhibition assay no such significant difference was observed among the developed compounds (% inhibition at 20 μ M 43.22 ± 0.10 , 34.92 ± 0.05 , 37.25 ± 0.07 , 36.58 ± 0.42 and 39.28 ± 0.15 , for **4j-4n**, respectively). Finally, the introduction of small electron-withdrawing groups onto the phenyl ring in order to explore the combined effect of electronic and steric features. This modification produced compounds **4o-4s**, bearing fluoro or nitrile in various positions of the terminal phenyl ring. Interestingly, the enzyme inhibition studies indicated the small EWG on the phenyl ring did not have much influence on AChE and BChE inhibitory properties (IC_{50} , AChE (μ M), **4o** = 17.23 ± 0.06 , **4p** = 22.12 ± 0.07 , **4q** = 12.93 ± 0.37 , **4r** = 16.01 ± 0.35 and **4s** = 17.43 ± 0.07 , for **4o-4s**, respectively).

The next goal of our study was to replace the aromatic phenyl ring with the heterocyclic moieties indole or quinolone in order to improve potency and target selectivity. This

modification resulted in the synthesis of compounds **7a** and **7b** with IC_{50} , AChE (μM) 5.74 ± 0.13 and 4.89 ± 0.37 , for **7a** and **7b**, respectively. The enhanced inhibition may be due to the aromatic- π interaction with Trp286 and Tyr341, and hydrogen bonding with Asp74 and Tyr337 in the case of **7a** (**Figure 4C & 4D**). To our surprise, the docking studies exposed two different binding modes of **7a**, as shown in the supporting information (**Figure S2**). Pose 1 had the indole ring pointed towards PAS while Pose 2 had the indole ring shifted towards the active site of substrate acetylcholine. Pose 1 showed higher docking and binding scores and therefore used this docked pose for molecular dynamics (MD) simulations in order to explore further the interactions with the protein. Introducing a heterocyclic nucleus (indole or quinoline) displayed a better BChE inhibitory activity with IC_{50} (μM), BChE, 14.05 ± 0.10 , 14.32 ± 0.04 , for **7a** and **7b**, respectively). These results indicated that the introduction of the indole or quinoline functionalities in place of the simple phenyl ring is well tolerated and could modulate the selectivity towards the target to a significant extent.

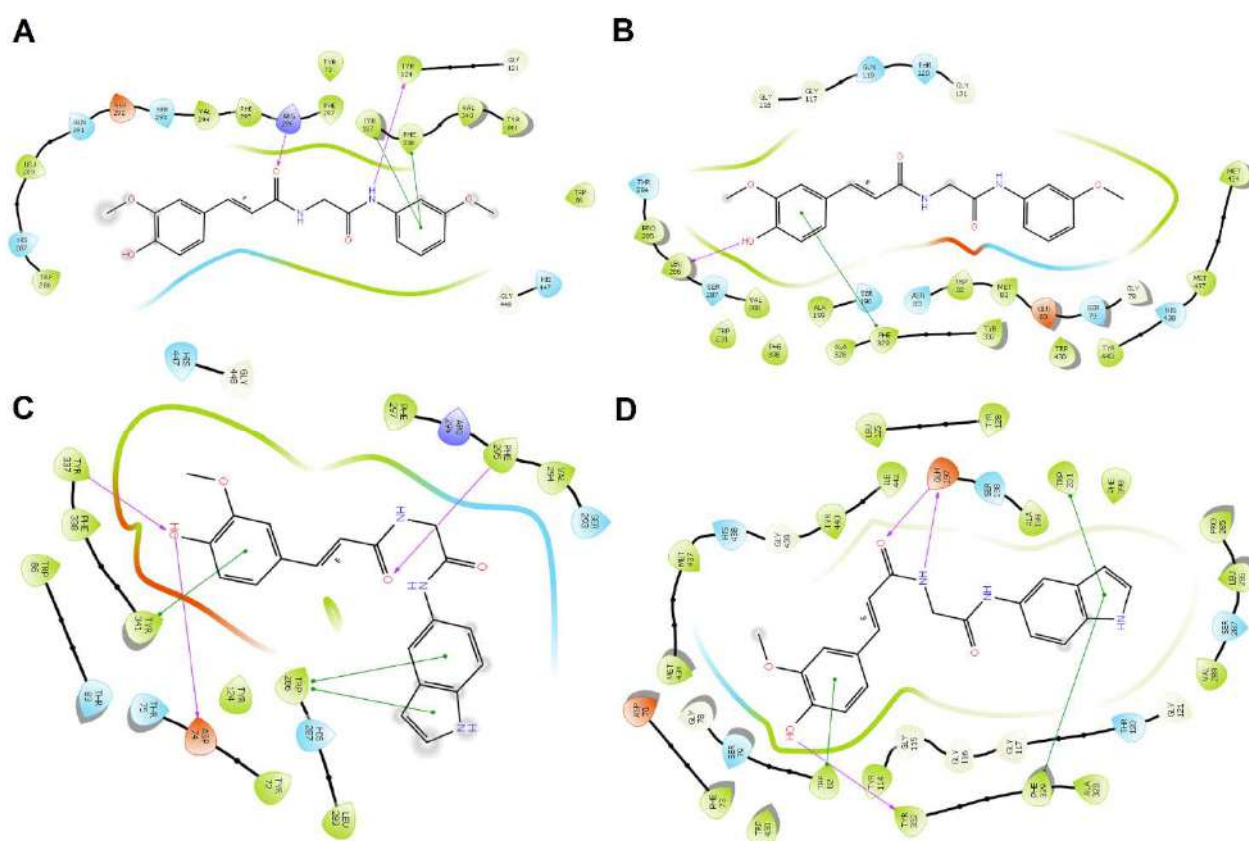
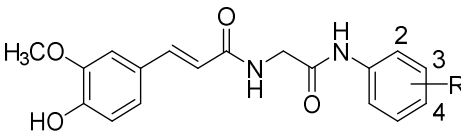
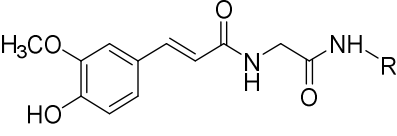
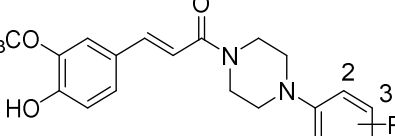


Fig. 4. 2D interaction diagram of (A) **4e** with AChE; (B) **4e** with BChE; (C) **7a** with AChE; and (D) **7a** with BChE.

In our next series of compounds, a piperazine moiety was introduced in order to impart rigidity and provide a site for protonation, to help improve BBB penetration and solubility. Our enzyme inhibition studies with **4a-4t** demonstrated that compounds having *m*-methoxy, *p*-chloro, fluoro or methyl substitutes are comparatively potent enzyme inhibitors over the other developed **FA** analogs. We specifically incorporated these groups in the development of piperazine-bearing molecules **10a-10g** to investigate the impact of these substitutes on enzymes inhibition. To our surprise, the introduction of the piperazine ring in place of glycine amide to connect the **FA** moiety and phenyl ring apparently led to a mixed impact on the enzyme's inhibition potencies. All the developed molecules were found to be moderate to weak inhibitors of the target enzymes compared to the other structural analogs reported in this work (**Table 1**). Intriguingly, a significant reduction in the enzyme inhibition activities was found in the case of *m*-methoxy or *p*-chloro derivatives, **10b** or **10f** compared to **4e** or **4i** (IC_{50} , AChE(μ M) 9.91 ± 0.07 , 11.15 ± 0.13 for **10b** and **10f** and BChE inhibition (in %) 26.89 ± 0.20 , 33.24 ± 1.56 for **10b** and **10f**, respectively). An increase in AChE inhibition and decrease in BChE inhibition activities were observed in *p*-fluoro or methoxy analogs (IC_{50} , AChE(μ M) 11.04 ± 0.06 , 12.05 ± 1.14 for **10c** and **10e**, %BChE inhibition 26.89 ± 0.20 , 33.24 ± 1.56 for **10b** and **10f**, respectively). This may be due to the complex interaction of these molecules with the enzymes. Binding interactions (2D diagram) of **10b** with amino acids of the AChE active cavity are shown in **Figure S3**. The SAR on this series has been summarized in **Figure 5**.

Table 1. Cholinesterase inhibitory activities of the target compounds

| <div style="display: flex; justify-content: space-around; align-items: center;"> <div style="text-align: center;">  <p>4a-4t</p> </div> <div style="text-align: center;">  <p>7a & 7b</p> </div> <div style="text-align: center;">  <p>10a-10g</p> </div> </div> | | | | |
|---|----------|--------------------------------------|------------------|------------------------|
| Compd | R | <i>h</i> AChE IC_{50}^a (μ M) | <i>eq</i> BChE | |
| | | | % inhibition | IC_{50}^a (μ M) |
| 4a | 2-methyl | 16.27 ± 0.62 | 36.82 ± 1.10 | nd |
| 4b | 3-methyl | 18.91 ± 0.17 | 36.12 ± 0.22 | nd |
| 4c | 4-methyl | 12.62 ± 0.05 | 35.60 ± 0.84 | nd |

| | | | | |
|------------------------|-----------------|--------------|--------------|--------------|
| 4d | 2-methoxy | 5.75 ± 0.24 | 43.33 ± 1.37 | nd |
| 4e | 3-methoxy | 2.42 ± 0.32 | 55.38 ± 0.17 | 15.29 ± 0.14 |
| 4f | 4-methoxy | 17.29 ± 0.07 | 49.85 ± 0.06 | 19.54 ± 0.01 |
| 4g | 2-chloro | 5.72 ± 0.03 | 47.36 ± 0.33 | nd |
| 4h | 3-chloro | 5.68 ± 0.04 | 48.54 ± 1.29 | nd |
| 4i | 4-chloro | 3.43 ± 0.03 | 46.85 ± 0.14 | nd |
| 4j | 2-trifluoro | 15.15 ± 0.30 | 43.22 ± 0.10 | nd |
| 4k | 3-trifluoro | 9.31 ± 0.03 | 34.92 ± 0.05 | nd |
| 4l | 4-trifluoro | 8.23 ± 0.12 | 37.25 ± 0.07 | nd |
| 4m | 3-bromo | 13.07 ± 0.05 | 36.58 ± 0.42 | nd |
| 4n | 4-bromo | 10.24 ± 0.14 | 39.28 ± 0.14 | nd |
| 4o | 2-fluoro | 17.23 ± 0.06 | 31.86 ± 0.57 | nd |
| 4p | 3-fluoro | 22.12 ± 0.07 | 38.31 ± 1.54 | nd |
| 4q | 4-fluoro | 12.93 ± 0.40 | 42.25 ± 0.56 | nd |
| 4r | 3-cyano | 16.01 ± 0.35 | 31.58 ± 0.69 | nd |
| 4s | 4-cyano | 17.43 ± 0.07 | 35.67 ± 0.27 | nd |
| 4t | Hydrogen | 21.94 ± 0.81 | 38.25 ± 0.25 | nd |
| 7a | 5-aminoindolyl | 5.74 ± 0.13 | 58.66 ± 0.17 | 14.05 ± 0.10 |
| 7b | 6-aminoquinolyl | 4.89 ± 0.37 | 57.73 ± 0.21 | 14.32 ± 0.04 |
| 10a | Hydrogen | 29.34 ± 0.03 | 37.03 ± 0.41 | nd |
| 10b | 3-methoxy | 9.91 ± 0.07 | 26.89 ± 0.20 | nd |
| 10c | 4-fluoro | 11.04 ± 0.06 | 27.66 ± 0.39 | nd |
| 10d | 3-nitro | 23.43 ± 1.98 | 37.92 ± 0.57 | nd |
| 10e | 4-methoxy | 12.05 ± 1.14 | 44.71 ± 0.05 | nd |
| 10f | 4-chloro | 11.15 ± 0.13 | 33.24 ± 1.56 | nd |
| 10g | 4-methyl | 19.48 ± 0.12 | 38.14 ± 0.12 | nd |
| FA^c | ----- | n.a. | 19.73 ± 0.91 | nd |
| DPZ^d | ----- | 0.03 ± 0.07 | 65.68 ± 0.01 | 2.89 ± 0.02 |

^aIC₅₀ = 50% inhibitory concentration (means ± SD of 2 to 3 independent experiments)

^bInhibition was determined at 20 μM inhibitor concentration (in triplicate)

^cFA (Ferulic acid) = used as negative control

^dDPZ (Donepezil) = used as positive control

n.a.: less than 10% inhibition at 20 μM

nd: not determined

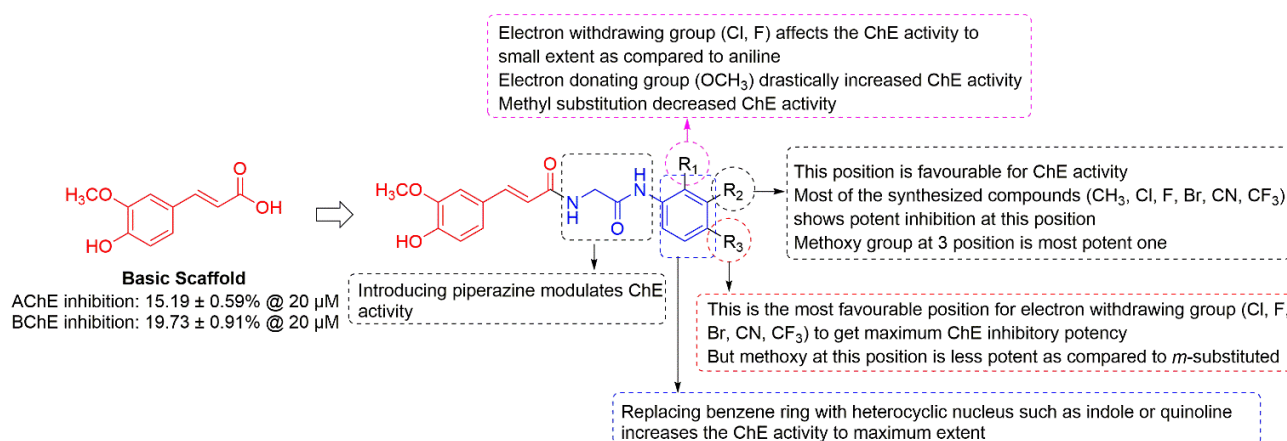


Fig. 5. Structural optimization and a brief summary of SAR with **FA** analogs.

2.3. AChE/BChE inhibition kinetic studies

On the basis of ChE inhibitory studies, lead compound **7a** was selected for AChE and BChE inhibition kinetics studies. Three fixed concentrations of the inhibitor **7a** were selected for this study and for each concentration, the velocity $[V]$ of the substrate hydrolysis was measured at six different substrate $[S]$ concentrations. For each inhibitor concentration, the reciprocal of the initial velocity ($1/[V]$) was plotted with respect to the reciprocal of the substrate concentration ($1/[S]$). As described in **Figure 6A & 6B**, the double reciprocal (Lineweaver–Burk) plot showed a non-competitive inhibition pattern for compound **7a** in the case of AChE, and mixed type inhibition in the case of BChE.

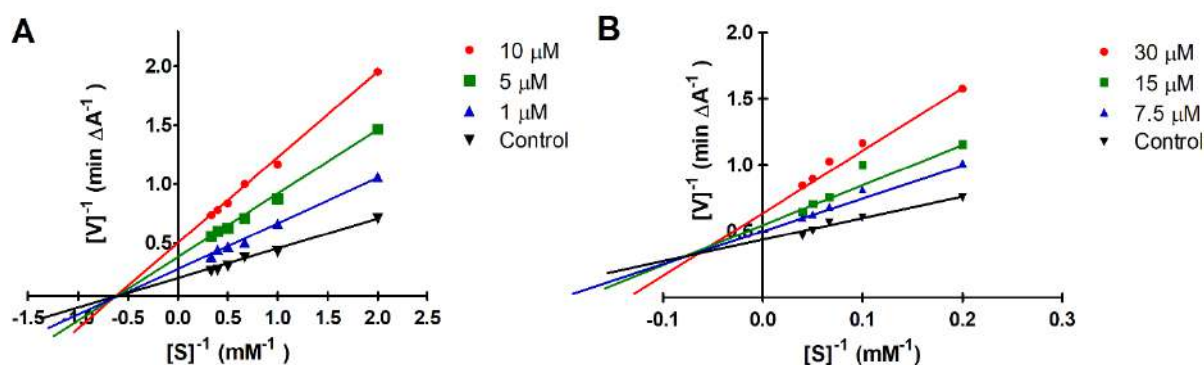


Fig. 6. Kinetics study on the mechanism of ChE inhibition by compound **7a**. **(A)** Overlaid Lineweaver–Burk reciprocal plots based on the *hAChE* initial velocity at increasing substrate concentration (0.5–3.0 mM) in the absence or presence of **7a** (1, 5, and 10 μM) are shown.

[S] = concentration of acetylthiocholine; [V] = initial velocity rate. **(B)** Merged Lineweaver–Burk reciprocal plots of eqBChE initial velocity with increasing substrate concentration (5, 10, 15, 20 and 25 mM) in the absence or presence of **7a** (7.5, 15 and 30 μ M) [S] = concentration of butyrylthiocholine; [V] = initial velocity rate. Lines were derived from a weighted least-squares analysis of data points. The experimental data are the means \pm SD of two independent experiments.

2.4. Measurement of propidium iodide displacement from the peripheral anionic site (PAS) of AChE

Enzyme kinetics study indicated that **7a** is a noncompetitive inhibitor of hAChE. To further gain insight and to assess whether **7a** has an affinity towards the PAS of AChE, a propidium iodide displacement assay was designed and performed. Propidium iodide is a specific ligand for the peripheral site of AChE that exhibits a 10-fold higher fluorescence when bound to AChE [39]. The decrease in the propidium iodide fluorescence in the presence of **7a** can be interpreted as propidium displacement from the PAS. **DPZ**, the marketed drug for AD, which is known to bind to the PAS site of the enzyme, served as a reference drug in this assay. The results obtained in this study clearly indicated that compound **7a** could effectively displace propidium iodide (9.06% to 28.53%) in comparison to **FA** 0.12 to 8.65% (**Table 2**). The reference drug **DPZ** gave 10.14% to 30.88% of propidium iodide displacement in this assay.

Table 2. Displacement of propidium iodide from the peripheral anionic site of AChE by **7a**, **FA** and **DPZ** at the indicated concentrations.

| | 5 μ M | 10 μ M | 20 μ M | 50 μ M |
|------------|------------------|------------------|------------------|------------------|
| 7a | 9.06 \pm 0.16 | 11.78 \pm 2.17 | 18.47 \pm 0.55 | 28.53 \pm 0.18 |
| FA | 0.12 \pm 0.35 | 2.22 \pm 0.37 | 5.10 \pm 0.19 | 8.65 \pm 0.25 |
| DPZ | 10.14 \pm 0.24 | 13.95 \pm 0.25 | 21.65 \pm 0.35 | 30.88 \pm 0.53 |

^aResults are the mean \pm SEM for two independent experiments.

2.5. Evaluation of antioxidant activity

Oxidative stress plays a major role in the progression of AD by the generation of excess reactive oxygen species (ROS) which impair multiple cellular functions including causing loss

of synaptic activity and finally can lead to neurodegeneration [40]. Thus, the reduction of oxidative stress is an important aspect of designing a new drug candidate for AD. **FA** probably exerts its antioxidant effect through free radical scavenging activity by transferring a hydrogen atom to its substrate [41]. The molecules exhibiting promising cholinergic inhibition were subjected to this study. The antioxidant property of the synthesized molecules **4e**, **4f**, **4h**, **4i**, **7a**, **7b**, and **10b** was evaluated by the 2,2-diphenyl-1-picrylhydrazyl (DPPH) method and compared with that of the parent molecule **FA**. Antioxidant activity is expressed as IC_{50} value, defined as the concentration of an antioxidant species required for a reduction of 50% of the DPPH radical concentration in a solution. All of the tested compounds demonstrated moderate antioxidant activity compared to **FA** (**Figure 7**, **Table 3**). We hypothesize that loss in the free radical quenching ability of the majority of the developed molecules compared to **FA** is probably due to the absence of the free acid functional group. It is noteworthy that we could compensate for this loss in the antioxidant property of developed analogs in the indole-bearing molecule **7a** and the piperazine derivative **10b**. The proposed mechanism for free radical quenching is shown in **Figure 8**. The free acid group on **FA** was found to be crucial to the radical scavenging ability. The compounds **7a** and **10b** presented moderate antioxidant activity, with IC_{50} of 57.35 ± 0.27 and 61.98 ± 0.30 μ M, respectively (**Table 3**).

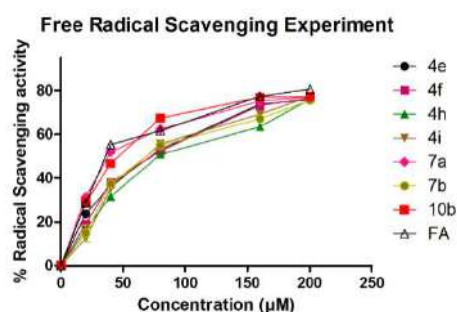


Fig. 7. Percent radical scavenging activity of **4e**, **4f**, **4h**, **4i**, **7a**, **7b**, **10b** and **ferulic acid (FA)**. Each point represents a value from the experiment done in triplicate and is expressed as the mean \pm SEM.

Table 3. Antioxidant activity (DPPH assay) of **4e**, **4f**, **4h**, **4i**, **7a**, **10b**, and **FA**

| Compound | Antioxidant activity (DPPH assay) | |
|-----------|-----------------------------------|-----------------------------------|
| | % Radical scavenging ^a | IC_{50} ^b (μ M) |
| 4e | 19.06 ± 0.20 | 94.29 ± 0.19 |

| | | |
|-----------------------|--------------|---------------|
| 4f | 23.64 ± 0.07 | 91.24 ± 0.61 |
| 4h | 12.66 ± 0.92 | 107.73 ± 0.93 |
| 4i | 16.66 ± 0.08 | 101.21 ± 0.85 |
| 7a | 31.33 ± 0.14 | 57.35 ± 0.27 |
| 7b | 18.59 ± 0.12 | 77.61 ± 0.58 |
| 10b | 28.82 ± 0.18 | 61.98 ± 0.30 |
| FA^c | 28.56 ± 0.02 | 56.49 ± 0.62 |

^aAll the values were obtained at a compound concentration of 20 μ M

^bIC₅₀: 50% inhibitory concentration (mean \pm SD of three experiments)

^cFA (ferulic acid) = used as a negative control

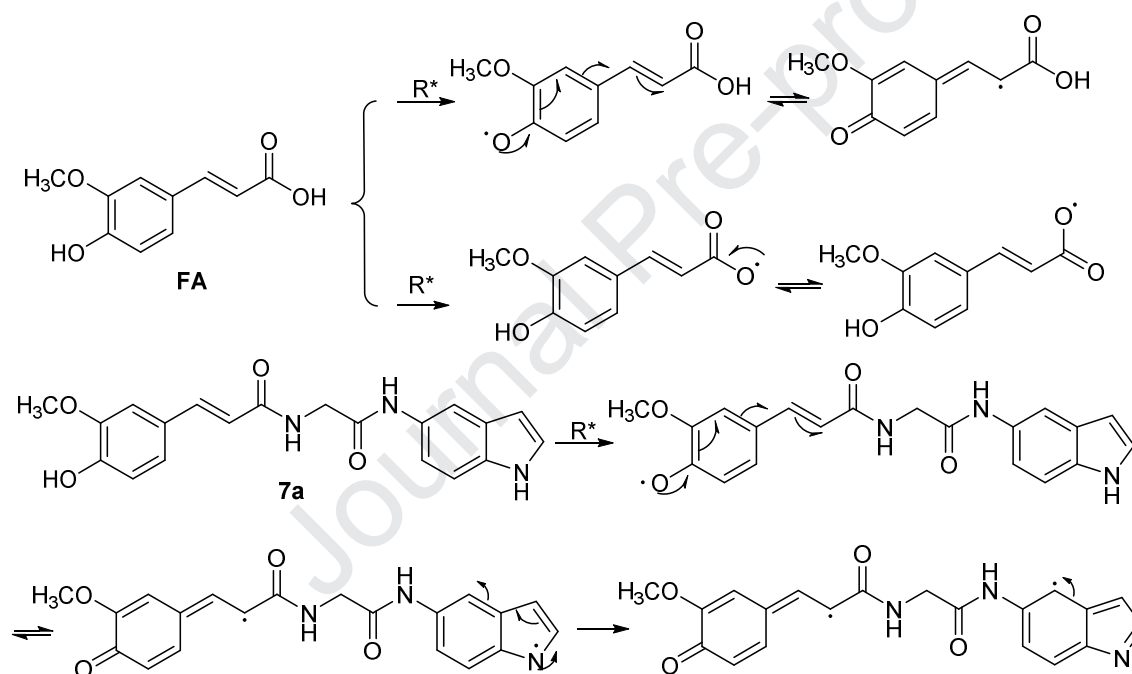


Fig. 8. Proposed mechanism of **FA** and **7a** radical scavenging activity.

2.6. Evaluation of iron chelation property of novel compounds

Oxidative stress, metal dyshomeostasis, and aging are presumably the common factors that play a major role in the onset of AD [42]. It has been shown in the literature that metal-derived ROS, especially those from iron and copper, are the major culprits responsible for the inhibition of mitochondrial respiration and the promotion of A β aggregation in the form of intracellular neurofibrillary plaques and tangles [43]. Given the fact that metals play a critical role in AD, metal chelating therapy is under investigation to see if it can be used to develop

disease-modifying agents. The metal chelation property of natural products depends on their chemical structure, including the number of electron-donating groups they contain and their position (Supporting Information, Figure S4). Therefore, the most potent compounds **4e** and **7a** were investigated for their metal chelating property by UV-vis spectroscopy with wavelengths ranging from 200 to 700 nm. In **Figure 9A & 9B**, UV-vis spectra of **7a** and **4e** with increasing Fe^{3+} concentration are shown. The absorbance peaks of **7a** and **4e** shifted from 306.5 to 446 nm, and in case of **4e** new peaks were observed at 454 and 620.5 nm, respectively. The increased absorbance indicated that there was an interaction between Fe^{3+} and compounds **4e** and **7a** (Supporting Information, Figure S5).

To further confirm the complex formation, MS-MS analysis of the solutions used in the UV analysis was carried out. As shown in **Figure 9C** the presence of molecular ion peaks corresponding to **7a-Fe³⁺** ($m/z = 420.35$ and 421.23) clearly demonstrated the metal chelating ability of **7a**. Interestingly, the appearance of peaks at $m/z = 411.35$ and 413.25 in the MS-MS spectrum of **4e-Fe³⁺** clearly indicated interaction of **4e** with Fe^{3+} (**Figure 9D**). These results supported the pH-dependent UV-vis spectroscopy metal complexation study.

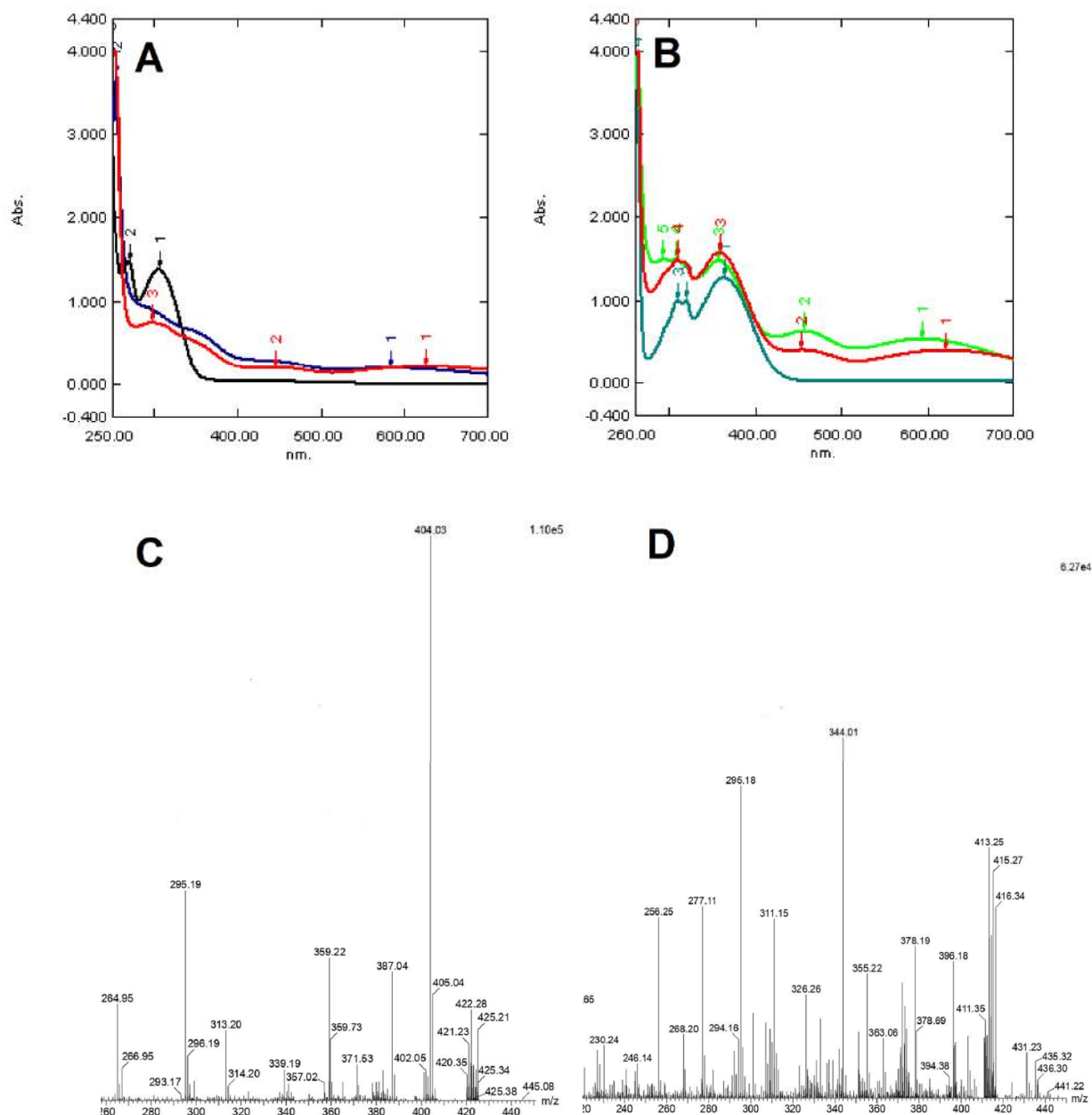


Fig. 9. UV absorbance spectrum of compounds **7a** and **4e** alone and in the presence of FeCl_3 in water at various pH. (A) **7a** alone (300 μ M) (black), **7a** (600 μ M) + FeCl_3 (600 μ M) at pH 4.2 (red) and **7a** (600 μ M) + FeCl_3 (600 μ M) at pH 7.4 (blue). (B) **4e** (300 μ M) (dark gray), **4e** (600 μ M) + FeCl_3 (600 μ M) at pH 4.2 (red) and **4e** (600 μ M) + FeCl_3 (600 μ M) at pH 7.4 (green). (C) Molecular ion peaks of complex formed from **7a** and FeCl_3 at pH 7.4. Peaks at m/z 420.35 and 421.23 correspond to **7a**- Fe^{3+} complex with 1:1 stoichiometry. (D) Molecular

ion peaks of complexes formed from **4e** and FeCl_3 at pH 7.4. Peaks at m/z 411.35 and 413.25 correspond to **4e**– Fe^{3+} complex with 1:1 stoichiometry.

2.7. Evaluation of $\text{A}\beta_{1-42}$ aggregation modulation activity of **7a**

AD is mainly associated with the deposition of self-aggregating $\text{A}\beta$ peptide. The accumulation of $\text{A}\beta_{1-42}$ induces the formation of toxic $\text{A}\beta$ oligomers and fibrils, which cause the impairment of synapses and neurons [44]. $\text{A}\beta_{1-42}$ aggregates were generated with a goal to evaluate the effect of the lead molecule on the aggregation process. In this experiment, $\text{A}\beta_{1-42}$ aggregates were formed to yield aggregated structures that were detected by atomic force microscopy (AFM). To achieve this, we incubated $\text{A}\beta_{1-42}$ ($0.39\ \mu\text{M}$) with mechanical shaking for 20 days. The main objective of this experiment was to find out the time point at which $\text{A}\beta_{1-42}$ monomers get converted into aggregated structures. The AFM image analysis (**Figure 10C & 10D**) revealed the aggregates generated at 10 days had clearly formed fibril structures and were different from the samples on day 20 (**Figure 10E & 10F**). The control sample $\text{A}\beta_{1-42}$ ($0.39\ \mu\text{M}$) at 10 days showed the presence of fibril structures bigger in size compared to protein alone at $t = 0$ (**Figure 10A & 10B**) and only a few characteristic monomer structures were observed in the sample of $\text{A}\beta_{1-42}$. We selected $t = 10$ days incubation time for further studies. Based on the enzyme inhibition studies and antioxidant property evaluation, **7a** was selected as the lead molecule to monitor the $\text{A}\beta_{1-42}$ aggregation modulation property. The reference drug **DPZ** and **FA** were also incubated with $\text{A}\beta_{1-42}$ for comparison. AFM images demonstrated the absence of a significant amount of fibril $\text{A}\beta$ samples incubated in the presence of **7a** (**Figure 10G & 10H**) and **FA** (**Figure 10I & 10J**). $\text{A}\beta_{1-42}$ incubated in the presence of **DPZ** exhibited distinct morphology (**Figure 10K & 10L**) compared to **7a**- or **FA**-treated samples. These results clearly indicate the potential interaction between **7a** and $\text{A}\beta_{1-42}$, which would thereby modulate the formation of $\text{A}\beta_{1-42}$ aggregates. The reference drug **DPZ** failed to confer significant structural changes in the aggregated form of $\text{A}\beta_{1-42}$, compared to **7a** or **FA**.

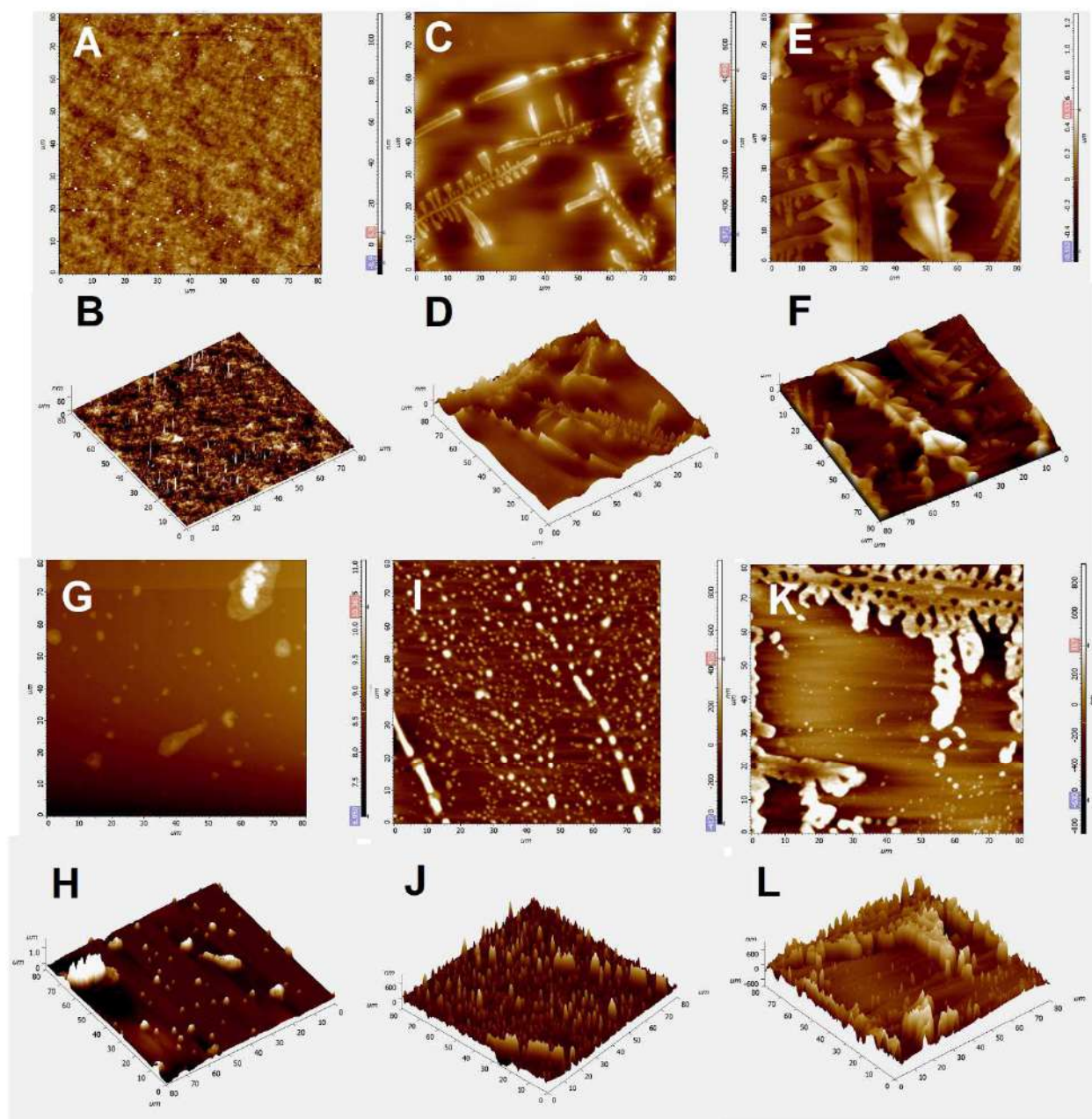


Fig. 10. Inhibition of self-induced $A\beta_{1-42}$ aggregation in the presence of **7a**, **FA** and **DPZ**. (AFM images). (**A&B**) Fresh $A\beta_{1-42}$ at $t = 0$ ($0.39 \mu\text{M}$). (**C&D**) $A\beta_{1-42}$ alone ($0.39 \mu\text{M}$) after 10 days of shaking at 37°C . (**E&F**) $A\beta_{1-42}$ alone ($0.39 \mu\text{M}$) after 20 days of shaking at 37°C . (**G&H**) $A\beta_{1-42}$ ($0.79 \mu\text{M}$) + **7a** ($1.58 \mu\text{M}$) after 10 days of shaking at 37°C . (**I&J**) $A\beta_{1-42}$ ($0.79 \mu\text{M}$) + **FA** ($1.58 \mu\text{M}$) after 10 days of shaking at 37°C . (**K&L**) $A\beta_{1-42}$ ($0.79 \mu\text{M}$) + **DPZ** ($1.58 \mu\text{M}$) after 10 days of shaking at 37°C .

2.8. Molecular docking study

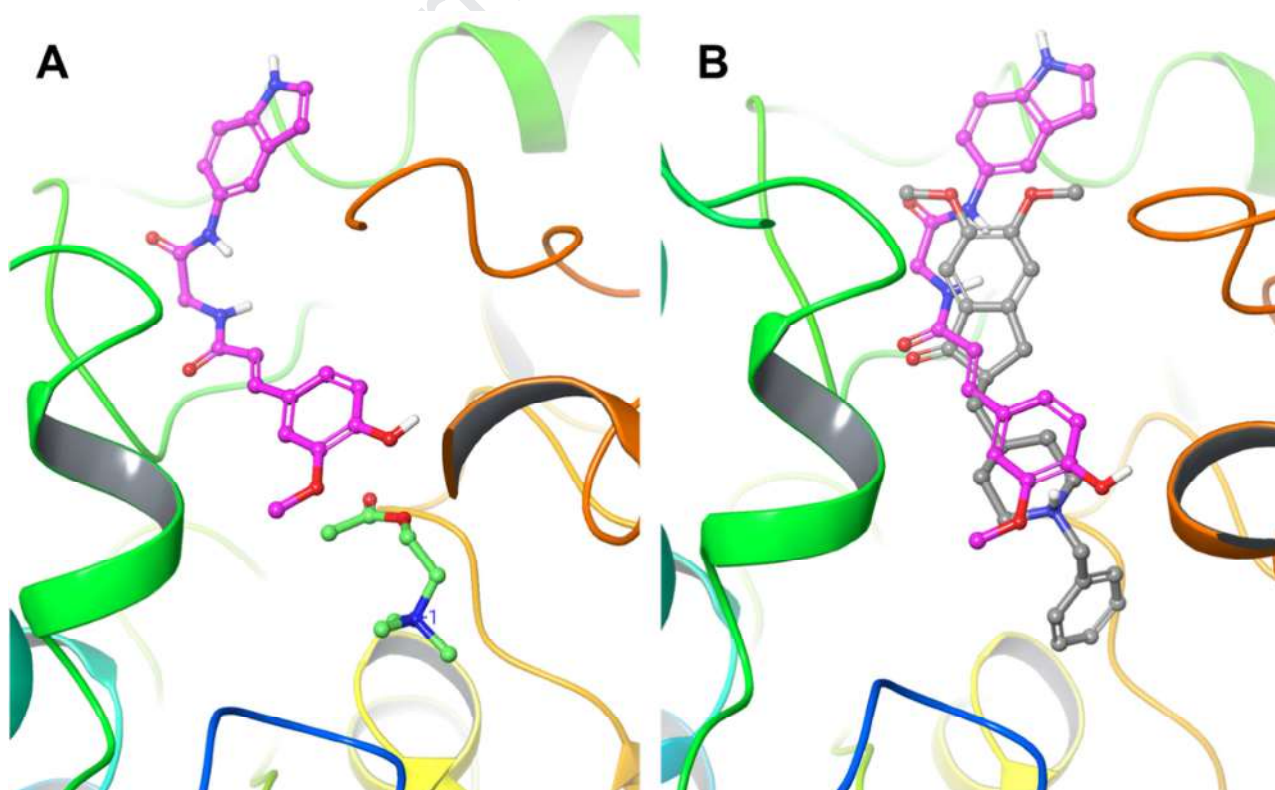
To investigate the binding mode of the compounds with their AChE (**PDB ID: 4EY7**) and BChE (**PDB ID: 4BDS**), molecular docking of the most potent compounds among ferulic acid and its analogs was performed using the Schrödinger software. The binding free-energies of the best complex of potent compounds were calculated using the Prime MM-GBSA module implemented in the Schrödinger software. The docking poses of the most potent compounds, **4e** and **7a** are presented in **Figure 4**. As mentioned in **Figure 4A**, compound **4e** formed two hydrogen bonds with Tyr124, Arg296, and two π - π stacks with Tyr337 and Phe338, resulting in its good inhibitory activity against AChE. However, in the case of BChE, **4e** formed only one hydrogen bond and one π - π stack with Leu286 and Phe329. This might be the reason for the reduced potency of **4e** against BChE (**Figure 4C**). As depicted in **Figure 4B**, in the case of **7a**, we observed binding at both the enzymatic catalytic active site (CAS) with Asp74, Tyr337, and Tyr341 and at the PAS with Trp286 and Phe295 (**Figure 4B**). This means that replacing the phenyl with indole could intensify AChE inhibitory activity. Further, in the case of BChE, **7a** formed three π - π stacks with Trp82, Trp321, Phe329, and hydrogen bonds with Glu197 and Tyr332. The docking scores and Prime MM-GBSA free energies of ferulic acid and its analogs are shown in Table 4.

Table 4. Docking scores and Prime MM-GBSA free energies of ferulic acid and its analog against AChE and BuChE.

| Compound | Glide GScores (kcal/mol) | | Prime MM-GBSA Free Energies (kcal/mol) | |
|-----------|-----------------------------|--------|---|--------|
| | AChE | BChE | AChE | BChE |
| FA | -5.332 | -5.984 | -9.47 | -6.78 |
| 4e | -7.912 | -5.42 | -62.59 | -27.19 |
| 4i | -7.770 | ND | -42.68 | ND |
| 4b | -6.555 | ND | -40.66 | ND |
| 4m | -6.925 | ND | -36.09 | ND |
| 7a | -7.358 (pose1) | -6.261 | -40.28 (pose 1) | -43.29 |
| | -8.016 (pose2) | | -34.70 (pose 2) | |

| | | | | |
|------------------|---------|--------|--------|--------|
| 7b | -7.105 | -6.622 | -44.44 | -57.37 |
| 10b | -8.462 | ND | -50.80 | ND |
| Donepezil | -13.208 | -7.386 | -77.01 | -54.47 |

The double reciprocal plot (Lineweaver–Burk) of enzyme kinetic inhibition showed a non-competitive inhibition pattern for compound **7a**. So, we aligned the X-ray crystal structure of mouse acetylcholinesterase complex with acetylcholine (**PDB ID: 2HA4**) (% identity with **4EY7** = 87 and % similarity = 92) and our docked complex of **7a** with AChE, manually shifted acetylcholine to the **7a–AChE** complex, and energy minimized the complex using the Prime minimization module of Schrödinger [45]. Interestingly, we found that acetylcholine can still be accommodated in the active site of AChE in the presence of **7a** (**Figure 11A**), which supports the non-competitive inhibition nature of **7a**. In addition, we also overlaid the docked pose of **7a** with **DPZ**, the co-crystallized ligand in the X-ray crystal structure of **4EY7**, and found that the **7a** indole moiety slightly shifted towards the PAS site, but most of the remaining part of **7a** overlapped with the **DPZ** pose (**Figure 11B**). Our finding matches well with the results of the propidium iodide displacement assay in which **7a** displaced propidium



iodide from the

Fig. 11. (A) Docked pose of **7a** (C in magenta) and acetylcholine (C in green) into the active site of AChE. (B) Overlaid docked pose of **7a** (C in magenta) and **DPZ** (C in grey) into the active site of AChE.

peripheral anionic site (PAS) of AChE (cf. section on measurement of propidium iodide displacement from the peripheral anionic site (PAS) of AChE).

2.9. Molecular dynamics (MD) simulations studies with AChE

In an effort to gain a better understanding of the interaction profile and mode of interactions between **7a** with AChE, we proceeded to do molecular dynamics (MD) simulations. MD is an important computational tool to check the thermodynamic stability of docked compounds [46]. We have selected the best docked ligand **7a** for the MD simulations. The MD simulations were performed for 30 ns, and the overall stability of the simulation was evaluated using the root mean square deviations (RMSD) of the backbone atoms, which ranged from 0.2 to 1.7 Å (**Figure 12A**). The graph suggests that the RMSD of the protein backbone is stable over the period of the MD simulation and attains equilibrium within 5 ns. The ligand root mean square fluctuation (L-RMSF) profile indicated ligand fragments interact with the protein and play an entropic role in the binding event (**Figure 12B**). In the graphical snapshot of the binding pattern shown in **Figure 12C**, the amide (NH), ferulic acid (OH) and indole (NH) of compound **7a** interact with the water molecules, playing a crucial role in the formation of hydrogen bonds with the amino acid residues Arg296, Ser293, Asp74, and Leu289. The stacked bar diagram indicates the normal interactions over the course of the MD simulations (**Figure 12D**). The stacked bar chart showed four types of ligand-protein interactions including H-bonding, hydrophobic interactions, ionic, and water bridge.

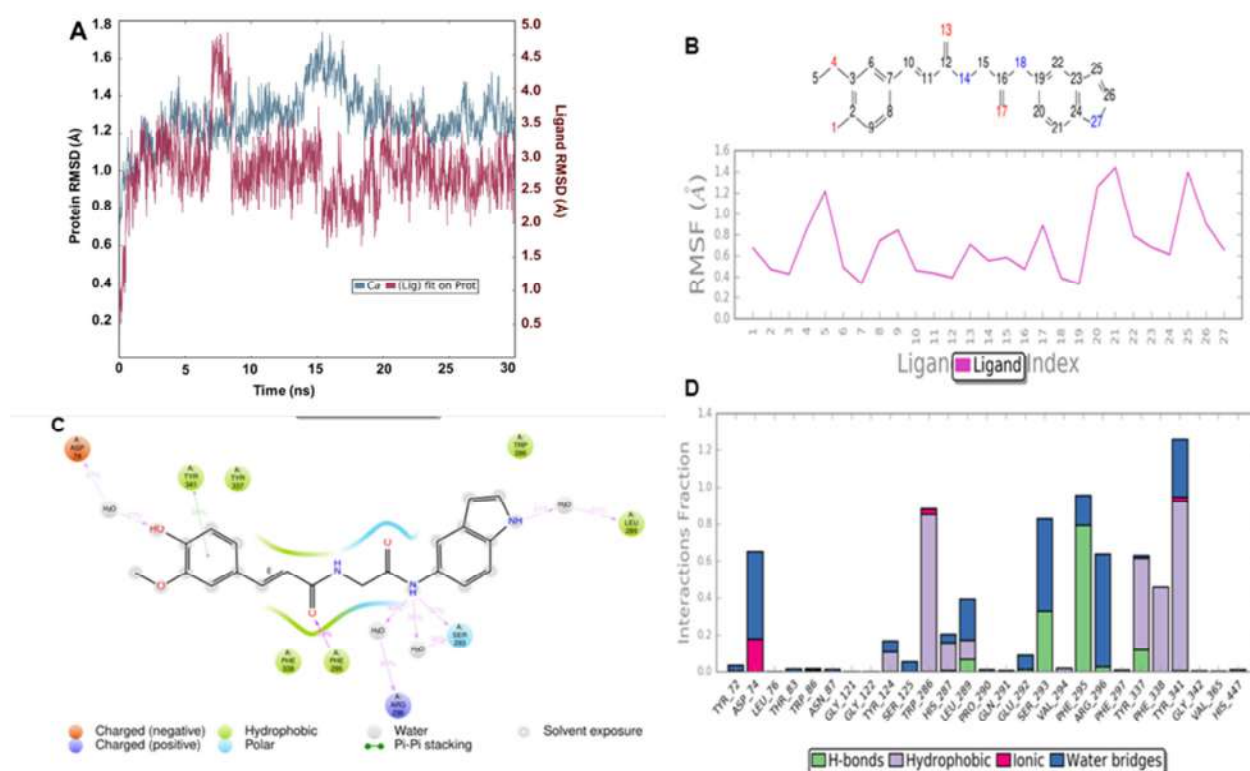


Fig. 12. (A) Protein-ligand RMSD. RMSD protein (left Y-axis); the ligand RMSD (right Y-axis) indicates the stability of ligand **7a** with respect to the protein and its active pocket. (B) Ligand Root Mean Square Fluctuation (L-RMSF). (C) A schematic of detailed **7a** atom interactions with the key amino acid residues. (D) Bar charts of protein interaction with ligand **7a** as monitored throughout the simulation (Green- H-bonding; Gray-Hydrophobic; Blue- Water bridges; Pink- Ionic interactions).

2.10. Molecular dynamics (MD) simulation studies with BChE

Since compound **7a** is active against both AChE and BChE, therefore, we also performed a 30 ns simulation for **7a** with the BChE complex. We used similar settings and protocols for the MD simulation as we used for **7a** with the AChE complex.

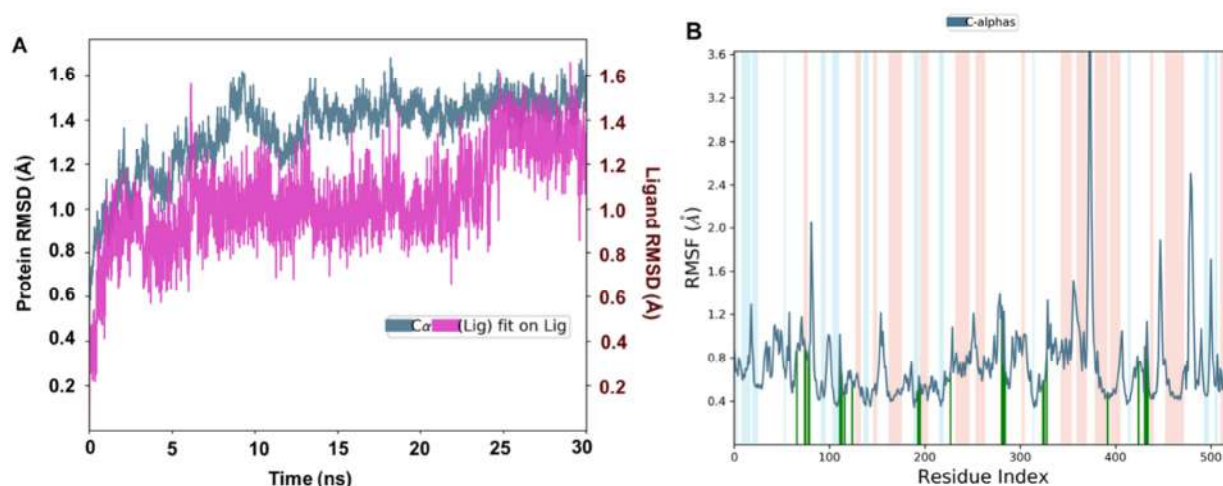


Fig. 13. (A) Protein RMSD (left Y-axis) and ligand RMSD (right Y-axis) indicate the stability of the ligand **7a** with respect to BChE and its active pocket. (B) RMSF plot based on C α atoms of BChE for the BChE–**7a** complex. Protein residues that interact with **7a** are marked with green vertical bars. Alpha-helical and beta-strand regions are highlighted in pink and blue backgrounds, respectively.

The RMSD plot of atom location vs. simulation time (**Figure 13A**) indicated that the protein (BChE) and **7a** attained a significantly stable state that was well maintained throughout the final 20 ns of the simulations. The RMSF plot (**Figure 13B**) based on C α atoms of BChE also showed very low fluctuation in the residues that form the ligand-binding site. The simulation interaction histogram (**Figure 14**) and 2D contact map (Supporting Information, Figure S6) showed that Gly115, Tyr128 (water-mediated H-bonding, ~60% contributions), Glu197 (H-bonding with carbonyl, 62% contribution), Trp231 (π - π stacking with indole moiety, 41% contribution), Leu286 (H-bonding with indole N-H, 74% contribution), Ala328 (H-bonding with phenolic hydroxyl, 81% contribution), and Phe329 (π - π stacking with indole moiety, 95% contribution) were the key residues for interactions with **7a** during the course of the simulation. Overall, **7a** maintained strong and stable interactions with BChE during the 30 ns of MD simulation.

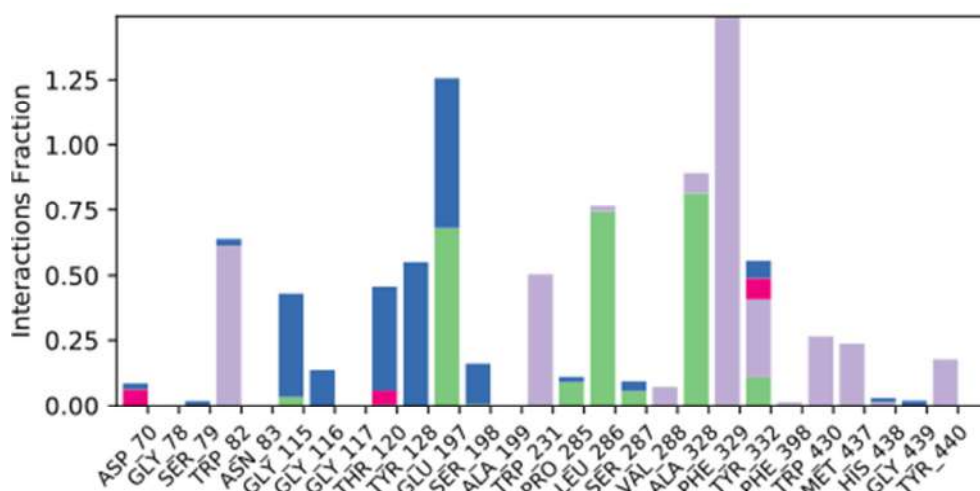


Fig. 14. The SID plot showing the protein-ligand interactions between the amino acid residues of the BChE binding site and **7a**. The stacked bar charts are categorized as follows: hydrogen bonding (green), hydrophobic interactions (violet), water bridges formed (blue) and ionic interactions (pink).

2.11. Calculation of physicochemical parameters and ADMET prediction

We used admetSAR and ChemDraw Professional 15.0 software to assess whether our synthesized series of compounds possess the correct parameters to exhibit drug-likeness or not. Compounds that fail the drug-likeness criteria often do not meet the requirements to be an effective clinical candidate due to excessive toxicity, poor bioavailability or other concerns [47]. We used admetSAR server to predict molecular descriptors such as lipophilicity (LogP), topological polar surface area (TPSA), molecular weight (MW), number of hydrogen bond donors (HBD) and hydrogen bond acceptors (HBA), number of rotatable bonds (RB), blood-brain barrier permeability (BBB) and Caco2 permeability (**Table 5**) [48]. According to Lipinski's Rule of Five, a compound is said to be membrane permeable if it matches the following criteria: (a) lipophilicity ≤ 5 , (b) molecular weight < 500 , (c) HBD ≤ 5 (OH and NH groups), (d) HBA ≤ 10 (N and O atoms). Compounds violating more than one of these rules could have problems related to bioavailability. All the synthesized compounds follow Lipinski's rule and exhibited significant brain permeability (**Table 5**).

Table 5. Physical properties and ADMET prediction of the compounds.

| Comp. | Mol.Wt. [†] | logP ^a | TPSA ^b | HBA ^c | HBD ^d | RBs ^e | BBB ^f | Caco-2 |
|------------|----------------------|-------------------|-------------------|------------------|------------------|------------------|------------------|--------|
| 4a | 340.38 | 2.48 | 87.66 | 4 | 3 | 6 | + | - |
| 4b | 340.38 | 2.48 | 87.66 | 4 | 3 | 6 | + | - |
| 4c | 340.38 | 2.48 | 87.66 | 4 | 3 | 6 | + | - |
| 4d | 356.38 | 2.18 | 96.89 | 5 | 3 | 7 | + | - |
| 4e | 356.38 | 2.18 | 96.89 | 5 | 3 | 7 | + | - |
| 4f | 356.38 | 2.18 | 96.89 | 5 | 3 | 7 | + | - |
| 4g | 360.79 | 2.82 | 87.66 | 4 | 3 | 6 | + | - |
| 4h | 360.79 | 2.82 | 87.66 | 5 | 3 | 7 | + | - |
| 4i | 360.79 | 2.82 | 87.66 | 5 | 3 | 7 | + | - |
| 4j | 394.11 | 3.19 | 87.66 | 4 | 3 | 6 | + | - |
| 4k | 394.35 | 3.19 | 87.66 | 4 | 3 | 6 | + | - |
| 4l | 394.35 | 3.19 | 87.66 | 4 | 3 | 6 | + | - |
| 4m | 404.25 | 2.93 | 87.66 | 4 | 3 | 6 | + | - |
| 4n | 404.25 | 2.93 | 87.66 | 4 | 3 | 6 | + | - |
| 4o | 344.34 | 2.31 | 87.66 | 4 | 3 | 6 | + | - |
| 4p | 344.34 | 2.31 | 87.66 | 4 | 3 | 6 | + | - |
| 4q | 344.34 | 2.31 | 87.66 | 4 | 3 | 6 | + | - |
| 4r | 351.36 | 2.04 | 111.45 | 5 | 3 | 6 | + | - |
| 4s | 351.36 | 2.04 | 111.45 | 5 | 3 | 6 | + | - |
| 4t | 326.35 | 2.17 | 87.66 | 4 | 3 | 6 | + | - |
| 7a | 365.39 | 2.65 | 99.69 | 4 | 4 | 6 | + | - |
| 7b | 377.40 | 2.72 | 100.02 | 5 | 3 | 6 | + | - |
| 10a | 338.41 | 2.76 | 53.01 | 4 | 1 | 4 | + | - |
| 10b | 368.43 | 2.77 | 62.24 | 5 | 1 | 5 | + | - |
| 10c | 356.40 | 2.90 | 53.01 | 4 | 1 | 4 | + | - |
| 10d | 383.40 | 2.67 | 104.82 | 6 | 1 | 5 | + | - |
| 10e | 368.43 | 2.77 | 62.24 | 5 | 1 | 5 | + | - |
| 10f | 372.85 | 3.62 | 53.0 | 5 | 1 | 4 | + | - |
| 10g | 352.43 | 3.39 | 53.0 | 5 | 1 | 4 | + | - |
| FA | 194.19 | 1.50 | 66.76 | 3 | 2 | 3 | + | - |
| DPZ | 379.50 | 4.36 | 111.45 | 4 | 0 | 6 | + | + |

All values were calculated using online software admetSAR except TPSA (ChemDraw).

[†] Daltons

^a Calculated logarithm of the octanol-water partition coefficient, ^b Topological polar surface area

^c Hydrogen-bond acceptor, ^d Hydrogen-bond donor, ^e Rotatable bonds, ^f Blood brain barrier

2.12. Evaluation of cytotoxicity of compound **7a**

The cytocompatibility, which is one of the important factors in the drug development process, was evaluated using the 3-(4,5-dimethylthiazol-2-yl)-2,5-diphenyltetrazolium

bromide (MTT) assay. The MTT assay is based on the reduction of MTT (yellow color) and other tetrazolium dyes and depends upon cellular metabolic activities due to NADPH dependent cellular oxidoreductase enzymes [49]. The healthy and fast-growing cells show increased reduction of MTT to formazan (purple color) and hence have higher absorbance, whereas the dead or inactive cells fail to do so.

The dose-dependent effect of **7a** on cell viability was carried out with SH-SY5Y cells, a widely used neuronal cell line. The cells were treated with different concentrations of **7a** and were quantitatively analyzed by the MTT-assay. As shown in **Figure 15**, **7a** showed cytocompatibility with SH-SY5Y cells at all the tested concentrations. At the highest tested concentration of **7a** i.e, 20 μM , 95.61% of cells were viable with 4.39% cytotoxicity as compared to control (100%) (**Figure 15**).

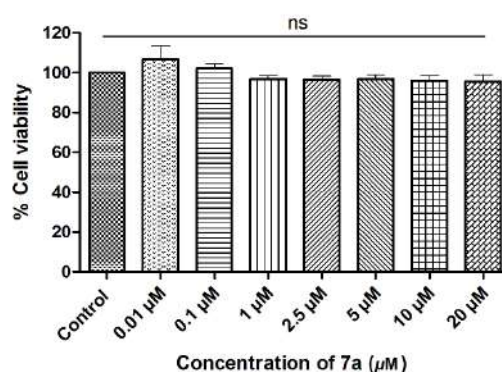


Fig. 15. Effect of **7a** on cell viability. Cells were treated with different concentrations of **7a** (20, 10, 5, 2.5, 1, 0.1 and 0.01 μM) for 24 hours. Cell percent viability was analyzed using the MTT assay. Data is represented as mean \pm SE of three independent experiments done in three replicates.

2.13. Acute toxicity studies

In-vivo acute toxicity and hepatotoxicity are two important criteria in the development of a compound as a new drug. Based on potent enzyme inhibitory activity and other multifunctional properties, compound **7a** was selected for acute toxicity and hepatotoxicity studies. The acute toxicity of compound **7a** was determined on healthy male Swiss albino mice (25-30 g), as per the OECD guidelines. From the first 4 h throughout 14 days after

administration of **7a**, no acute toxicity symptoms, such as death, abnormal behavior, changes in water or food consumption or weight loss (**Figure 16**) were observed. All animals were sacrificed on the 14th day after drug administration and microscopically examined for possible damage to the liver (**Figure 16**). The results showed that the animals treated with compound **7a** did not develop any sign of toxicity and well-tolerated **7a** at doses up to 500 mg/kg.

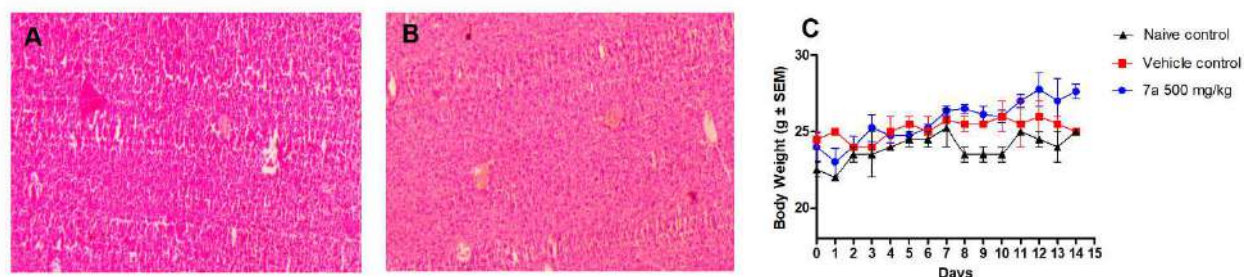


Fig. 16. Histomorphological appearance of liver of mice (A) no treatment (Naïve control); (B) **7a**, 500 mg/kg. (C) Mean daily body weight profile of each group of mice during the 14-day drug administration period.

2.14. Evaluation of in-vivo efficacy of **7a** in scopolamine-induced AD mice model

A learning and memory improvement experiment was performed using the Y maze involving daily p.o. administration of compound **7a** to mice suffering from learning and memory dysfunction [50]. Learning and memory impairment in mice can be produced by scopolamine-induced blockage of the muscarinic cholinergic receptor nerve terminals, which is a well-established animal model for AD [51]. The test compound (**7a**) was administered daily to healthy male Swiss albino mice at the dose of 6.25, 12.5 and 25 mg/kg, p.o., for 7 days and body weights were analyzed (**Figure 17A**).

On the 7th day, the Y maze experiment was performed to assess the spatial working memory in mice after intraperitoneal (3.0 mg/kg) administration of scopolamine hydrochloride. The animals were treated with **7a** or **FA** or **DPZ**, 30 min prior to scopolamine administration and spontaneous alterations were calculated 15 min after scopolamine treatment. A significant reduction in spontaneous alternation was observed in the scopolamine hydrochloride (3 mg/kg, i.p.) treated group compared to the vehicle control group, which indicated the development of amnesia in the mice (**Figure 17B**, *** $p < 0.001$). The **DPZ**

treated group (5.0 mg/kg, p.o.) showed significantly increased spontaneous alternations ($###p < 0.001$) compared to the scopolamine treated group. A similar result was observed with **7a** (6.25, 12.5 and 25 mg/kg), which showed statistically significant difference in % spontaneous alternations compared to scopolamine and **DPZ** treated group (**Figure 17B**, $###p < 0.001$ vs scopolamine, $\pi\pi p < 0.01$, $\pi p < 0.05$ vs **DPZ**, ns to **DPZ** in case of 6.25 mg/kg). On the other hand, **FA** (12.5 and 25 mg/kg) did not show any significant difference in spontaneous alternation compared to scopolamine (**Figure 17B**, $p = ns$). The mechanism of the spontaneous alternation stimulation in the scopolamine model is likely mediated by the anti-AChE activity of the compound **7a**, suggesting that **7a** is a potent cholinesterase inhibitor that can cross the blood-brain barrier effectively. The total arm entries (**Figure 17C**) remained unchanged in all treated groups, indicating that scopolamine did not affect the locomotor activity in mice. The overall results of the scopolamine-induced amnesia model suggested that **7a** showed significant potential for improving spatial and immediate memory in mice.

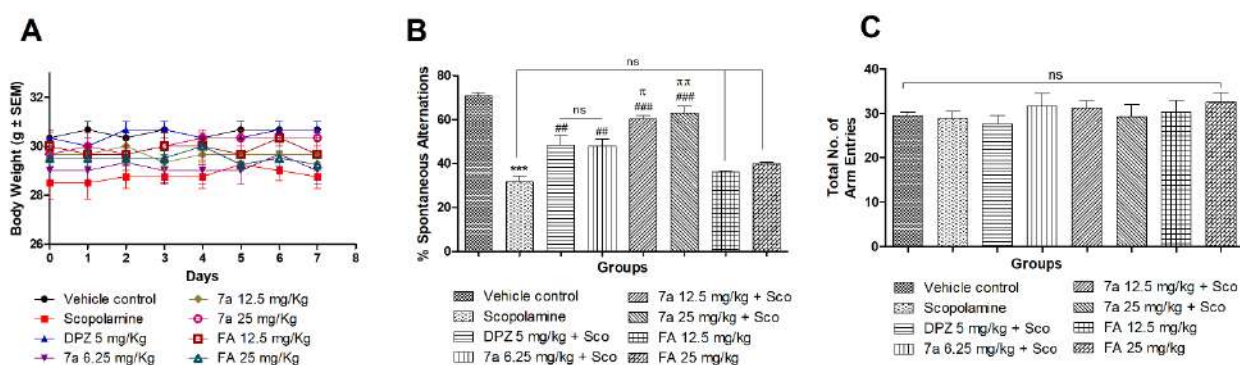


Fig. 17. Scopolamine-induced memory deficit in mice. **(A)** Mean daily bodyweight profile of each group of mice during the 7-day drug administration period. **(B)** Effect of **7a** on scopolamine-induced memory deficit in the Y-maze test. Compound **7a** (6.25, 12.5, and 25 mg/kg, p.o.), **FA** (12.5, and 25 mg/kg, p.o.), **DPZ** (5 mg/kg, p.o.) were given for 7 days. On the 7th day, the mice were treated with scopolamine (3 mg/kg, i.p.) and subjected to the Y-maze test after 15 min of scopolamine administration. **(C)** Number of arm entries in the Y-maze test. Data are expressed as the mean \pm SEM ($n = 5$), $***p < 0.001$ vs vehicle control; $###p < 0.001$, $##p < 0.01$ vs scopolamine; $\pi\pi p < 0.01$, $\pi p < 0.05$ vs **DPZ**; ns = nonsignificant (One-way ANOVA followed by Tukey's multiple comparison test).

2.15. Neurochemicals estimation and antioxidant property evaluation

To investigate levels of AChE, BChE and antioxidant effect of **7a**, *ex vivo* studies were performed with the treated animals. AChE and BChE levels in the brain were assessed by Ellman's colorimetric method with slight modifications. As described in **Figure 18A** and **18B**, scopolamine significantly elevates AChE (**Figure 18A**) and BChE (**Figure 18B**) levels compared to the vehicle control group, while **DPZ** and **7a** groups showed a significant reduction in elevated AChE and BChE levels (**Figure 18A** and **18B**). However, the non-significant difference was observed in elevated levels of AChE (**Figure 18A**) and BChE (**Figure 18B**) in the case of **FA** at 12.5 and 25 mg/kg. These findings suggest that **7a** significantly attenuates the cholinesterase levels in the brain, but **FA** is not able to reverse the scopolamine-induced increase in AChE and BChE levels. The *ex-vivo* antioxidant property of **7a** was estimated using various biochemical parameters such as superoxide dismutase (SOD), catalase (CAT) and malondialdehyde (MDA). SOD is an enzyme that protects cellular components from oxidation by ROS and eventually reduces cellular damage. It catalyzes the dismutation of the superoxide ($O_2^{\cdot -}$) radical into molecular oxygen (O_2) and hydrogen peroxide (H_2O_2). CAT is a common enzyme that catalyzes the decomposition of hydrogen peroxide (H_2O_2) to water and oxygen. MDA (a byproduct of lipid peroxidation) is a marker for oxidative stress. MDA undergoes condensation with thiobarbituric acid to give red fluorescence. As shown in **Figure 18c**, the scopolamine treated mice group showed a significant reduction in SOD levels. Interestingly, the SOD level was noticed to be significantly increased in **DPZ** (**Figure 18C**) treated animals. Treatment with the lead molecules **7a** and **FA** could effectively reverse the reduced level of SOD in scopolamine treated animals. Additionally, significant increases in catalase (CAT) activity in brain supernatant was observed in the **DPZ** (**Figure 18D**), **7a** and **FA** (**Figure 18D**) treatment group, while the MDA contents were correspondingly decreased in **DPZ** (**Figure 18D**), **7a** (**Figure 18D**) and **FA** (**Figure 18D**) compared to those of the scopolamine treated group. These findings collectively suggest the potent *in-vivo* ChE inhibitory and antioxidant activities of **7a**.

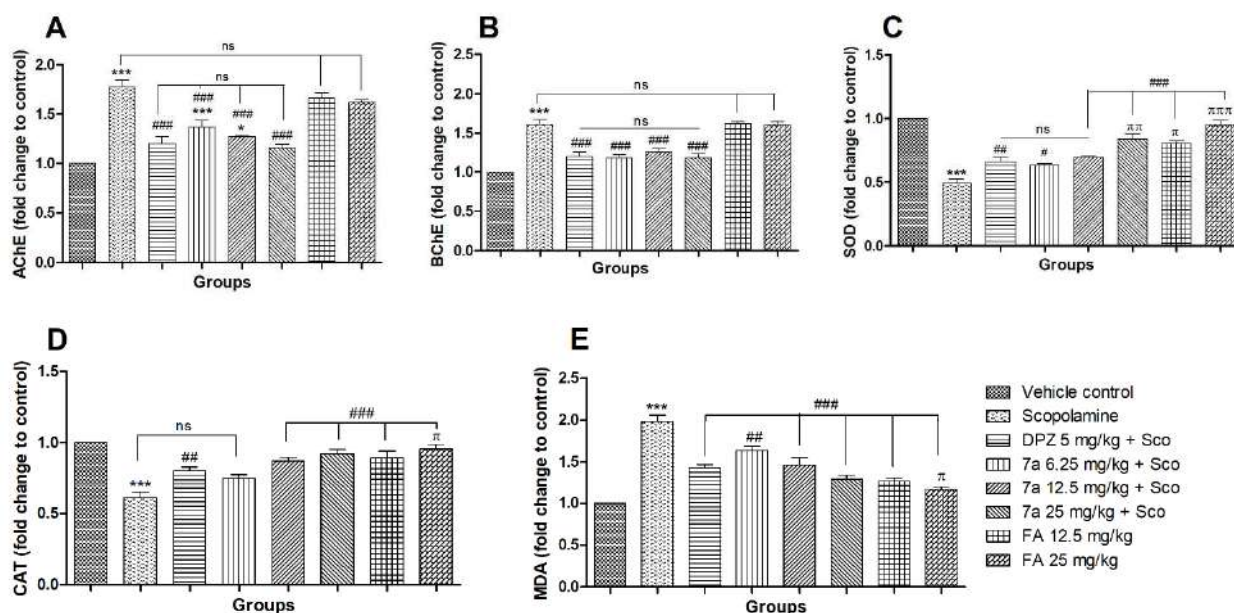


Fig. 18. The *ex-vivo* AChE, BChE and antioxidant effect of **DPZ** (5 mg/kg), compound **7a** (6.25, 12.5 and 25 mg/kg), **FA** (12.5, 25 mg/kg) and scopolamine (3 mg/kg). **(A)** Elevated AChE. **(B)** BChE levels by scopolamine treatment were significantly reduced by **7a**. **(C)** SOD (Fold change to vehicle control). **(D)** Catalase (CAT) (fold change to vehicle control). **(E)** MDA (fold change to vehicle control). Data are expressed as mean \pm SEM ($n = 5$), *** $p < 0.001$ vs vehicle control; ### $p < 0.001$, ## $p < 0.01$ and # $p < 0.05$ vs scopolamine group; $\pi\pi\pi p < 0.001$, $\pi\pi p < 0.01$, $\pi p < 0.05$ vs **DPZ**; ns = nonsignificant (One-way ANOVA followed by Tukey's multiple comparison test).

3. Conclusion

Based on the **FA** template, we designed and developed a novel series of glycine amide derivatives and related analogs as a part of our approach to developing naturally inspired multifunctional drugs for the management of AD. The rationale behind the design of the novel molecules is to have improved cholinergic inhibitory activities along with an increase in LogP of **FA** analogs. The introduction of an amide linker followed by an aromatic or substituted aromatic or heterocyclic or substituted piperazine feature leads to significant improvement in the enzyme's inhibition properties. The developed molecules were tested for *in-vitro* AChE and BChE inhibitory activities. Among the tested compounds, **4e**, **4i**, **7b**, **4h**, **7a**, and **4d**

showed the highest inhibitory activities for AChE. All the compounds were further evaluated for BChE. From among all the compounds, **7a**, **7b**, **4e**, and **4f** showed potent BChE inhibition property.

The molecular docking studies revealed that **7a** is able to bind to peripheral and catalytic sites and exposed the two different binding modes of **7a** with AChE. The stabilities of the best complexes between **7a** and AChE and BChE were confirmed with the help of MD studies. The calculated physicochemical properties and ADMET clearly demonstrated the druggable properties of the developed novel molecules. The data from the enzyme kinetic study proved that **7a** caused noncompetitive inhibition of AChE and mixed inhibition of BChE.

The lead molecule **7a** also exhibited significant antioxidant activity in the DPPH assay and iron-chelating property in the pH-dependent UV based complexation study and mass spectrometric analysis. Based on the enzyme inhibition and antioxidant studies, **7a** was selected as a lead molecule for further *in-vitro* and *in-vivo* studies. The data from the AFM analysis demonstrated **7a** is able to modulate aggregation of A β ₁₋₄₂. The results from cell-based toxicity studies showed cytocompatibility of **7a** with SH-SY5Y cells at all of the tested concentrations. In the acute toxicity studies, **7a** was found to be well-tolerated and non-toxic up to 500 mg/kg, oral dose. Compound **7a** exhibited promising *in-vivo* activity upon administration through the oral route in the scopolamine-induced AD model without affecting locomotor activity in the mice. Finally, compound **7a** is able to significantly reduce the levels of AChE and BChE and had potent anti-oxidant property in *ex-vivo* studies. Based on the promising *in-vitro* and *in-vivo* activities of the developed molecules in AD models, this first generation of **FA** analogs could serve for further structural modifications and formulation development for naturally inspired multifunctional drug development for the management of AD.

4. Experimental section

4.1. Chemistry

All the solvents required for the synthesis of the compounds were dried by solvent distillation techniques before use [52]. All the chemicals and reagents were obtained from the Sigma-Aldrich (St. Louis, MO, USA), Alfa Aesar (Massachusetts), S.D. Fine Chemicals

(India) and Avrachemicals (India). All reactions were performed under inert atmosphere (N_2) unless otherwise noted. The reactions were monitored by thin-layer chromatography (TLC) on precoated silica gel 60 F₂₅₄ (MerckKGaA) and were visualized under UV light, iodine vapors or by treatment with ninhydrin and bromocresol green reagents. Column chromatographic purifications were performed using silica gel 60-120 mesh size (CDH Laboratory Reagents, India). Proton nuclear magnetic resonance (1H NMR) and ^{13}C NMR spectra were measured on Bruker Advance, 500 MHz spectrometers with tetramethylsilane (TMS) as the internal standard. The NMR solvents used were $CDCl_3$ or $DMSO-d_6$ as indicated. Chemical shifts were measured in ppm and coupling constants (J) were measured in Hz. The following abbreviations are used to describe peak splitting patterns when appropriate: d = doublet, t = triplet, q = quartet, m = multiplet, dd = doublet of doublet, br = broad. Coupling constants J are reported in Hertz (Hz). High-resolution mass spectra (HRMS) were obtained by electrospray (HRMS/ESI), recorded with Agilent 1100 LC-Q-TOF and HRMS-6540-UHD machines at Indian Institute of Integrative Medicine (IIIM), Jammu, India, and Indian Institute of Technology, Ropar, India.

4.1.1. General procedure for synthesis of 2-chloro-*N*-phenyl substituted acetamides (**2a-2t** and **5a-5b**)

To a solution of substituted aniline (compounds **1a-1t**) or 5-aminoindole and 6-aminoquinoline (1.0 equiv.) in dichloromethane (CH_2Cl_2) (15 mL) at 0 °C, potassium carbonate (K_2CO_3) (2.0 equiv.) was added. The reaction was stirred at 0 °C for 15 min. Into this stirring solution, chloroacetyl chloride (1.0 equiv.) was added dropwise at 0 °C. The mixture was stirred for 2 h at room temperature. After completion of the reaction, water (20 mL) was added, and the mixture was extracted with dichloromethane. The organic solvent phase was concentrated under vacuum to afford the desired compounds **2a-2t**, **5a** and **5b**.

4.1.1.1. 2-chloro-*N*-(2-methylphenyl)acetamide (**2a**)

White powder, 68% yield. 1H NMR ($DMSO-d_6$, 500 MHz): δ 9.65 (bs, 1H), 7.38 (d, J = 7.5 Hz, 1H), 7.23 (d, J = 7.5 Hz, 1H), 7.19-7.17 (m, 1H), 7.13 (dd, J_1 = 7.5 Hz, J_2 = 1.0 Hz, 1H), 4.30 (bs, 2H), 2.20 (s, 3H).

4.1.1.2. 2-chloro-*N*-(3-methylphenyl)acetamide (**2b**)

White powder, 62% yield. 1H NMR ($DMSO-d_6$, 500 MHz): δ 10.21 (bs, 1H), 7.42 (s, 1H), 7.37 (d, J = 8.0 Hz, 1H), 7.20 (t, J = 8.0 Hz, 1H), 6.90 (d, J = 7.5 Hz, 1H), 4.23 (bs, 2H), 2.28 (s, 3H).

4.1.1.3. 2-chloro-N-(4-methylphenyl)acetamide (2c)

Brown powder, 70% yield. ^1H NMR (DMSO- d_6 , 500 MHz): δ 10.18 (bs, 1H), 7.47 (d, J = 8.5 Hz, 2H), 7.12 (d, J = 8.5 Hz, 2H), 4.22 (s, 2H), 2.25 (s, 3H).

4.1.1.4. 2-chloro-N-(2-methoxyphenyl)acetamide (2d)

White powder, 64% yield. ^1H NMR (DMSO- d_6 , 500 MHz): δ 10.27 (bs, 1H), 7.21-7.28 (m, 2H), 7.12 (d, J = 8.0 Hz, 1H), 6.68-6.66 (m, 1H), 4.24 (bs, 2H), 3.73 (s, 3H).

4.1.1.5. 2-chloro-N-(3-methoxyphenyl)acetamide (2e)

Black powder, 70% yield. ^1H NMR (DMSO- d_6 , 500 MHz): δ 10.30 (s, 1H), 7.28 (s, 1H), 7.28-7.21 (m, 1H), 7.13 (t, J = 8.0 Hz, 1H), 6.68- 6.64 (m, 1H), 4.24 (bs, 2H), 3.73 (s, 3H).

4.1.1.6. 2-chloro-N-(4-methoxyphenyl)acetamide (2f)

Brown powder, 76% yield. ^1H NMR (DMSO- d_6 500 MHz): δ 10.18 (bs, 1H), 7.50 (dd, J_1 = 7.0 Hz, J_2 = 2.0 Hz, 2H), 6.90 (dd, J_1 = 7.0 Hz, J_2 = 2.0 Hz, 2H), 4.21 (s, 2H), 3.72 (s, 3H).

4.1.1.7. 2-chloro-N-(2-chlorophenyl)acetamide (2g)

White powder, 71% yield. ^1H NMR (DMSO- d_6 , 500 MHz): δ 9.85 (bs, 1H), 7.73 (dd, J_1 = 8.0 Hz, J_2 = 1.5 Hz, 1H), 7.51 (dd, J_1 = 8.0 Hz, J_2 = 1.5 Hz, 1H), 7.35 (t, J = 6.5 Hz, 1H), 7.24 (t, J = 6.5 Hz, 1H), 4.37 (s, 2H).

4.1.1.8. 2-chloro-N-(3-chlorophenyl)acetamide (2h)

White powder, 69% yield. ^1H NMR (DMSO- d_6 , 500 MHz): δ 10.65 (bs, 1H), 8.06 (bs, 1H), 7.81-7.80 (m, 1H), 7.55 (dd, J_1 = 4.0 Hz, J_2 = 1.0 Hz, 2H), 4.29 (s, 2H).

4.1.1.9. 2-chloro-N-(4-chlorophenyl)acetamide (2i)

White powder, 74% yield. ^1H NMR (DMSO- d_6 , 500 MHz): δ 10.39 (bs, 1H), 7.62-7.59 (m, 2H), 7.16 (t, J = 9.0 Hz, 2H), 4.26 (s, 2H).

4.1.1.10. 2-chloro-N-(2-(trifluoromethyl)phenyl)acetamide (2j)

White powder, 61% yield. ^1H NMR (DMSO- d_6 , 500 MHz): δ 9.92 (bs, 1H), 7.75 (d, J = 8.0 Hz, 1H), 7.70 (t, J = 7.5 Hz, 1H), 7.53-7.47 (m, 2H), 4.32 (s, 2H).

4.1.1.11. 2-chloro-N-(3-(trifluoromethyl) phenyl)acetamide (2k)

Brown powder, 61% yield. ^1H NMR (DMSO- d_6 , 500 MHz): δ 10.64 (s, 1H), 8.07 (s, 1H), 7.78 (d, J = 8.5 Hz, 1H), 7.57 (t, J = 8.0 Hz, 1H), 7.43 (d, J = 8.0 Hz, 1H), 4.29 (s, 2H).

4.1.1.12. 2-chloro-N-(4-(trifluoromethyl) phenyl)acetamide (2l)

White powder, 61% yield. ^1H NMR (DMSO- d_6 , 500 MHz): δ 8.24 (bs, 1H), 7.50 (dd, J_1 = 7.0 Hz, J_2 = 2.0 Hz, 2H), 7.33 (dd, J_1 = 7.0 Hz, J_2 = 2.0 Hz, 2H), 4.19 (s, 1H).

4.1.1.13. 2-chloro-N-(3-bromophenyl)acetamide (2m)

White powder, 69% yield. ^1H NMR (DMSO- d_6 , 500 MHz): δ 10.64 (bs, 1H), 8.06 (s, 1H), 7.81-7.80 (m, 1H), 7.55 (d, J = 5.0 Hz, 2H), 4.29 (s, 2H).

4.1.1.14. 2-chloro-N-(4-bromophenyl)acetamide (2n)

White powder, 67% yield. ^1H NMR (DMSO- d_6 , 500 MHz): δ 7.68-7.76 (m, 1H), 7.82 (bs, 2H), 7.50 (d, J = 8.0 Hz, 2H), 4.30 (bs, 2H).

4.1.1.15. 2-chloro-*N*-(2-fluorophenyl)acetamide (**2o**)

White powder, 64% yield. ^1H NMR (DMSO- d_6 , 500 MHz): δ 7.82 (bs, 1H), 7.27-7.23 (m, 1H), 7.18-7.17 (m, 2H), 4.31 (bs, 2H).

4.1.1.16. 2-chloro-*N*-(3-fluorophenyl)acetamide (**2p**)

White powder, 64% yield. ^1H NMR (DMSO- d_6 , 500 MHz): δ 9.92 (bs, 1H), 7.75 (d, J = 7.5 Hz, 1H), 7.70 (t, J = 7.5 Hz, 1H), 7.53-7.47 (m, 2H), 4.32 (s, 2H).

4.1.1.17. 2-chloro-*N*-(4-fluorophenyl)acetamide (**2q**)

White powder, 65% yield. ^1H NMR (DMSO- d_6 , 500 MHz): δ 7.77 (d, J_1 = 8.5 Hz, 2H), 7.69 (d, J_1 = 8.5 Hz, 2H), 4.27 (bs, 2H).

4.1.1.18. 2-chloro-*N*-(3-cyanophenyl)acetamide (**2r**)

Brown powder, 60% yield. ^1H NMR (DMSO- d_6 , 500 MHz): δ 8.04 (bs, 1H), 7.79-7.81 (m, 1H), 7.55 (t, J = 7.0 Hz, 2H), 4.27 (bs, 2H).

4.1.1.19. 2-chloro-*N*-(4-cyanophenyl)acetamide (**2s**)

White powder, 67% yield. ^1H NMR (DMSO- d_6 , 500 MHz): δ 10.67 (bs, 1H), 7.80 (d, J = 8.0 Hz, 2H), 7.71 (d, J = 8.0 Hz, 2H), 4.30 (s, 2H).

4.1.1.20. 2-chloro-*N*-(phenyl)acetamide (**2t**)

White powder, 66% yield. ^1H NMR (CDCl₃, 500 MHz): δ 8.25 (bs, 1H), 7.56 (d, J = 8.0 Hz, 2H), 7.38 (t, J = 7.5 Hz, 2H), 7.19 (t, J = 7.0 Hz, 1H), 4.21 (bs, 2H).

4.1.1.21. 2-chloro-*N*-(1*H*-indol-5-yl)acetamide (**5a**)

Black powder, 78% yield. ^1H NMR (DMSO- d_6 , 500 MHz): δ 11.03 (bs, 1H), 10.09 (bs, 1H), 7.86 (bs, 1H), 7.31-7.34 (m, 2H), 7.20 (dd, J_1 = 8.5 Hz, J_2 = 2.0 Hz, 1H), 6.39 (t, J = 4.5 Hz, 1H), 4.23 (s, 2H).

4.1.1.22. 2-chloro-*N*-(quinolin-6-yl)acetamide (**5b**)

White powder, 75% yield. ^1H NMR (DMSO- d_6 , 500 MHz): δ 10.65 (bs, 1H), 8.80 (dd, J_1 = 4.0 Hz, J_2 = 1.5 Hz, 1H), 8.36 (s, 1H), 8.32 (d, J = 8.0 Hz, 1H), 8.00 (d, J = 5.0 Hz, 1H), 7.80 (dd, J_1 = 9.0 Hz, J_2 = 2.5 Hz, 1H), 7.50 (dd, J_1 = 8.0 Hz, J_2 = 4.0 Hz, 1H), 4.34 (s, 2H).

4.1.2. General procedure for synthesis of compounds 2-amino-*N*-phenyl substituted acetamide (**3a-3t**, **6a** and **6b**)

To a solution of substituted phenyl acetamide, **2a-2t** or **5a** or **5b** (0.25 g, 1.0 equiv) excess of liquid ammonia (NH₃) (10 mL) was added, and the reaction was heated at 60 °C for 6 h. The reaction mixture was allowed to cool to room temperature, after which 30 mL of ethyl acetate was added and the organic layer was separated and dried over anhydrous Na₂SO₄,

and concentrated in vacuo, which provided the free amine of compounds **3a-3t**, **6a**, and **6b** as a solid/oily product with 50-60% yield. Purification of the crude products was done by column chromatography using DCM:MeOH (9.5:0.5) as eluents to afford the aforementioned compounds.

4.1.2.1. 2-amino-N-(o-tolyl)acetamide (3a)

White oily product, 60% yield. ¹H NMR (DMSO-*d*₆, 500 MHz) δ 9.75 (bs, 1H), 7.39-7.44 (m, 2H), 7.10 (t, *J* = 7.5 Hz, 1H), 6.82 (d, *J* = 7.0 Hz, 1H), 3.23 (s, 2H), 2.24 (s, 3H).

4.1.2.2. 2-amino-N-(m-tolyl)acetamide (3b)

White oily product, 57% yield. ¹H NMR (DMSO-*d*₆, 500 MHz): δ 9.76 (bs, 1H), 7.45 - 7.40 (m, 2H), 7.12 (t, *J* = 8.0 Hz, 1H), 6.85 (d, *J* = 7.0 Hz, 1H), 3.23 (s, 2H), 2.26 (s, 3H).

4.1.2.3. 2-amino-N-(p-tolyl)acetamide (3c)

White oily product, 59% yield. ¹H NMR (DMSO-*d*₆, 500 MHz): δ 10.38 (bs, 1H), 7.48 (d, *J* = 8.5 Hz, 2H), 7.27 (d, *J* = 2.5 Hz, 1H), 7.12 (d, *J* = 8.0 Hz, 2H), 4.25 (s, 2H), 2.24 (s, 3H).

4.1.2.4. 2-amino-N-(2-methoxyphenyl)acetamide (3d)

Oily product, 54% yield. ¹H NMR (DMSO-*d*₆, 500 MHz) δ 7.83 (d, *J* = 7.0 Hz, 1H), 7.21-7.15 (m, 2H), 7.02 (d, *J* = 7.0 Hz, 1H), 3.30 (s, 2H), 2.23 (bs, 3H).

4.1.2.5. 2-amino-N-(3-methoxyphenyl)acetamide (3e)

Brown oily product, 60% yield. ¹H NMR (DMSO-*d*₆, 500 MHz): δ 9.77 (bs, 1H), 7.33 (bs, 1H), 7.19-7.16 (m, 2H), 6.61 (d, *J* = 7.5 Hz, 1H), 3.71 (s, 3H), 3.23 (bs, 2H), 3.16 (s, 2H).

4.1.2.6. 2-amino-N-(4-methoxyphenyl)acetamide (3f)

Brown oily product, 58% yield. ¹H NMR (DMSO-*d*₆, 500 MHz) δ 9.71 (bs, 1H), 7.53 (d, *J* = 8.0 Hz, 2H), 6.86 (d, *J* = 8.0 Hz, 2H), 3.71 (s, 3H), 3.22 (bs, 2H), 3.16 (s, 2H).

4.1.2.7. 2-amino-N-(2-chlorophenyl)acetamide (3g)

White solid product, 53% yield. ¹H NMR (DMSO-*d*₆, 500 MHz): δ 8.26 (d, *J* = 7.5 Hz, 1H), 7.51 (d, *J* = 8.0 Hz, 1H), 7.34 (t, *J* = 7.0 Hz, 1H), 7.13 (t, *J* = 7.0 Hz, 1H), 3.40 (s, 2H).

4.1.2.8. 2-amino-N-(3-chlorophenyl)acetamide (3h)

White solid product, 50% yield. ¹H NMR (DMSO-*d*₆, 500 MHz): δ 10.18 (bs, 1H), 7.85 (bs, 1H), 7.52 (d, *J* = 8.0 Hz, 1H), 7.34 (t, *J* = 8.0 Hz, 1H), 7.11 (d, *J* = 7.5 Hz, 1H), 3.40 (s, 2H).

4.1.2.9. 2-amino-N-(4-chlorophenyl)acetamide (3i)

White solid product, 55% yield. ¹H NMR (DMSO-*d*₆, 500 MHz) δ 9.71 (bs, 1H), 7.51 (d, *J* = 7.5 Hz, 2H), 6.84 (d, *J* = 7.5 Hz, 2H), 3.30 (s, 2H), 3.14 (s, 2H).

4.1.2.10. 2-amino-N-(2-(trifluoromethyl)phenyl)acetamide (3j)

Oily product, 58% yield. ¹H NMR (DMSO-*d*₆, 500 MHz): δ 8.14 (bs, 1H), 7.88 (d, *J* = 8.0 Hz, 1H), 7.52-7.51 (m, 2H), 3.29 (s, 2H).

4.1.2.11. 2-amino-N-(3-(trifluoromethyl)phenyl)acetamide (3k)

Oily product, 56% yield. ^1H NMR (DMSO- d_6 , 500 MHz): δ 8.15 (bs, 1H), 7.84 (d, J = 7.5 Hz, 1H), 7.54 (t, J = 8.0 Hz, 1H), 7.38 (d, J = 7.5 Hz, 1H).

4.1.2.12. 2-amino-N-(4-(trifluoromethyl)phenyl)acetamide (3l)

Oily product, 51% yield. ^1H NMR (DMSO- d_6 , 500 MHz) δ 7.85 (d, J = 8.5 Hz, 2H), 7.66 (d, J = 8.5 Hz, 2H), 4.12 (bs, 2H), 3.30 (bs, 2H)

4.1.2.13. 2-amino-N-(3-bromophenyl)acetamide (3m)

Oily product, 59% yield. ^1H NMR (DMSO- d_6 , 500 MHz) δ 8.15 (bs, 1H), 7.28 (t, J = 8.0 Hz, 1H), 7.18-7.11 (m, 2H).

4.1.2.14. 2-amino-N-(4-bromophenyl)acetamide (3n)

Oily product, 54% yield. ^1H NMR (DMSO- d_6 , 500 MHz): δ 7.62 (d, J = 8.5 Hz, 2H), 7.47 (d, J = 8.5 Hz, 2H), 4.02 (bs, 2H), 1.98 (bs, 2H).

4.1.2.15. 2-amino-N-(2-fluorophenyl)acetamide (3o)

Brown oily product, 60% yield. ^1H NMR (DMSO- d_6 , 500 MHz): δ 8.90 (t, J = 8.0 Hz, 1H), 7.26-7.22 (m, 1H), 7.17-7.08 (m, 2H), 3.45 (bs, 2H).

4.1.2.16. 2-amino-N-(3-fluorophenyl)acetamide (3p)

Oily product, 52% yield. ^1H NMR (DMSO- d_6 , 500 MHz): δ 7.83 (d, J = 7.0 Hz, 1H), 7.21-7.15 (m, 2H), 7.19-7.17 (m, 1H), 7.02 (d, J = 7.0 Hz, 1H), 3.30 (s, 2H), 2.23 (bs, 2H).

4.1.2.17. 2-amino-N-(4-fluorophenyl)acetamide (3q)

White solid product, 54% yield. ^1H NMR (DMSO- d_6 , 500 MHz): δ 7.65-7.63 (m, 2H), 7.13 (t, J = 9.0 Hz, 2H), 3.27 (s, 2H).

4.1.2.18. 2-amino-N-(3-cyanophenyl)acetamide (3r)

Oily product, 58% yield. ^1H NMR (DMSO- d_6 , 500 MHz): δ 8.12 (s, 2H), 7.86 (dd, J_1 = 7.5 Hz, J_2 = 1.5 Hz, 1H), 7.53-7.48 (m, 2H) 3.29 (bs, 2H).

4.1.2.19. 2-amino-N-(4-cyanophenyl)acetamide (3s)

Oily product, 60% yield. ^1H NMR (DMSO- d_6 , 500 MHz) δ 7.83 (dd, J_1 = 6.0 Hz, J_2 = 2.5 Hz, 1H), 7.65 (dd, J_1 = 6.0 Hz, J_2 = 2.5 Hz, 1H), 3.44 (bs, 2H), 3.29 (bs, 2H).

4.1.2.20. 2-amino-N-(phenyl)acetamide (3t)

White solid powder, 55% yield. ^1H NMR (DMSO- d_6 , 500 MHz) δ 7.59 (d, J = 7.5 Hz, 2H), 7.29 (d, J = 7.0 Hz, 2H), 7.03 (t, J = 6.5 Hz, 1H), 3.24 (bs, 2H), 3.15 (s, 2H).

4.1.2.21. 2-amino-N-(1H-indol-5-yl)acetamide (6a)

Oily product, 56% yield. ^1H NMR (DMSO- d_6 , 500 MHz): δ 10.98 (bs, 1H), 9.68 (bs, 1H), 7.89 (bs, 1H), 7.30-7.22 (m, 3H), 3.24 (s, 2H), 3.16 (s, 2H).

4.1.2.22. 2-amino-N-(quinolin-6-yl)acetamide (6b)

White solid product, 53% yield. ^1H NMR (DMSO- d_6 , 500 MHz): δ 8.77 (bs, 1H), 8.40 (bs, 1H), 8.27 (d, J = 7.5 Hz, 1H), 7.96 (d, J = 8.5 Hz, 1H), 7.86 (d, J = 8.5 Hz, 1H), 7.47 (bs, 1H), 4.13 (bs, 2H), 3.16 (s, 2H).

4.1.3. General procedure for synthesis of target compounds **4a-4t**, **7a**, and **7b**

Into a stirring solution of ferulic acid (0.3 g, 1.54 mmol) in anhydrous dichloromethane (10 mL), N-hydroxybenzotriazole (HOBt) (0.52 g, 3.86 mmol), 1-[3-(dimethylamino)-propyl]-3-ethylcarbodiimide hydrochloride (EDC) (0.35 g, 2.31 mmol) and DIPEA (0.49 g, 3.86 mmol) were added. The reaction was stirred at room temperature for 15 min. Thereafter, a 2-amino-N-phenyl substituted acetamide (1.54 mmol) was added, and the reaction mixture was allowed to stir overnight at room temperature. After completion of the reaction, it was quenched by addition of water and extracted with CH₂Cl₂ (3 × 25 mL). The combined organic layer was washed with brine, dried over Na₂SO₄ and concentrated under vacuum. The residue was subjected to silica gel chromatography or crystallization to afford the aforementioned compounds.

4.1.3.1. (E)-3-(4-hydroxy-3-methoxyphenyl)-N-(2-oxo-2-(o-tolylamino)ethyl)acrylamide (**4a**)

White solid powder, 67% yield. ¹H NMR (DMSO-*d*₆, 500 MHz): δ 9.48 (bs, 1H), 9.38 (bs, 1H), 8.31 (t, *J* = 5.5 Hz, 1H), 7.44-7.36 (m, 2H), 7.21 (d, *J* = 7.0 Hz, 1H), 7.16 (t, *J* = 9.0 Hz, 1H), 7.08 (d, *J* = 7.0 Hz, 1H), 7.03 (dd, *J*₁ = 6.5 Hz, *J*₂ = 1.5 Hz, 1H), 6.80 (d, *J* = 8.0 Hz, 1H), 6.60 (d, *J* = 15.5 Hz, 1H), 4.06 (s, 2H), 3.81 (s, 3H), 2.20 (bs, 3H). ¹³C NMR (DMSO-*d*₆, 125 MHz) δ 168.02, 164.84, 149.53, 148.36, 144.95, 136.37, 133.33, 129.65, 126.23, 123.22, 119.87, 116.06, 115.98, 111.59, 56.14, 43.98, 20.90. HRMS [*M* + *H*]⁺ Found 341.1508, calculated 341.1500 for C₁₉H₂₀N₂O₄.

4.1.3.2. (E)-3-(4-hydroxy-3-methoxyphenyl)-N-(2-oxo-2-(*m*-tolylamino)ethyl)acrylamide (**4b**)

White solid powder, 61% yield. ¹H NMR (DMSO-*d*₆, 500 MHz): δ 9.37 (bs, 1H), 8.30 (bs, 1H), 7.42 (d, *J* = 7.5 Hz, 1H), 7.37 (d, *J* = 16.0 Hz, 1H), 7.20 (d, *J* = 7.0 Hz, 1H), 7.16 (bs, 2H), 7.08 (t, *J* = 7.0 Hz, 1H), 7.02 (d, *J* = 8.0 Hz, 1H), 6.80 (d, *J* = 8.0 Hz, 1H), 6.60 (d, *J* = 16.0 Hz, 1H), 4.05 (bs, 2H), 3.81 (s, 3H), 2.20 (s, 3H). ¹³C NMR (DMSO-*d*₆, 125 MHz) δ 168.37, 166.41, 148.84, 148.29, 139.99, 136.53, 131.94, 130.77, 126.81, 126.45, 125.61, 125.12, 122.09, 119.04, 116.13, 111.37, 56.01, 43.23, 18.38. HRMS [*M* + *H*]⁺ Found 341.1501, calculated 341.1505 for C₁₉H₂₀N₂O₄.

4.1.3.3. (E)-3-(4-hydroxy-3-methoxyphenyl)-N-(2-oxo-2-(*p*-tolylamino)ethyl)acrylamide (**4c**)

White solid powder, 69% yield. ¹H NMR (DMSO-*d*₆, 500 MHz): δ 9.48 (bs, 1H), 9.39 (bs, 1H), 8.32 (bs, 1H), 7.43-7.36 (m, 2H), 7.21-7.16 (m, 3H), 7.09-7.01 (m, 2H), 6.80 (d, *J* = 7.5 Hz, 1H), 6.60 (d, *J* = 15.5 Hz, 1H), 4.06 (bs, 2H), 3.81 (s, 3H), 2.20 (bs, 3H). ¹³C NMR (DMSO-*d*₆, 125 MHz) δ 168.02, 166.34, 148.83, 148.29, 139.96, 136.81, 132.63, 129.56, 126.83, 122.08, 119.05, 116.12, 111.34, 56.02, 43.32, 20.89. HRMS [*M* + *H*]⁺ Found 341.1503, calculated 341.1505 for C₁₉H₂₀N₂O₄.

4.1.3.4. (*E*)-3-(4-hydroxy-3-methoxyphenyl)-(2-((2-methoxyphenyl)amino)-2-oxoethyl)acrylamide (**4d**)

White solid powder, 62% yield. ^1H NMR (DMSO- d_6 , 500 MHz): δ 9.48 (bs, 1H), 9.19 (bs, 1H), 8.37 (bs, 1H), 8.01 (d, J = 7.5 Hz, 1H), 7.38 (d, J = 15.5 Hz, 1H), 7.17 (bs, 1H), 7.07-7.03 (m, 3H), 6.91 (t, J = 7.0 Hz, 1H), 6.80 (d, J = 8.0 Hz, 1H), 6.60 (d, J = 16.0 Hz, 1H), 4.05 (bs, 2H), 3.81 (s, 6H). ^{13}C NMR (DMSO- d_6 , 125 MHz): δ 167.90, 165.83, 159.51, 148.37, 147.82, 140.08, 139.47, 129.56, 126.34, 121.58, 118.58, 111.39, 110.90, 108.59, 104.96, 55.53, 54.94, 42.91. HRMS $[\text{M} + \text{H}]^+$ Found 357.1431 calculated 356.1449 for $\text{C}_{19}\text{H}_{20}\text{N}_2\text{O}_5$.

4.1.3.5. (*E*)-3-(4-hydroxy-3-methoxyphenyl)-*N*-(2-((3-methoxyphenyl)amino)-2-oxoethyl)acrylamide (**4e**)

White solid powder, 66% yield. ^1H NMR (DMSO- d_6 , 500 MHz): δ 10.03 (bs, 1H), 9.47 (bs, 1H), 8.26 (t, J = 6.0 Hz, 1H), 7.35 (d, J = 16.0 Hz, 1H), 7.30 (t, J = 1.5 Hz, 1H), 7.23-7.19 (m, 1H), 7.15 (d, J = 2.0 Hz, 1H), 7.12 (d, J = 8.5 Hz, 1H), 7.02 (dd, J_1 = 6.5 Hz, J_2 = 2.0 Hz, 1H), 6.80 (d, J = 8.0 Hz, 1H), 6.64-6.58 (m, 2H), 4.01 (bs, 2H), 3.72 (s, 3H). ^{13}C NMR (DMSO- d_6 , 125 MHz): δ 168.37, 166.31, 159.97, 148.84, 148.29, 140.55, 139.94, 130.03, 126.80, 122.05, 119.04, 116.13, 111.85, 111.35, 109.06, 105.42, 55.99, 55.40, 43.38. HRMS $[\text{M} + \text{H}]^+$ Found 357.1457, calculated 357.1450 for $\text{C}_{19}\text{H}_{20}\text{N}_2\text{O}_5$.

4.1.3.6. (*E*)-3-(4-hydroxy-3-methoxyphenyl)-*N*-(2-((4-methoxyphenyl)amino)-2-oxoethyl)acrylamide (**4f**)

White solid powder, 62% yield. ^1H NMR (DMSO- d_6 , 500 MHz): δ 9.89 (bs, 1H), 9.46 (bs, 1H), 8.25 (t, J = 6.0 Hz, 1H), 7.50 (d, J = 8.0 Hz, 2H), 7.35 (d, J = 15.5 Hz, 1H), 7.15 (bs, 1H), 7.02 (dd, J_1 = 6.0 Hz, J_2 = 2.0 Hz, 1H), 6.89 (d, J = 8.0 Hz, 1H), 6.80 (d, J = 7.5 Hz, 1H), 6.60 (d, J = 15.5 Hz, 1H), 3.98 (bs, 2H), 3.81 (s, 3H), 3.71 (s, 3H). ^{13}C NMR (DMSO- d_6 , 125 MHz): δ 167.86, 165.81, 159.49, 148.35, 147.80, 140.05, 139.44, 129.53, 126.33, 121.56, 118.57, 115.65, 111.37, 110.90, 108.59, 104.96, 55.52, 54.92, 42.89. HRMS $[\text{M} + \text{H}]^+$ Found 357.1458, calculated 357.1450 for $\text{C}_{19}\text{H}_{20}\text{N}_2\text{O}_5$.

4.1.3.7. (*E*)-*N*-(2-((2-chlorophenyl)amino)-2-oxoethyl)-3-(4-hydroxy-3-methoxyphenyl)acrylamide (**4g**)

White solid powder, 70% yield. ^1H NMR (DMSO- d_6 , 500 MHz): δ 10.23 (bs, 1H), 9.47 (bs, 1H), 8.31 (t, J = 6.0 Hz, 1H), 7.95 (bs, 1H), 7.80 (bs, 1H), 7.46 (d, J = 8.0 Hz, 1H), 7.37-7.33 (m, 2H), 7.16-7.10 (m, 2H), 7.02 (d, J = 8.0 Hz, 1H), 6.80 (d, J = 8.0 Hz, 1H), 6.59 (d, J = 16.0 Hz, 1H), 4.02 (s, 2H), 3.81 (s, 3H). ^{13}C NMR (DMSO- d_6 , 125 MHz): δ 167.77, 165.82, 148.36, 147.81, 139.45, 135.29, 126.32, 123.98, 121.57, 120.87, 120.81, 118.56, 115.65, 115.38, 115.20, 110.90, 55.53, 42.80. HRMS $[\text{M} + \text{H}]^+$ Found 361.0955, calculated 361.0947 for $\text{C}_{18}\text{H}_{17}\text{ClN}_2\text{O}_4$.

4.1.3.8. (*E*)-*N*-(2-((3-chlorophenyl)amino)-2-oxoethyl)-3-(4-hydroxy-3-methoxyphenyl)acrylamide (**4h**)

White solid powder, 69% yield. ^1H NMR (DMSO- d_6 , 500 MHz): δ 10.20 (s, 1H), 9.46 (bs, 1H), 8.30-8.27 (m, 2H), 7.93 (t, J = 4.0 Hz, 1H), 7.52-7.50 (m, 1H), 7.35 (d, J = 16.0 Hz, 1H), 7.29-7.22 (m, 3H), 7.15 (d, J = 2.0 Hz, 1H), 7.02 (dd, J_1 = 8.5 Hz, J_2 = 1.0 Hz, 2H), 6.82 (d, J = 8.0 Hz, 1H), 6.60 (d, J = 15.5 Hz, 1H), 4.01 (s, 2H), 3.81 (s, 3H). ^{13}C NMR (DMSO- d_6 , 125 MHz): δ 168.75, 166.42, 148.86, 148.30, 140.92, 140.06, 131.24, 126.79, 126.34, 122.11, 122.01, 121.94, 118.93, 118.36, 116.14, 111.39, 56.04, 43.42. HRMS $[\text{M} + \text{H}]^+$ Found 361.0959, calculated 360.0945 for $\text{C}_{18}\text{H}_{17}\text{ClN}_2\text{O}_4$.

4.1.3.9. (*E*)-*N*-(2-((4-chlorophenyl)amino)-2-oxoethyl)-3-(4-hydroxy-3-methoxyphenyl)acrylamide (**4i**)

White solid powder, 69% yield. ^1H NMR (DMSO- d_6 , 500 MHz): δ 9.55 (s, 1H), 8.38 (t, J = 5.5 Hz, 1H), 7.81 (d, J = 8.0 Hz, 1H), 7.50 (dd, J_1 = 8.0 Hz, J_2 = 1.0 Hz, 1H), 7.40-7.32 (m, 2H), 7.20-7.16 (m, 2H), 7.03 (dd, J_1 = 8.5 Hz, J_2 = 1.0 Hz, 1H), 6.81 (d, J = 8.0 Hz, 1H), 6.59 (d, J = 15.5 Hz, 1H), 4.08 (s, 2H), 3.81 (s, 3H). ^{13}C NMR (DMSO- d_6 , 125 MHz) δ 168.29, 165.89, 148.37, 147.81, 140.46, 139.54, 130.79, 126.30, 125.84, 121.59, 121.54, 121.41, 118.46, 117.85, 115.65, 110.89, 55.52, 42.94. HRMS $[\text{M} + \text{H}]^+$ Found 361.0951, calculated 361.095 for $\text{C}_{18}\text{H}_{17}\text{ClN}_2\text{O}_4$.

4.1.3.10. (*E*)-3-(4-hydroxy-3-methoxyphenyl)-*N*-(2-oxo-2-((3(trifluoromethyl)phenyl)amino)ethyl) acrylamide (**4j**)

White solid powder, 61% yield. ^1H NMR (DMSO- d_6 , 500 MHz): δ 10.40 (bs, 1H), 9.50 (bs, 1H), 8.30 (bs, 1H), 8.11 (d, J = 7.5 Hz, 1H), 7.85-7.80 (m, 2H), 7.56 (s, 1H), 7.40 (d, J = 15.5 Hz, 1H), 7.38 (s, 1H), 7.16 (s, 1H), 7.02 (d, J = 7.5 Hz, 1H), 6.81 (d, J = 6.0 Hz, 1H), 6.61 (d, J = 15.5 Hz, 1H), 4.01 (s, 2H), 3.81 (s, 3H). ^{13}C NMR (DMSO- d_6 , 125 MHz) δ 168.91, 165.97, 148.40, 147.82, 139.67, 135.10, 133.07, 129.07, 126.29, 121.62, 118.33, 115.66, 110.94, 55.53, 42.59. HRMS $[\text{M} + \text{H}]^+$ Found 395.1178, calculated 395.1172 for $\text{C}_{19}\text{H}_{17}\text{F}_3\text{N}_2\text{O}_4$.

4.1.3.11. (*E*)-3-(4-hydroxy-3-methoxyphenyl)-*N*-(2-oxo-2-((3(trifluoromethyl)phenyl)amino)ethyl) acrylamide (**4k**)

White solid powder, 62% yield. ^1H NMR (DMSO- d_6 , 500 MHz): δ 9.82 (bs, 1H), 9.44 (bs, 1H), 8.30 (t, J = 5.5 Hz, 1H), 7.89 (bs, 1H), 7.37 (d, J = 15.5 Hz, 1H), 7.28-7.24 (m, 1H), 7.18-7.15 (m, 3H), 7.02 (dd, J_1 = 8.0 Hz, J_2 = 1.5 Hz, 2H), 6.81 (d, J = 8.0 Hz, 1H), 6.59 (d, J = 15.5 Hz, 1H), 4.08 (s, 2H), 3.82 (s, 3H). ^{13}C NMR (DMSO- d_6 , 125 MHz) δ 165.10, 149.14, 142.77, 138.14, 136.68, 133.63, 128.51, 127.90, 127.13, 126.94, 125.10, 122.79, 122.31, 119.59, 117.17, 110.12, 78.03. HRMS $[\text{M} + \text{H}]^+$ Found 395.1101, calculated 395.1120 for $\text{C}_{19}\text{H}_{17}\text{F}_3\text{N}_2\text{O}_4$.

4.1.3.12. (*E*)-3-(4-hydroxy-3-methoxyphenyl)-*N*-(2-oxo-2-((4(trifluoromethyl)phenyl)amino)ethyl)acrylamide (**4l**)

White solid powder, 65% yield. ^1H NMR (DMSO- d_6 , 500 MHz): δ 8.30 (t, J = 6.0 Hz, 1H), 7.89-7.85 (m, 1H), 7.36 (d, J = 15.0 Hz, 1H), 7.26-7.22 (m, 1H), 7.18-7.12 (m, 3H), 7.02 (dd, J_1 = 5.0 Hz, J_2 = 1.5 Hz, 1H), 6.80 (d, J = 8.0 Hz, 1H), 6.57 (d, J = 15.0 Hz, 1H), 4.06 (bs, 2H), 3.80 (bs, 3H). ^{13}C NMR (DMSO- d_6 , 125 MHz) δ 169.07, 166.39, 148.87, 148.47, 148.30, 142.94, 140.07, 126.78, 126.59, 126.57, 125.92, 123.92, 123.84, 123.76, 123.58, 122.09, 119.44, 118.92, 116.14, 111.38, 56.00, 43.47. HRMS $[\text{M} + \text{H}]^+$ Found 395.1217, calculated 395.1215 for $\text{C}_{19}\text{H}_{17}\text{F}_3\text{N}_2\text{O}_4$.

4.1.3.13. (*E*)-*N*-(2-((3-bromophenyl)amino)-2-oxoethyl)-3-(4-hydroxy-3-methoxyphenyl)acrylamide (**4m**)

White solid powder, 61% yield. ^1H NMR (DMSO- d_6 , 500 MHz): δ 10.20 (bs, 1H), 8.29 (bs, 1H), 7.93 (bs, 1H), 7.50 (d, J = 8.0 Hz, 1H), 7.36 (d, J = 15.5 Hz, 1H), 7.29-7.22 (m, 2H), 7.15 (bs, 1H), 7.01 (d, J = 8.0 Hz, 1H), 6.80 (d, J = 8.5 Hz, 1H), 6.58 (d, J = 15.5 Hz, 1H), 4.00 (bs, 2H), 3.81 (s, 1H). ^{13}C NMR (DMSO- d_6 , 125 MHz) δ 168.73, 166.44, 148.87,

148.30, 140.90, 140.09, 131.21, 126.78, 126.34, 122.22, 122.01, 121.95, 118.90, 118.36, 116.13, 11.36, 56.03, 43.42. HRMS $[M + H]^+$ Found 405.0443, calculated 405.0425 for $C_{18}H_{17}BrN_2O_4$.

4.1.3.14. (E)-N-(2-((4-bromophenyl)amino)-2-oxoethyl)-3-(4-hydroxy-3-methoxyphenyl)acrylamide (4n)

White solid powder, 68% yield. 1H NMR (DMSO- d_6 , 500 MHz): δ 10.18 (s, 1H), 9.46 (s, 1H), 8.29 (t, $J = 5.5$ Hz, 1H), 7.58 (d, $J = 9.0$ Hz, 2H), 7.49 (d, $J = 9.0$ Hz, 2H), 7.35 (d, $J = 16.0$ Hz, 1H), 7.15 (bs, 1H), 7.02 (d, $J = 8.0$ Hz, 1H), 6.80 (d, $J = 8.0$ Hz, 1H), 6.59 (d, $J = 16.0$ Hz, 1H), 4.0 (bs, 2H), 3.18 (bs, 3H). ^{13}C NMR (DMSO- d_6 , 125 MHz) δ 168.56, 166.33, 148.84, 148.28, 139.99, 138.75, 132.05, 126.79, 122.49, 121.49, 118.98, 116.13, 115.26, 111.36, 56.00, 43.40. HRMS $[M + H]^+$ Found 407.0420, calculated 407.0426 for $C_{18}H_{17}BrN_2O_4$.

4.1.3.15. (E)-N-(2-((2-fluorophenyl)amino)-2-oxoethyl)-3-(4-hydroxy-3-methoxyphenyl)acrylamide (4o)

White solid powder, 65% yield. 1H NMR (DMSO- d_6 , 500 MHz): δ 8.31 (t, $J = 6.0$ Hz, 1H), 7.87 (dd, $J_1 = 9.5$, $J_2 = 5.0$ Hz, 1H), 7.37 (d, $J = 15.5$ Hz, 1H), 7.27-7.22 (m, 1H), 7.18-7.15 (m, 4H), 7.02 (dd, $J_1 = 8.5$ Hz, $J_2 = 2.0$ Hz, 1H), 6.80 (d, $J = 8.5$ Hz, 1H), 6.58 (d, $J = 16$ Hz, 1H), 4.08 (bs, 2H), 3.80 (bs, 3H). ^{13}C NMR (DMSO- d_6 , 125 MHz) δ 168.84, 166.42, 154.97, 153.03, 148.86, 148.30, 140.09, 126.80, 126.42, 126.33, 125.76, 125.71, 124.86, 124.83, 124.44, 122.11, 118.95, 116.14, 116.04, 115.88, 111.37, 56.00, 43.20. HRMS $[M + H]^+$ Found 345.1257, calculated 345.1253 for $C_{18}H_{17}FN_2O_4$.

4.1.3.16. (E)-N-(2-((3-fluorophenyl)amino)-2-oxoethyl)-3-(4-hydroxy-3-methoxyphenyl)acrylamide (4p)

White solid powder, 68% yield. 1H NMR (DMSO- d_6 , 500 MHz): δ 10.29 (bs, 1H), 9.50 (bs, 1H), 8.33 (bs, 1H), 7.60 (d, $J = 10.5$ Hz, 1H), 7.32-7.37 (m, 3H), 7.16 (bs, 1H), 7.03 (bs, 1H), 6.88-6.80 (m, 1H), 6.59 (d, $J = 15.5$ Hz, 1H), 4.02 (bs, 2H), 3.81 (s, 3H). ^{13}C NMR (DMSO- d_6 , 125 MHz) δ 169.20, 166.48, 148.85, 148.29, 139.98, 134.17, 133.82, 128.58, 126.82, 126.53, 126.32, 126.06, 125.84, 123.27, 122.09, 119.09, 116.13, 111.34, 56.00, 43.00. HRMS $[M + H]^+$ Found 345.1254, calculated 345.125 for $C_{18}H_{17}FN_2O_4$.

4.1.3.17. (E)-N-(2-((4-fluorophenyl)amino)-2-oxoethyl)-3-(4-hydroxy-3-methoxyphenyl)acrylamide (4q)

White solid powder, 60% yield. 1H NMR (DMSO- d_6 , 500 MHz): δ 7.60 (dd, $J_1 = 7.5$ Hz, $J_2 = 5.0$ Hz (m, 2H), 7.34 (d, $J = 15.5$ Hz, 1H), 7.16-7.13 (m, 3H), 7.02 (dd, $J_1 = 8.0$ Hz, $J_2 = 1.5$ Hz, 1H), 6.80 (d, $J = 8.0$ Hz, 1H), 6.57 (d, $J = 15.5$ Hz, 1H), 3.99 (bs, 2H), 3.80 (bs, 3H). ^{13}C NMR (DMSO- d_6 , 125 MHz) δ 168.14, 166.36, 148.66, 148.23, 140.10, 135.56, 126.81, 122.16, 121.35, 121.29, 118.88, 116.01, 115.89, 115.71, 111.31, 56.01, 43.09. HRMS $[M + H]^+$ Found 345.1243, calculated 345.1251 for $C_{18}H_{17}FN_2O_4$.

4.1.3.18. (E)-N-(2-((3-cyanophenyl)amino)-2-oxoethyl)-3-(4-hydroxy-3-methoxyphenyl)acrylamide (4r)

White solid powder, 62% yield. 1H NMR (DMSO- d_6 , 500 MHz): δ 8.33 (t, $J = 5.5$ Hz, 1H), 8.06 (bs, 1H), 7.81 (d, $J = 8.0$ Hz, 1H), 7.55-7.49 (m, 2H), 7.35 (d, $J = 16.0$ Hz, 1H), 7.15 (bs, 1H), 7.02 (d, $J = 7.5$ Hz, 1H), 6.80 (d, $J = 8.0$ Hz, 1H), 6.57 (d, $J = 16.0$ Hz, 1H), 4.02 (bs, 1H), 3.80 (bs, 3H). ^{13}C NMR (DMSO- d_6 , 125 MHz) δ 168.95, 166.47, 148.69, 148.23, 140.22,

139.96, 130.80, 127.34, 126.78, 124.10, 122.18, 119.16, 118.74, 116.02, 112.02, 111.32, 56.01, 43.24, 29.43. HRMS (ESI) m/z $[M + H]^+$ 352.1294, calculated 352.1297 for $C_{19}H_{17}N_3O_4$.

4.1.3.19. (E)-N-(2-((4-cyanophenyl)amino)-2-oxoethyl)-3-(4-hydroxy-3-methoxyphenyl)acrylamide (4s)

White solid powder, 65% yield. 1H NMR (DMSO- d_6 , 500 MHz): δ 9.82 (bs, 1H), 9.44 (bs, 1H), 8.29 (t, $J = 5.5$ Hz, 1H), 7.88 (bs, 1H), 7.37 (d, $J = 15.5$ Hz, 1H), 7.28-7.24 (m, 1H), 7.18-7.15 (m, 3H), 7.02 (d, $J = 1.5$ Hz, 1H), 6.80 (d, $J = 8.0$ Hz, 1H), 6.59 (d, $J = 15.5$ Hz, 1H), 4.07 (bs, 2H), 3.81 (s, 3H). ^{13}C NMR (DMSO- d_6 , 125 MHz) δ 167.86, 165.81, 159.49, 148.35, 147.80, 140.05, 139.44, 129.53, 126.33, 121.56, 118.57, 115.65, 111.37, 110.37, 108.59, 104.96, 55.52, 54.92, 42.89. HRMS (ESI) m/z $[M + H]^+$ 378.1457, calculated 378.1461 for $C_{20}H_{17}N_3O_4$.

4.1.3.20. (E)-N-(2-((phenyl)amino)-2-oxoethyl)-3-(4-hydroxy-3-methoxyphenyl)acrylamide (4t)

White solid powder, 65% yield. 1H NMR (DMSO- d_6 , 500 MHz): δ 7.58 (d, $J = 7.5$ Hz, 2H), 7.35 (d, $J = 15.5$ Hz, 1H), 7.30 (t, $J = 8.0$ Hz, 2H), 7.15 (bs, 1H), 7.05-7.01 (m, 2H), 6.80 (d, $J = 8.0$ Hz, 1H), 6.58 (d, $J = 16.0$ Hz, 1H), 4.00 (bs, 2H), 3.80 (s, 3H). ^{13}C NMR (DMSO- d_6 , 125 MHz) δ 168.20, 166.40, 148.66, 148.25, 140.10, 139.16, 129.24, 126.84, 123.80, 122.16, 119.64, 119.54, 118.91, 116.03, 111.33, 56.03, 43.19. HRMS $[M + H]^+$ Found 327.1340, calculated 327.1345 for $C_{18}H_{18}N_2O_4$.

4.1.3.21. (E)-N-(2-((1H-indol-5-yl)amino)-2-oxoethyl)-3-(4-hydroxy-3-methoxyphenyl)acrylamide (7a)

Brown solid powder, 70% yield. 1H NMR (DMSO- d_6 , 500 MHz): δ 11.0 (s, 1H), 9.82 (bs, 1H), 9.47 (bs, 1H), 8.25 (t, $J = 5.5$ Hz, 1H), 7.85 (bs, 1H), 7.37-7.29 (m, 3H), 7.20 (dd, $J_1 = 9.0$ Hz, $J_2 = 2.0$ Hz, 1H), 7.16 (d, $J = 2.0$ Hz, 1H), 7.02 (dd, $J_1 = 8.0$ Hz, $J_2 = 2.0$ Hz, 1H), 6.80 (d, $J = 8.5$ Hz, 1H), 6.62 (d, $J = 15.5$ Hz, 1H), 6.37 (bs, 1H), 4.02 (d, $J = 6.0$ Hz, 2H), 3.81 (s, 3H). ^{13}C NMR (DMSO- d_6 , 125 MHz) δ 169.20, 166.48, 148.85, 148.30, 139.99, 134.18, 133.82, 128.58, 126.82, 126.53, 126.32, 126.06, 125.85, 123.28, 122.10, 119.10, 116.14, 111.34, 56.20, 43.36. HRMS $[M + H]^+$ Found 366.1451, calculated 366.1446 for $C_{20}H_{19}N_3O_4$.

4.1.3.22. (E)-3-(4-hydroxy-3-methoxyphenyl)-N-(2-oxo-2-(quinolin-6-ylamino)ethyl)acrylamide (7b)

Brown solid powder, 69% yield. 1H NMR (DMSO- d_6 , 500 MHz): δ 10.41 (bs, 1H), 9.50 (bs, 1H), 8.78 (bs, 1H), 8.35 (bs, 2H), 8.27 (d, $J = 7.5$ Hz, 1H), 7.98 (d, $J = 8.0$ Hz, 1H), 7.82 (d, $J = 9.0$ Hz, 1H), 7.47 (s, 1H), 7.37 (d, $J = 16.0$ Hz, 1H), 7.16 (bs, 1H), 7.02 (d, $J = 7.5$ Hz, 1H), 6.80 (d, $J = 6.5$ Hz, 1H), 6.63 (d, $J = 15.5$ Hz, 1H), 4.08 (s, 2H), 3.81 (s, 3H). ^{13}C NMR (DMSO- d_6 , 125 MHz) δ 167.12, 165.76, 148.34, 147.81, 139.34, 132.69, 130.82, 127.42, 126.37, 125.87, 123.69, 121.55, 118.73, 115.66, 114.78, 111.15, 110.90, 110.68, 111.04, 55.53, 42.86. HRMS $[M + H]^+$ Found 377.1509, calculated 377.1504 for $C_{21}H_{19}N_3O_4$.

4.1.4. General procedure for synthesis of substituted phenylpiperazine compounds 9a-9g

In an atmosphere of dry N₂, a mixture of substituted aniline (1.0 equiv.), bis(2-chloroethyl)amine hydrochloride (1.0 equiv.), and diethylene glycol monomethyl ether (5 mL) was refluxed at 150 °C for 8–10 h. After being cooled to room temperature, the mixture was dissolved in MeOH (4 mL) followed by addition of Et₂O (100 mL). The precipitate was filtered off and washed with Et₂O to provide HCl salt. The compound HCl salt **9a-9g**, which was used without purification in the next step.

4.1.4.1. 1-phenylpiperazine (**9a**)

Compound aniline **8a** (0.3 g, 1.0 equiv.) was reacted with bis(2-chloroethyl)amine hydrochloride (0.42 g, 1.0 equiv.) in diethylene glycol monomethyl ether (5 mL) by following the general procedure to yield compound **9a** (0.480 g, 68%).

4.1.4.2. 1-(3-methoxyphenyl)piperazine (**9b**)

Compound *m*-anisidine **8b** (0.3 g, 1.0 equiv.) was reacted with bis(2-chloroethyl)amine hydrochloride (0.44 g, 1.0 equiv.) in diethylene glycol monomethyl ether (5 mL) by following the general procedure to yield compound **9b** (0.370 g, 69%).

4.1.4.3. 1-(4-fluorophenyl)piperazine (**9c**)

Compound 4-Fluoroaniline **8c** (0.3 g, 1.0 equiv.) was reacted with bis(2-chloroethyl)amine hydrochloride (0.46 g, 1.0 equiv.) in diethylene glycol monomethyl ether (5 mL) by following the general procedure to yield compound **9c** (0.410 g, 67%).

4.1.4.4. 1-(3-nitrophenyl)piperazine (**9d**)

Compound 3-nitroaniline **8d** (0.3 g, 1.0 equiv.) was reacted with bis(2-chloroethyl)amine hydrochloride (0.39g, 1.0 equiv.) in diethylene glycol monomethyl ether (5 mL) by following the general procedure to yield compound **9d** (0.510g, 68%).

4.1.4.5. 1-(4-methoxyphenyl)piperazine (**9e**)

Compound *p*-anisidine **8e** (0.3 g, 1.0 equiv.) was reacted with bis(2-chloroethyl)amine hydrochloride (0.45 g, 1.0 equiv.) in diethylene glycol monomethyl ether (5 mL) by following the general procedure to yield compound **9e** (0.420 g, 66%).

4.1.4.6. 1-(4-chlorophenyl)piperazine (**9f**)

Compound *p*-chloroaniline **8f** (0.3 g, 1.0 equiv.) was reacted with bis(2-chloroethyl)amine hydrochloride (0.45 g, 1.0 equiv.) in diethylene glycol monomethyl ether (5 mL) by following the general procedure to yield compound **9f** (0.390 g, 66%).

4.1.4.7. 1-(*p*-tolyl)piperazine (**9g**)

Compound *p*-toluidine **8g** (0.3 g, 1.0 equiv.) was reacted with bis(2-chloroethyl)amine hydrochloride (0.45 g, 1.0 equiv.) in diethyleneglycolmonomethylether (5 mL) by following the general procedure to yield compound **9g** (0.490 g, 70%).

4.1.5. General procedure for synthesis of compounds **10a-g**

To a solution of ferulic acid (0.3 g, 1.54 mmol) and N-substituted-piperazine (1.2 mmol) in tetrahydrofuran (30 mL), N-hydroxybenzotriazole (HOBt) (0.20 g, 1.54 mmol) and 1-[3-(dimethylamino)-propyl]-3-ethylcarbodiimide hydrochloride (EDCI) (0.59 g, 3.86 mmol) and DIPEA (0.49 g, 3.86 mmol) were added. The mixture was stirred at room temperature under nitrogen atmosphere for 10–12 h. After completion of the reaction, the solution was washed successively with 5% HCl, saturated NaHCO₃ and brine, respectively, then dried over anhydrous Na₂SO₄, and concentrated in vacuum. The crude material was purified by column chromatography over silica gel (hexane/EtOAc, 6:4) to give the final compound.

4.1.5.1. (E)-3-(4-hydroxy-3-methoxyphenyl)-1-(4-phenylpiperazin-1-yl)prop-2-en-1-one (10a)

White solid product, 80% yield. ¹H NMR (DMSO-*d*₆, 500 MHz): δ 9.44 (bs, 1H), 7.44 (d, *J* = 15.0 Hz, 1H), 7.34 (s, 1H), 7.23 (t, *J* = 8.0 Hz, 2H), 7.12–7.09 (m, 2H), 6.97 (d, *J* = 8.0 Hz, 2H), 6.83–6.77 (m, 2H), 3.83 (s, 4H), 3.71 (s, 1H), 3.16 (s, 4H). ¹³C NMR (DMSO-*d*₆, 125 MHz) δ 165.37, 151.32, 148.97, 148.32, 142.87, 129.46, 127.16, 123.08, 119.79, 116.34, 115.90, 114.87, 111.66, 56.27, 49.27, 48.95, 45.27, 41.99. HRMS [*M* + *H*]⁺ Found 339.1708, calculated 339.1702 for C₂₀H₂₂N₂O₃.

4.1.5.2. (E)-3-(4-hydroxy-3-methoxyphenyl)-1-(4-(3-methoxyphenyl)piperazin-1-yl)prop-2-en-1-one (10b)

White solid product, 82% yield. ¹H NMR (DMSO-*d*₆, 500 MHz): δ 9.47 (s, 1H), 7.44 (d, *J* = 15.0 Hz, 1H), 7.35 (s, 1H), 7.13–7.10 (m, 2H), 6.94 (d, *J* = 8.5 Hz, 2H), 6.84 (d, *J* = 5.0 Hz, 2H), 6.77 (d, *J* = 6.5 Hz, 1H), 3.69 (bs, 5H), 3.68 (bs, 5H), 3.02 (s, 4H). ¹³C NMR (DMSO-*d*₆, 125 MHz) δ 165.33, 153.79, 148.95, 148.32, 145.67, 142.85, 127.16, 123.08, 118.51, 115.89, 114.88, 114.77, 111.63, 56.26, 55.64, 51.11, 50.44, 45.44, 42.10. HRMS [*M* + *H*]⁺ Found 369.1816, calculated 369.1818 for C₂₁H₂₄N₂O₄.

4.1.5.3. ((E)-1-(4-(4-fluorophenyl)piperazin-1-yl)-3-(4-hydroxy-3-methoxyphenyl)prop-2-en-1-one (10c)

Pale yellow solid product, 81% yield. ¹H NMR (DMSO-*d*₆, 500 MHz): δ 9.44 (bs, 1H), 7.43 (d, *J* = 15.0 Hz, 1H), 7.34 (bs, 1H), 7.12–7.05 (m, 4H), 7.01 (bs, 2H), 6.78 (d, *J* = 15.0 Hz, 1H), 3.83 (s, 5H), 3.71 (bs, 2H), 3.09 (bs, 4H). ¹³C NMR (DMSO-*d*₆, 125 MHz) δ 165.36, 157.71, 155.83, 148.97, 148.32, 148.23, 148.22, 142.90, 127.15, 123.08, 118.25, 118.19, 115.90, 115.72, 114.84, 111.66, 56.27, 50.37, 49.74, 45.28, 42.00. HRMS [*M* + *H*]⁺ Found 357.1611, calculated 357.1605 for C₂₀H₂₁FN₂O₃.

4.1.5.4. (E)-3-(4-hydroxy-3-methoxyphenyl)-1-(4-(3-nitrophenyl)piperazin-1-yl)prop-2-en-1-one (10d)

Yellow solid product, 83% yield. ¹H NMR (DMSO-*d*₆, 500 MHz): δ 9.45 (bs, 1H), 7.44 (d, *J* = 15.0 Hz, 1H), 7.34 (s, 1H), 7.12–7.06 (m, 4H), 7.01–6.99 (m, 2H), 6.77 (d, *J* = 8.0 Hz, 1H), 3.83 (s, 5H), 3.80 (bs, 2H), 3.09 (s, 4H). ¹³C NMR (DMSO-*d*₆, 125 MHz) δ 164.93, 157.28, 155.40, 148.53, 147.88, 147.80, 142.51, 126.70, 122.69, 117.83, 117.77, 115.48, 115.45, 115.30, 114.37, 111.16, 55.81, 49.93, 49.31, 44.85, 41.55. HRMS [*M* + *H*]⁺ Found 384.1561, calculated 384.1556 for C₂₀H₂₁FN₂O₃.

4.1.5.5. (E)-3-(4-hydroxy-3-methoxyphenyl)-1-(4-(4-methoxyphenyl)piperazin-1-yl)prop-2-en-1-one (**10e**)

White solid product, 85% yield. ^1H NMR (DMSO- d_6 , 500 MHz): δ 9.47 (s, 1H), 7.43 (d, J = 15.0 Hz, 1H), 7.35 (bs, 1H), 7.13-7.10 (s, 1H), 6.94 (d, J = 8.5 Hz, 2H), 6.83 (d, J = 9.0 Hz, 2H), 6.78 (d, J = 8.0 Hz, 1H), 3.68 (s, 5H), 3.35 (s, 5H), 3.02 (s, 4H). ^{13}C NMR (DMSO- d_6 , 125 MHz) δ 164.89, 153.34, 148.50, 147.87, 145.22, 142.45, 126.71, 122.67, 118.08, 115.43, 114.40, 114.31, 111.12, 55.80, 55.19, 50.75, 47.56, 42.32, 41.89. HRMS $[\text{M} + \text{H}]^+$ Found 369.1819, calculated 369.1812 for $\text{C}_{21}\text{H}_{24}\text{N}_2\text{O}_4$.

4.1.5.6. (E)-1-(4-(4-chlorophenyl)piperazin-1-yl)-3-(4-hydroxy-3-methoxyphenyl)prop-2-en-1-one (**10f**)

White solid product, 83% yield. ^1H NMR (DMSO- d_6 , 500 MHz): δ 9.44 (bs, 1H), 7.43 (d, J = 15.5 Hz, 1H), 7.32 (bs, 1H), 7.10-6.98 (m, 6H), 6.78 (d, J = 8.5 Hz, 1H), 3.83 (bs, 7H), 3.08 (bs, 4H). ^{13}C NMR (DMSO- d_6 , 125 MHz) δ 170.16, 162.48, 160.60, 153.72, 153.06, 152.93, 147.70, 131.89, 127.79, 123.00, 122.94, 120.65, 120.45, 119.55, 116.43, 116.35, 61.01, 55.13, 54.54, 50.06, 46.75. HRMS $[\text{M} + \text{H}]^+$ Found 373.1502, calculated 373.1509 for $\text{C}_{20}\text{H}_{21}\text{ClN}_2\text{O}_3$.

4.1.5.7. (E)-3-(4-hydroxy-3-methoxyphenyl)-1-(4-(p-tolyl)piperazin-1-yl)prop-2-en-1-one (**10g**)

White solid product, 80% yield. ^1H NMR (DMSO- d_6 , 500 MHz): δ 9.44 (bs, 1H), 7.44 (d, J = 15.5 Hz, 1H), 7.32 (bs, 1H), 7.10-7.07 (m, 2H), 6.91 (d, J = 8.5 Hz, 1H), 6.83-6.77 (m, 3H), 3.83 (bs, 6H), 3.68 (bs, 6H), 3.01 (bs, 4H). ^{13}C NMR (DMSO- d_6 , 125 MHz) δ 170.14, 158.56, 153.71, 153.07, 150.38, 147.65, 131.91, 127.78, 123.27, 120.66, 119.59, 119.50, 116.39, 61.00, 60.38, 55.84, 55.20, 50.27, 46.93. HRMS $[\text{M} + \text{H}]^+$ Found 353.1254, calculated 353.1260 for $\text{C}_{21}\text{H}_{24}\text{N}_2\text{O}_3$.

4.2. Biological evaluation

4.2.1. Determination of IC_{50} values

Human acetylcholinesterase (hAChE), from human erythrocytes AChE (CAS No. 9000-81-1, Sigma Aldrich), butyryl cholinesterase from equine serum eqBChE (CAS NO. 9001-08-5, Sigma Aldrich), 5,5'-dithiobis-2-nitrobenzoic acid (Ellman's reagent, DTNB CAS No.69-78-3), acetylthiocholine iodide (ATCI, CAS No. 1866-15-5) and butyryl thiocholine iodide (BTCl, CAS No. 1866-16-6) were purchased from Sigma Aldrich. The determinations of AChE inhibitory capacity of the compounds were tested by Ellman assay with slight modification [53]. Ferulic acid (Sigma Aldrich, CAS No. 1261170-81-3) and **DPZ** hydrochloride (Sigma Aldrich, CAS No. 120011-70-3) were used as reference compounds. All the experiments were conducted in 50 mM Tris-HCl buffer at pH 8. Briefly, 50 μL of AChE (0.022 U mL^{-1}) and 10 μL of the test or standard compound were incubated in 96-well plates at room temperature for 30 min. Additional, 30 μL of the substrate viz. ATCI (1.5 mM) was added and the solution was incubated for an additional 30 min at room temperature. Finally, 160 μL of DTNB (0.15

mM) was added to it and after 30 sec the absorbance was measured at 415 nm wavelength using a 96 well microplate reader (SynergyTM HT, Bio-Tek Instruments, Inc.). Each assay was performed in triplicate and each experiment was repeated at least two-three times independently. The blank contained all components except enzyme. The inhibition percent was calculated using the following expression: $[(Ac-Ai)/Ac] \times 100$, where Ai and Ac are the absorbances obtained for AChE in the presence and absence of inhibitors. The *in-vitro* BChE assay was performed using the same procedure as mentioned above. Briefly, 50 μ L of BChE (0.06 U mL⁻¹) and 10 μ L of the test or standard compound were incubated in 96-well plates at room temperature for 30 min. Further, 30 μ L of the substrate viz. BTCI (15 mM) was added and the solution was incubated for an additional 30 min at room temperature. Finally, 160 μ L of DTNB (1.5 mM) was added to it and after 30 sec the absorbance was measured at 415 nm wavelength using a 96-well microplate reader. Each assay was performed in triplicate and each experiment was repeated at least two-three times independently. The inhibition percent was calculated by the following expression: $[(Ac-Ai)/Ac] \times 100$, where Ai and Ac are the absorbance obtained for BChE in the presence and absence of inhibitors.

4.2.2. Kinetic Characterization of AChE and BChE Inhibition

To study the ChE inhibitory mechanism of action of **7a**, reciprocal plots of $1/[V]$ versus $1/[S]$ were constructed using six different concentrations of the substrate acetylthiocholine iodide (ATCI) or five concentrations of butyryl thiocholine iodide (BTCI) (0.5, 1.0, 1.5, 2.0, 2.5, and 3.0 mM for hAChE; 5, 10, 15, 20, and 25 mM for *equine* BChE) by using the Ellman method. Briefly, compound **7a** (10 μ L) at different concentrations (1, 5 and 10 μ M for hAChE; 7.5, 15 and 30 μ M for *equine* BChE) was pre-incubated with hAChE (50 μ L of 0.022 U/mL) or *equine* BChE (50 μ L of 0.06 U/mL) and DTNB (160 μ L of 0.15 mM for AChE; 160 μ L of 1.5 mM for *equine* BChE), at 37 °C for 30 min, followed by the addition of 30 μ L of the substrate at different concentrations. The kinetic characterization of the hydrolysis of ATCI or BTCI catalyzed by AChE or *equine* BChE was done spectrometrically using a 96-well microplate reader (SynergyTM HT, Bio-Tek Instruments, Inc.) at 415 nm.

4.2.3. Propidium iodide displacement assay

A solution of hAChE at a concentration of 5.0 U/mL in 0.1 mM Tris buffer, pH 8.0, was used. Aliquots of the compounds (1:1) to get the final concentrations of 5, 10, 20 and 50 μ M

were added, and the solutions were kept at room temperature for 6 h at 25 °C. Finally, the samples were incubated for 20 min with propidium iodide at a final concentration of 20 μ M, and the fluorescence was measured in a fluorescence microplate reader (SynergyTM HT, Bio-Tek Instruments, Inc.). Wavelengths of excitation and emission were 535 and 595 nm, respectively.

4.2.4. DPPH radical-scavenging potency

The DPPH (2,2-diphenyl-1-picryl-hydrazyl-hydrate) free radical method is an antioxidant assay based on reduction of DPPH. DPPH gets reduced in the presence of an antioxidant molecule, giving rise to a yellow-colored diphenyl picrylhydrazine. Thus, the assay measures hydrogen atom donating ability and hence provides measurement of antioxidant activity of a compound [54]. All the experiments were performed in methanol. Five different concentrations 200, 160, 80, 40 and 20 μM of test compounds (**4d**, **4e**, **4h**, **4i**, **7a**, **10b**, and ferulic acid) were used. In brief, 75 μL of different concentrations (200, 160, 80, 40, and 20 μM), of the test compounds were added to a 96-well plate. To this, 75 μL of DPPH (100 μM final concentration) solution was added. Finally, a 96-well microplate was incubated at 37 $^{\circ}\text{C}$ for 25 min in a shaking water bath with moderate shaking. The absorbance was measured at 520 nm wavelength using a 96-well microplate reader (SynergyTM HT, Bio-Tek Instruments, Inc.). A low absorbance indicates an effective free radical scavenging capacity. The reducing percentage (RP) of the DPPH was determined by the equation $\text{RP} = [(\text{absorbance of control} - \text{absorbance of the test}) / \text{absorbance of control}] \times 100$. All the experiments were performed in duplicate or triplicate.

4.2.5. *In-vitro metal chelating assay*

The chelating studies were performed using a UV-vis spectrophotometer (Agilent Cary 60 UV-Vis spectrophotometer) wavelength ranging from 200 to 700 nm. Desired concentrations of the compounds (**7a** and **4e**) were dissolved in deionized water to make a 600 μM solution and pH was monitored using a pH meter. Further, the compounds (**7a** and **4e**) were diluted to make a 300 μM solution. The solution obtained was scanned under a UV-vis spectrophotometer in the range of 200-700 nm. Finally, FeCl_3 (1.2 mM) was dissolved in deionized water to prepare a colorless stock solution. The two solutions, FeCl_3 (600 μM), and compound (600 μM) were mixed in equal proportions, and the pH was monitored and scanned with a UV-vis spectrophotometer. The pH of the solution was raised to 7.4 by adding diisopropylethylamine (50 μL DIPEA + 950 μL DI water) to the solution followed by UV scanning. The absorption spectra of each compound (300 μM) alone or in the presence of FeCl_3 (300 μM , final concentration) for were recorded in the range of 200-700 nm for 30 min at 25 $^{\circ}\text{C}$. The graph was plotted to compare the UV shift before and after the complexation. The metal chelation assay was performed in triplicate. The above samples were analyzed by the MS-MS technique to further confirm the stoichiometry of the complex.

4.2.6. Amyloid- β aggregation studies

A β aggregation study was performed using atomic force microscopy with a NT-MDT Ntegra Prima Atomic Force Microscope (AFM). Amyloid β Protein Fragment 1-42 (CAS Number 107761-42-2) was purchased from Sigma Aldrich and Genscript. For the A β_{1-42} aggregation inhibition experiment, the A β stock solution was diluted with phosphate buffer saline (pH 7.4) to 0.79 μ M before use. The A β_{1-42} working concentration was estimated through the NanoDropTM 2000/2000c spectrophotometer (Thermo Scientific instrument). To carry out the aggregation studies, a mixture of the peptide (50 μ L, 0.39 μ M, final concentration) with or without the test compound (50 μ L, 0.79 μ M final concentration in ratio 1:2) were incubated on an Eppendorf thermomixture C with condensation-prevention top (Eppendorf, catalog No. 5382000015) with agitation at 1400 rpm, at 37 °C for 10 days.

4.2.7. Substrate preparation and plate casting

For AFM film generation, three samples were prepared (1) Fresh A β Protein (0.39 μ M), (2) A β Protein alone (0.39 μ M), (3) A β Protein with **7a** (in a 1:2 ratio). The samples for the AFM imaging were prepared by the drop-casting method using a silicon dioxide substrate [free gift from Dr. BholaNath Pal, SMST, IIT (BHU)]. The plates were washed through ultrasonic agitation on a GT sonic ultrasonic cleaner (AnTech, Product Code: VGT-1990QTS) by placing silicon dioxide plates on the substrate holding tray (made up of Teflon) into the beaker, followed by acetone washing for 5 min. After acetone washing, the substrate was rinsed with isopropyl alcohol using the same procedure as mentioned above. Thereafter, plates were subjected to drying in desiccators for 1 h.

In plate casting, fresh A β_{1-42} Protein, A β_{1-42} alone and protein A β_{1-42} with compound sample (1: 2) were subjected to the substrate by placing 10 μ L of the protein sample on the freshly washed silicon dioxide plates, which were dried at room temperature or placed under vacuum for AFM imaging. The images were visualized using the Nova Px image analysis software (NT-MDTNtegraPrima, Russia).

4.2.8. Molecular docking studies

Molecular docking studies can provide some valuable information on the mode of interaction of the synthesized ligands at the active site of AChE and BChE enzymes. Molecular docking studies were performed using Schrödinger software. X-ray crystal structures of AChE (**PDB ID: 4EY7**) and BChE (**PDB ID: 4BDS**) enzymes were obtained from the Protein Data Bank (www.rscb.org) and proteins were prepared using the “protein preparation wizard” module implemented in the Schrodinger software [45, 55]. Energy was minimized using the OPLS3 force field. Validation and optimization of the docking protocol were performed by redocking the co-crystallized ligands into the active site of the enzymes (AChE and BChE). The 2D structures of compounds **4b**, **4e**, **4i**, **4m**, **7a**, **7b**, **10b**, **DPZ**, **FA**, and tacrine were sketched in the 2D sketcher module of Maestro and 3D minimized using the LigPrep module of the Schrodinger software [56]. The active site of the proteins was defined by the centroid of the co-crystallized ligands present in the X-ray crystal structures of 4EY7 and 4BDS. Standard precision with flexible ligand sampling was used in the Glide docking. The Prime-MMGBSA module of Schrödinger was used to calculate the binding free energies of the best-docked complex of the compounds with the AChE and BChE proteins.

4.2.9. Molecular dynamics simulations

The binding stability and interaction profile of the docked complex of potent inhibitor **7a** were analyzed on AChE and BChE. For this study, a 30 ns molecular dynamics simulation was performed using the Desmond module of Schrödinger [57]. Solvation of the protein–ligand complex was performed using the TIP4P water model and a buffer distance of 10 Å between the box edge and atoms of the complex. The system was neutralized by adding 0.15 M NaCl. The system was energy minimized with a maximum of 20,000 steps, and a modified relaxation protocol was applied for equilibration of the system as described in our previous publication [58]. The constant NPT production run of 30 ns using a time step of 2 fs was performed with no constraints.

4.2.10. Cytotoxicity studies

4.2.10.1. Cell preparation

Human neuroblastoma, SH-SY5Y cells (National Centre for Cell Science, Pune) were used for cytotoxicity studies. SH-SY5Y cells were cultured in 25 cm² tissue culture flasks and incubated in DMEM (Cell clone) and Ham's F12 (Sigma) media, (1:1) supplemented with penicillin-streptomycin (1X), plasmocin prophylactic (1X) and heat-inactivated fetal bovine serum (10%) at 37 °C in a humidified incubator with 5% CO₂ humidified atmosphere. The growth medium was replaced every third day and cells were passaged at 75% confluence.

4.2.10.2. Assessment of cell viability by MTT assay

The cytotoxicity of **7a** on SH-SY5Y cells was determined by MTT assay. SH-SY5Y cells were seeded at a concentration of 1×10^4 cells/well in 96-well plates and were incubated overnight for adherence. The compound, **7a** was added in SH-SY5Y cells at a concentration of 20, 10, 5, 2.5, 1, 0.1 and 0.01 μ M in triplicates and incubated for 24 h at 5% CO₂ at 37 °C. Cells without **7a** were used as control. Post incubation, 3-[4,5-dimethylthiazol-2-yl]-2,5-diphenyltriazolium bromide (MTT) (Himedia) (5 mg/mL) was added. After four hours, 0.04 M HCl isopropanol was added to the medium having an MTT solution and incubated at 37 °C for 1 h in dark. Absorbance was measured at 570 nm using a 96-well microplate reader (SynergyTM HT, Bio-Tek Instruments, Inc.). Mean absorbance (OD₅₇₀) values were plotted against different concentrations of **7a** used. Percent cell viability was calculated by using the formula:

$$\text{Percentage of viability} = \frac{\text{Mean OD value of the experimental sample (treated)}}{\text{Mean OD value of experimental control (untreated)}} \times 100$$

Percentage cytotoxicity was calculated by the following formula:

$$\% \text{ cytotoxicity} = 100\% - \% \text{ cell viability [59].}$$

4.2.11. Animal studies

Adult male Swiss albino mice, 6 weeks old and weighing 30 ± 2 g were obtained from the Central Animal House of the University and acclimatized in an animal room for 7 days (12:12 h light/dark cycle, temperature 25 ± 2 °C) in the Department of Pharmaceutical Engineering & Technology, Indian Institute of Technology (Banaras Hindu University). Mice were supplied with commercial food pellets and tap water unless otherwise stated. All the experimental methods and procedures conducted in this study were in accordance with the guidelines

approved by the Committee for the Purpose of Control and Supervision of Experiments on Animals, Ministry of Environment, Forests and Climate Change, Government of India and approved by the Central Animal Ethical Committee of the University (Banaras Hindu University, Varanasi, India) (**Dean/2018/ CAEC/1189, dated 20.04.2019**).

4.2.11.1. *Acute toxicity test*

Compound **7a** was tested for acute oral toxicity as per OECD guidelines. Compound **7a** was administered in graded doses up to 500 mg/kg. Mice were observed regularly for the first 24 h to notice behavioral changes, seizures, or diarrhea and then observed for mortality up to 14 days. All the mice were sacrificed on the 14th day after drug administration and were microscopically examined for possible damage to the liver.

4.2.11.2. *Scopolamine-induced amnesia model and Y maze test*

4.2.11.2.1. *Drugs and chemicals*

Scopolamine hydrochloride (CAS No. 55-16-3) and donepezil hydrochloride (CAS No. 120011-70-3) were purchased from Sigma–Aldrich. All other reagents used in this study were obtained from commercial suppliers and used without further purification.

4.2.11.2.2. *Drug preparation and treatment protocol [5, 60]*

Scopolamine hydrochloride (3 mg/kg), **DPZ** (5 mg/kg) and compound **7a** suspensions (6.25, 12.5 and 25 mg/kg) were freshly prepared in 0.5% v/v TWEEN 80. The animals were randomly allocated into eight groups (n=5) namely, (i) vehicle control, (ii) scopolamine 3 mg/kg, i.p., (iii) **DPZ** 5 mg/kg, (iv) **7a** 6.25 mg/kg, p.o., (v) **7a** 12.5 mg/kg, p.o., (vi) **7a** 25 mg/kg, p.o., (vii) **FA** 12.5 mg/kg, p.o., (viii) **FA** 25 mg/kg, p.o. Test compounds or **DPZ** were administered daily up to 7 days. On the seventh day, scopolamine was administered to groups ii, iii, iv, v, vi, vii and viii after 30 min of drug administration. The vehicle control group received only the vehicle. Then, all the animals were subjected to a Y-maze test 15 min after vehicle or scopolamine administration.

4.2.11.2.3. *Y-maze test*

The Y-maze test is a simple, rapid, and sensitive test for the evaluation of exploratory behavior and spatial working memory in rodents. The Y-maze is a three-arm horizontal maze separated apart by 120°. The three arms of the maze were designated A, B, and C. During experimentation, each mouse was placed at the end of one arm and allowed to move freely through the maze for 8-min, during which the number of times it made a full entry (entry of all four limbs) into each arm was recorded using a video camera. Later, the data was analyzed, and the number of spontaneous alternations was calculated. Spontaneous alternations occur when a mouse enters into three different arms in three consecutive entries (ABC, ACB, BAC, BCA, CAB and CBA). The percentage of alternation was then calculated using the equation: % spontaneous alternation (SA) = [(number of alternations/total arm entries) – 2] X 100. This measure of %SA reflects the short-term memory in mice.

4.2.11.3. Neurochemicals estimation and antioxidant property evaluation

After the completion of the Y-maze experiment, all mice according to their respective groups were sacrificed immediately through cervical dislocation and whole brains were isolated from the skull and homogenized with glass homogenizer in 5 mL of 12.5 mM sodium phosphate buffer (pH 7.4). The homogenates were centrifuged at 7000 rpm for 30 min at 4 °C. The supernatants were collected, and utilized for estimations of different biochemical parameters.

The cholinergic biomarker levels (AChE/BChE) were determined by Ellman's colorimetric method with slight modification. Briefly, 100 µL of the supernatant was incubated with ATCI or BTCl (15 mM of 100 µL) for 5 min. After that 100 µL of 1.5 mM DTNB was added, and the absorbance was recorded at 415 nm, immediately.

The estimation of antioxidant parameter superoxide dismutase (SOD) was performed as per reported protocol. All of the reagent for this assay was prepared in phosphate buffer saline (PBS pH 7.4). Briefly, the reagent was prepared by dissolving 50 mM of anhydrous sodium carbonate (Na₂CO₃), 0.1 mM of ethylenediaminetetraacetic acid (EDTA) and 25 µM of nitro blue tetrazolium (NBT) in PBS (0.1 M, pH 7.4). For the experiment, 100 µL of prepared reagent, 25 µL of hydroxylamine hydrochloride (NH₂OH·HCl) and 50 µL of supernatant were mixed thoroughly, and the absorbance was recorded at 570 for 3 min at regular intervals.

Catalase (CAT) is an enzyme that catalyzes the decomposition of hydrogen peroxide to water and oxygen. The CAT activity was evaluated as per the reported protocol described by Sinha. The assay mixture consisted of 50 μ M of PBS (0.1 M; pH 7.4), 50 μ L of 800 mM of hydrogen peroxide (H_2O_2), 50 μ M of brain supernatant and 100 μ L of dichromate/acetic acid solution (5% $\text{K}_2\text{Cr}_2\text{O}_7$ /glacial acetic acid; 1:3 v/v). Briefly, in a 96-well plate, 50 μ M of brain supernatant, 50 μ M of PBS (0.1 M pH 7.4) and 50 μ L of 800 mM of hydrogen peroxide (H_2O_2) were incubated at 37 °C for 1 min. After incubation, 150 μ L of dichromate/acetic acid solution (coloring reagent) was added followed by boiling at 100 °C for 10 min. Finally, the absorbance was recorded at 570 nm using a 96-well microplate reader.

A malondialdehyde (MDA) assay was used to access antioxidant properties on lipid peroxidation in the brain homogenate. Briefly, 0.2 mL of 8.1% sodium lauryl sulfate (SLS), 1.5 mL of 20% glacial acetic acid and 1.5 mL of 0.8% aqueous solution of thiobarbituric acid (TBA) was added to the 0.2 mL of processed brain homogenate. The mixture was made up to 4.0 mL with deionized water and heated at 95 °C for 60 min. After cooling with tap water, 5 mL of n-butanol and pyridine mixture (15:1 v/v) and 1 mL of distilled water were added and centrifuged. The organic layer (200 μ L) was separated out in a 96-well plate and absorbance was measured at 532 nm using a 96-well microplate reader.

Declaration of competing interest

The authors declare that there is no conflict of interest.

Acknowledgments

GM is thankful to the Central Instrument Facility (CIF) Indian Institute of Technology (BHU) for providing NMR and AFM facilities. GM is also thankful to Indian Institute of Integrative Medicine (IIIM) Jammu and Indian Institute of Technology, Ropar for the HRMS study. GPM is thankful to Dr. Bhola Nath Pal, SMST, IIT (BHU) for providing silicon dioxide substrate for AFM imaging. GPM also acknowledges the National Centre for Cell Science for the SHSY5Y cell line.

Funding

This work is supported by Science and Engineering Research Board under Core Research Grant (**SERB-CRG/2018/003490**) and Indian Institute of Technology (BHU) (**SM/2016-17/1198/L**). Y.P.S., A.P., G.N.V.C.T., S.V. are thankful to Indian Institute of Technology (BHU) and MHRD, India for fellowship.

Appendix A. Supplementary data

Supplementary data to this article can be found online at <https://ees.elsevier.com/ejmech/default.asp>

References

- [1] Q. Li, S. He, Y. Chen, F. Feng, W. Qu, H. Sun, Donepezil-based multi-functional cholinesterase inhibitors for treatment of Alzheimer's disease, *European journal of medicinal chemistry*, 158 (2018) 463-477.
- [2] <http://www.alz.org/facts/>, in, 2017 Alzheimer's Disease Facts and Figures - Alzheimer's Association, 2017.
- [3] J. Cheung, M.J. Rudolph, F. Burshteyn, M.S. Cassidy, E.N. Gary, J. Love, M.C. Franklin, J.J. Height, Structures of human acetylcholinesterase in complex with pharmacologically important ligands, *Journal of medicinal chemistry*, 55 (2012) 10282-10286.
- [4] T.H. Ferreira-Vieira, I.M. Guimaraes, F.R. Silva, F.M. Ribeiro, Alzheimer's disease: Targeting the Cholinergic System, *Current neuropharmacology*, 14 (2016) 101-115.
- [5] D. Kumar, S.K. Gupta, A. Ganeshpurkar, G. Gutti, S. Krishnamurthy, G. Modi, S.K. Singh, Development of Piperazinediones as dual inhibitor for treatment of Alzheimer's disease, *European journal of medicinal chemistry*, 150 (2018) 87-101.
- [6] P. Salahuddin, M.T. Fatima, A.S. Abdelhameed, S. Nusrat, R.H. Khan, Structure of amyloid oligomers and their mechanisms of toxicities: Targeting amyloid oligomers using novel therapeutic approaches, *European journal of medicinal chemistry*, 114 (2016) 41-58.
- [7] Y.P. Singh, A. Pandey, S. Vishwakarma, G. Modi, A review on iron chelators as potential therapeutic agents for the treatment of Alzheimer's and Parkinson's diseases, *Molecular Diversity*, (2018).
- [8] G. Mushtaq, N.H. Greig, J.A. Khan, M.A. Kamal, Status of acetylcholinesterase and butyrylcholinesterase in Alzheimer's disease and type 2 diabetes mellitus, *CNS & neurological disorders drug targets*, 13 (2014) 1432-1439.
- [9] S. West, P. Bhugra, Emerging drug targets for A β and tau in Alzheimer's disease: a systematic review, *British journal of clinical pharmacology*, 80 (2015) 221-234.
- [10] N. Guzior, A. Wieckowska, D. Panek, B. Malawska, Recent development of multifunctional agents as potential drug candidates for the treatment of Alzheimer's disease, *Current medicinal chemistry*, 22 (2015) 373-404.
- [11] L.S. Schneider, F. Mangialasche, N. Andreasen, H. Feldman, E. Giacobini, R. Jones, V. Mantua, P. Mecocci, L. Pani, B. Winblad, M. Kivipelto, Clinical trials and late-stage drug development for Alzheimer's disease: an appraisal from 1984 to 2014, *Journal of internal medicine*, 275 (2014) 251-283.
- [12] J. Wang, D. Land, K. Ono, J. Galvez, W. Zhao, P. Vempati, J.W. Steele, A. Cheng, M. Yamada, S. Levine, P. Mazzola, G.M. Pasinetti, Molecular topology as novel strategy for discovery of drugs with β lowering and anti-aggregation dual activities for Alzheimer's disease, *PloS one*, 9 (2014) e92750.

- [13] D. Kumar, A. Ganeshpurkar, D. Kumar, G. Modi, S.K. Gupta, S.K. Singh, Secretase inhibitors for the treatment of Alzheimer's disease: Long road ahead, *European journal of medicinal chemistry*, 148 (2018) 436-452.
- [14] S.K. Singh, A. Dutta, G. Modi, alpha-Synuclein aggregation modulation: an emerging approach for the treatment of Parkinson's disease, *Future medicinal chemistry*, 9 (2017) 1039-1053.
- [15] K. Chalupova, J. Korabecny, M. Bartolini, B. Monti, D. Lamba, R. Caliandro, A. Pesaresi, X. Brazzolotto, A.J. Gastellier, F. Nachon, J. Pejchal, M. Jarosova, V. Hepnarova, D. Jun, M. Hrabanova, R. Dolezal, J. Zdarova Karasova, M. Mzik, Z. Kristofikova, J. Misik, L. Muckova, P. Jost, O. Soukup, M. Benkova, V. Setnicka, L. Habartova, M. Chvojkova, L. Kleteckova, K. Vales, E. Mezeiova, E. Uliassi, M. Valis, E. Nepovimova, M.L. Bolognesi, K. Kuca, Novel tacrine-tryptophan hybrids: Multi-target directed ligands as potential treatment for Alzheimer's disease, *European journal of medicinal chemistry*, 168 (2019) 491-514.
- [16] A. Gandini, M. Bartolini, D. Tedesco, L. Martinez-Gonzalez, C. Roca, N.E. Campillo, J. Zaldivar-Diez, C. Perez, G. Zuccheri, A. Miti, A. Feoli, S. Castellano, S. Petralla, B. Monti, M. Rossi, F. Moda, G. Legname, A. Martinez, M.L. Bolognesi, Tau-Centric Multitarget Approach for Alzheimer's Disease: Development of First-in-Class Dual Glycogen Synthase Kinase 3beta and Tau-Aggregation Inhibitors, *Journal of medicinal chemistry*, 61 (2018) 7640-7656.
- [17] K. Liu, T.L. Guo, J. Chojnacki, H.-G. Lee, X. Wang, S.L. Siedlak, W. Rao, X. Zhu, S. Zhang, Bivalent ligand containing curcumin and cholesterol as fluorescence probe for A β plaques in Alzheimer's disease, *ACS Chem Neurosci*, 3 (2012) 141-146.
- [18] E.P. Lebois, J.P. Schroeder, T.J. Esparza, T.M. Bridges, C.W. Lindsley, P.J. Conn, D.L. Brody, J.S. Daniels, A.I. Levey, Disease-Modifying Effects of M1 Muscarinic Acetylcholine Receptor Activation in an Alzheimer's Disease Mouse Model, *ACS chemical neuroscience*, 8 (2017) 1177-1187.
- [19] M. Bakou, K. Hille, M. Kracklauer, A. Spanopoulou, C.V. Frost, E. Malideli, L.M. Yan, A. Caporale, M. Zacharias, A. Kapurniotu, Key aromatic/hydrophobic amino acids controlling a cross-amyloid peptide interaction versus amyloid self-assembly, *The Journal of biological chemistry*, 292 (2017) 14587-14602.
- [20] R. Cukalevski, B. Boland, B. Frohm, E. Thulin, D. Walsh, S. Linse, Role of Aromatic Side Chains in Amyloid β -Protein Aggregation, *ACS chemical neuroscience*, 3 (2012) 1008-1016.
- [21] N.S. de Groot, I. Pallarés, F.X. Avilés, J. Vendrell, S. Ventura, Prediction of "hot spots" of aggregation in disease-linked polypeptides, *BMC Structural Biology*, 5 (2005) 18.
- [22] H. Liu, L. Wang, W. Su, X.Q. Xie, Advances in recent patent and clinical trial drug development for Alzheimer's disease, *Pharmaceutical patent analyst*, 3 (2014) 429-447.
- [23] K. Honarnejad, A. Daschner, A.P. Gehring, A. Szybinska, A. Giese, J. Kuznicki, F. Bracher, J. Herms, Identification of tetrahydrocarbazoles as novel multifactorial drug candidates for treatment of Alzheimer's disease, *Translational Psychiatry*, 4 (2014) e489.
- [24] K. Jomova, D. Vondrakova, M. Lawson, M. Valko, Metals, oxidative stress and neurodegenerative disorders, *Molecular and cellular biochemistry*, 345 (2010) 91-104.
- [25] K. Li, H. Reichmann, Role of iron in neurodegenerative diseases, *Journal of Neural Transmission*, 123 (2016) 389-399.
- [26] R.J. Ward, F.A. Zucca, J.H. Duyn, R.R. Crichton, L. Zecca, The role of iron in brain ageing and neurodegenerative disorders, *The Lancet. Neurology*, 13 (2014) 1045-1060.
- [27] S. Masaldan, A.I. Bush, D. Devos, A.S. Rolland, C. Moreau, Striking while the iron is hot: Iron metabolism and ferroptosis in neurodegeneration, *Free radical biology & medicine*, 133 (2019) 221-233.
- [28] D. Pratico, Oxidative stress hypothesis in Alzheimer's disease: a reappraisal, *Trends in pharmacological sciences*, 29 (2008) 609-615.
- [29] C. Voshavar, M. Shah, L. Xu, A.K. Dutta, Assessment of Protective Role of Multifunctional Dopamine Agonist D-512 Against Oxidative Stress Produced by Depletion of Glutathione in PC12 Cells: Implication in Neuroprotective Therapy for Parkinson's Disease, *Neurotoxicity research*, 28 (2015) 302-318.
- [30] D.J. Newman, G.M. Cragg, Natural Products as Sources of New Drugs from 1981 to 2014, *Journal of Natural Products*, 79 (2016) 629-661.

- [31] M. Estrada, C. Herrera-Arozamena, C. Pérez, D. Viña, A. Romero, J.A. Morales-García, A. Pérez-Castillo, M.I. Rodríguez-Franco, New cinnamic – N-benzylpiperidine and cinnamic – N,N-dibenzyl(N-methyl)amine hybrids as Alzheimer-directed multitarget drugs with antioxidant, cholinergic, neuroprotective and neurogenic properties, *European journal of medicinal chemistry*, 121 (2016) 376-386.
- [32] Z. Sang, K. Wang, X. Han, M. Cao, Z. Tan, W. Liu, Design, Synthesis, and Evaluation of Novel Ferulic Acid Derivatives as Multi-Target-Directed Ligands for the Treatment of Alzheimer's Disease, *ACS Chem Neurosci*, 10 (2019) 1008-1024.
- [33] C. Chen, X. Yang, H. Fang, X. Hou, Design, synthesis and preliminary bioactivity evaluations of 8-hydroxyquinoline derivatives as matrix metalloproteinase (MMP) inhibitors, *European journal of medicinal chemistry*, 181 (2019) 111563.
- [34] P. Gisbert, P. Trillo, I.M. Pastor, Comparative Study of Catalytic Systems Formed by Palladium and Acyl-Substituted Imidazolium Salts, 3 (2018) 887-893.
- [35] J. Verghese, T. Nguyen, L.M. Oppgaard, L.M. Seivert, H. Hiasa, K.C. Ellis, Flavone-based analogues inspired by the natural product simocyclinone D8 as DNA gyrase inhibitors, *Bioorganic & medicinal chemistry letters*, 23 (2013) 5874-5877.
- [36] M. Iwamura, R. Koyama, Y. Nonaka, F. Dai, R. Matsuoka, M. Nakamura, H. Iwabuchi, T. Okada, T. Hasegawa, High-Throughput Evaluation System based on Fluorescence Intensity Distribution Analysis-Polarization to Investigate Carbohydrate–Carbohydrate Interactions, 89 (2016) 617-625.
- [37] K.G. Liu, A.J. Robichaud, A general and convenient synthesis of N-aryl piperazines, *Tetrahedron Letters*, 46 (2005) 7921-7922.
- [38] G.L. Ellman, Tissue sulfhydryl groups, *Archives of biochemistry and biophysics*, 82 (1959) 70-77.
- [39] P. Taylor, S. Lappi, Interaction of fluorescence probes with acetylcholinesterase. Site and specificity of propidium binding, *Biochemistry*, 14 (1975) 1989-1997.
- [40] W.-J. Huang, X. Zhang, W.-W. Chen, Role of oxidative stress in Alzheimer's disease, *Biomedical reports*, 4 (2016) 519-522.
- [41] S. Losada-Barreiro, C. Bravo-Díaz, Free radicals and polyphenols: The redox chemistry of neurodegenerative diseases, *European journal of medicinal chemistry*, 133 (2017) 379-402.
- [42] A. Robert, Y. Liu, M. Nguyen, B. Meunier, Regulation of Copper and Iron Homeostasis by Metal Chelators: A Possible Chemotherapy for Alzheimer's Disease, *Accounts of Chemical Research*, 48 (2015) 1332-1339.
- [43] A. Nunes, S.M. Marques, C. Quintanova, D.F. Silva, S.M. Cardoso, S. Chaves, M.A. Santos, Multifunctional iron-chelators with protective roles against neurodegenerative diseases, *Dalton Transactions*, 42 (2013) 6058-6073.
- [44] X. Zhang, Z. Fu, L. Meng, M. He, Z. Zhang, The Early Events That Initiate β -Amyloid Aggregation in Alzheimer's Disease, *Front Aging Neurosci*, 10 (2018) 359-359.
- [45] Maestro, Schrödinger, LLC, New York, NY, USA, 2018.
- [46] P. Pandey, K.K. Roy, R.J. Doerksen, Negative allosteric modulators of cannabinoid receptor 2: protein modeling, binding site identification and molecular dynamics simulations in the presence of an orthosteric agonist, *Journal of biomolecular structure & dynamics*, 38 (2020) 32-47.
- [47] I. Khan, K.R. Garikapati, A. Setti, A.B. Shaik, V.K. Kanth Makani, M.A. Shareef, H. Rajpurohit, N. Vangara, M. Pal-Bhadra, A. Kamal, C.G. Kumar, Design, synthesis, in silico pharmacokinetics prediction and biological evaluation of 1,4-dihydroindeno[1,2-c]pyrazole chalcone as EGFR /Akt pathway inhibitors, *European journal of medicinal chemistry*, 163 (2019) 636-648.
- [48] Z. Sang, W. Pan, K. Wang, Q. Ma, L. Yu, Y. Yang, P. Bai, C. Leng, Q. Xu, X. Li, Z. Tan, W. Liu, Design, synthesis and evaluation of novel ferulic acid-O-alkylamine derivatives as potential multifunctional agents for the treatment of Alzheimer's disease, *European journal of medicinal chemistry*, 130 (2017) 379-392.
- [49] M.V. Berridge, P.M. Herst, A.S. Tan, Tetrazolium dyes as tools in cell biology: New insights into their cellular reduction, in: *Biotechnology Annual Review*, Elsevier, 2005, pp. 127-152.
- [50] W. Wang, W. Wang, G. Yao, Q. Ren, D. Wang, Z. Wang, P. Liu, P. Gao, Y. Zhang, S. Wang, S. Song, Novel sarsasapogenin-triazolyl hybrids as potential anti-Alzheimer's agents: Design, synthesis and biological evaluation, *European journal of medicinal chemistry*, 151 (2018) 351-362.

- [51] B.H. Chen, J.H. Park, D.W. Kim, J. Park, S.Y. Choi, I.H. Kim, J.H. Cho, T.-K. Lee, J.C. Lee, C.-H. Lee, I.K. Hwang, Y.-M. Kim, B.C. Yan, I.J. Kang, B.N. Shin, Y.L. Lee, M.C. Shin, J.H. Cho, Y.J. Lee, Y.H. Jeon, M.-H. Won, J.H. Ahn, Melatonin Improves Cognitive Deficits via Restoration of Cholinergic Dysfunction in a Mouse Model of Scopolamine-Induced Amnesia, *ACS Chem Neurosci*, 9 (2018) 2016-2024.
- [52] D.B.G. Williams, M. Lawton, Drying of Organic Solvents: Quantitative Evaluation of the Efficiency of Several Desiccants, *The Journal of Organic Chemistry*, 75 (2010) 8351-8354.
- [53] M. Shidore, J. Machhi, K. Shingala, P. Murumkar, M.K. Sharma, N. Agrawal, A. Tripathi, Z. Parikh, P. Pillai, M.R. Yadav, Benzylpiperidine-Linked Diarylthiazoles as Potential Anti-Alzheimer's Agents: Synthesis and Biological Evaluation, *Journal of medicinal chemistry*, 59 (2016) 5823-5846.
- [54] Y. Chen, J. Sun, L. Fang, M. Liu, S. Peng, H. Liao, J. Lehmann, Y. Zhang, Tacrine–Ferulic Acid–Nitric Oxide (NO) Donor Trihybrids as Potent, Multifunctional Acetyl- and Butyrylcholinesterase Inhibitors, *Journal of medicinal chemistry*, 55 (2012) 4309-4321.
- [55] G.M. Sastry, M. Adzhigirey, T. Day, R. Annabhimoju, W. Sherman, Protein and ligand preparation: parameters, protocols, and influence on virtual screening enrichments, *Journal of computer-aided molecular design*, 27 (2013) 221-234.
- [56] LigPrep, Schrödinger, LLC, NY, USA, 2018.
- [57] D.E.S. Research, Desmond Molecular Dynamics System, in: D.E.S. Research (Ed.) *Maestro-Desmond Interoperability Tools*, Schrödinger, LLC, New York, NY, 2019.
- [58] N.D. Chaurasiya, J. Zhao, P. Pandey, R.J. Doerksen, I. Muhammad, B.L. Tekwani, Selective Inhibition of Human Monoamine Oxidase B by Acacetin 7-Methyl Ether Isolated from *Turnera diffusa* (Damiana), *Molecules* (Basel, Switzerland), 24 (2019) 810.
- [59] A.H. Cory, T.C. Owen, J.A. Barltrop, J.G. Cory, Use of an aqueous soluble tetrazolium/formazan assay for cell growth assays in culture, *Cancer Commun*, 3 (1991) 207-212.
- [60] D.V. Patel, N.R. Patel, A.M. Kanhed, S.P. Patel, A. Sinha, D.D. Kansara, A.R. Mecwan, S.B. Patel, P.N. Upadhyay, K.B. Patel, D.B. Shah, N.K. Prajapati, P.R. Murumkar, K.V. Patel, M.R. Yadav, Novel Multitarget Directed Triazinoindole Derivatives as Anti-Alzheimer Agents, *ACS chemical neuroscience*, 10 (2019) 3635-3661.

Highlights

- Naturally inspired *in-vivo* active multifunctional anticholinesterase molecules were synthesized
- Novel ferulic acid analog was more efficacious antioxidant than ferulic acid itself
- Ferulic acid analog modulated aggregation of amyloid β_{1-42}
- Demonstrated reversal of scopolamine-induced learning and memory impairment in mice
- Docking and molecular dynamics revealed stable interactions of new analog with AChE

Declaration of interests

☒ The authors declare that they have no known competing financial interests or personal relationships that could have appeared to influence the work reported in this paper.

☐ The authors declare the following financial interests/personal relationships which may be considered as potential competing interests:

| |
|-------------------|
| Gyan Prakash Modi |
|-------------------|